Remote sensing of North Sea water quality

A comparison between Sentinel-3 OLCI and in-situ measurements

E.M.J. Stierman

Technische Universiteit Delft

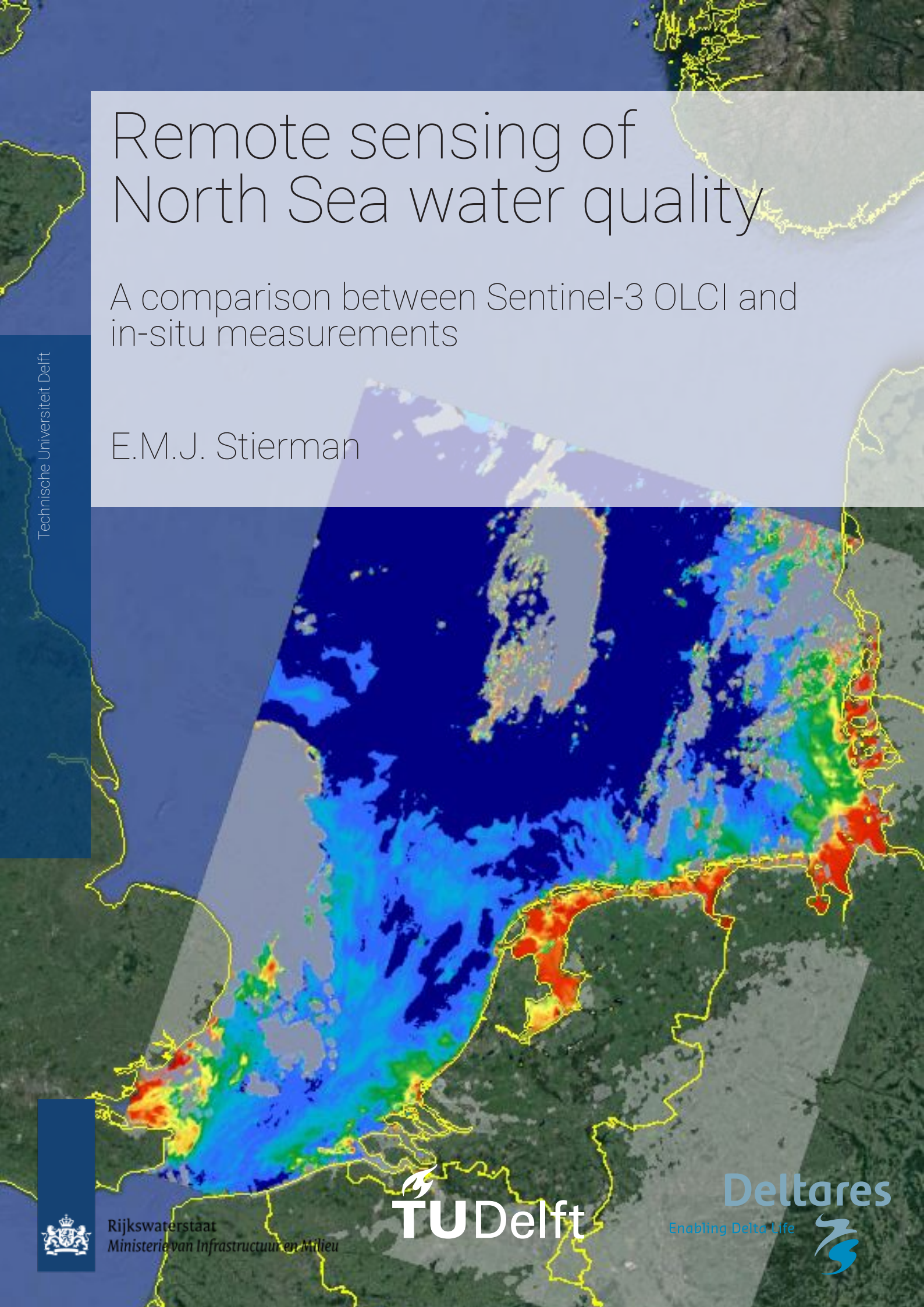

Rijkswaterstaat
Ministerie van Infrastructuur en Milieu

TU Delft

Deltares
Enabling Delta Life

Remote sensing of North Sea water quality

A comparison between Sentinel-3 OLCI and in-situ measurements

by

E.M.J. Stierman

to obtain the degree of Master of Science
at the Delft University of Technology,
to be defended on Wednesday December 20, 2017 at 11:00 AM.

Student number:	4173376	
Project duration:	May 1, 2017 – December 20, 2017	
Thesis committee:	Dr. R. C. Lindenbergh,	TU Delft
	Prof. Dr. P. F. Levelt,	TU Delft, KNMI
	Dr. J. P. Veefkind,	TU Delft, KNMI
	J. J. Chimot,	TU Delft
	Dr. M. A. Eleveld,	Deltares
	A. Oyen,	CIV, Rijkswaterstaat

An electronic version of this thesis is available at `http://repository.tudelft.nl/`.

TU Delft

Abstract

Chlorophyll (Chl) and Total Suspended Matter (TSM) are both important water quality parameters since they influence the amount of oxygen & amount of light penetrating the water. Oxygen and light are vital in marine ecosystems. The Dutch governmental organisation, Rijkswaterstaat (RWS), has been monitoring the water quality of the Dutch part of the North Sea for the last 35 years. A research vessel takes off to sample parameters such as chlorophyll and TSM every few weeks at fixed locations. Recently, Sentinel-3 satellites started to provide satellite-based information on air or water quality. It is expected that products from the Ocean Land Colour Instrument (OLCI) sensor, on board of Sentinel-3, can greatly improve both the geographical and temporal coverage of these parameters. For the Dutch coastal waters this is challenging, because they predominantly consist of complex coastal waters.

This study focusses on the validation of water quality parameters (Chl and TSM) available from Sentinel-3A OLCI observations. To verify the processing line of the OLCI data products it was desired to evaluate the following variables as well: 1) the aerosol optical thickness used in the atmospheric aerosol correction process, which is an important step for deriving the water-leaving reflectance, and 2) the water-leaving reflectance itself used as the main signal for deriving Chl and TSM.

OLCI water quality data products were compared to Rijkswaterstaat in-situ measurements for the months May until September of 2017. Furthermore, OLCI's Chl and TSM were compared with climatologies of MERIS data. The OLCI water-leaving reflectance and aerosol optical thickness data products were compared with observations from the Belgian AERONET-OC station Thornton. To evaluate the spatial distribution of OLCI's aerosol optical thickness comparisons with nearly coincident MODIS-AQUA observations were made. To evaluate the spatial variability of OLCI's data products boxplots were created of Chl, TSM and the aerosol optical thickness.

The water quality products of OLCI consist of a Chl product determined by the OC4Me algorithm and a Chl & TSM product derived from a neural network. OLCI Chl obtained from the OC4Me algorithm showed an overestimation of a factor 2 compared to the in-situ measurements. The Chl results of the neural network compared well with the in-situ measurements showing a correlation coefficient of 0.77. OLCI TSM showed an unrealistic underestimation of a factor 4 compared to in-situ measurements. Boxplots showed that the largest spatial variability is found at stations <50 km from the coast for the three water quality products. This unrealistic underestimation of scattering TSM would imply an underestimation of the water-leaving reflectance in all the bands. Comparing OLCI's water-leaving reflectance with AERONET's showed underestimations in the blue and green bands only. OLCI's water-leaving reflectance of the red and near-infra-red (NIR) bands correlated well with the AERONET-OC measurements. The aerosol optical thickness data product showed unrealistic overestimations of OLCI compared to AERONET-OC, but had a correlation coefficient of 0.58 when comparing it to MODIS aerosol optical thickness product. The spatial variability of OLCI's aerosol optical thickness is very high with differences of more than 40% per kilometre. In general, all products seem to have unrealistic values around clouds and in coastal areas, especially the aerosol optical thickness product. The pixels in those regions are different from other pixels.

These results imply that further research into the software implementation of the radiative transfer models, lookup tables, vicarious calibrations and Neural Networks is needed to understand how retrievals of Chl and TSM concentrations are influenced. Such a fundamental understanding is ultimately also of interest for end users and all parties providing products and services for marine applications.

Preface

The master of Applied Earth Sciences (AES) at the Delft University of Technology is concluded with a graduation research project, also known as the master thesis project. This document presents the report for a master thesis in the field of optical remote sensing and atmospheric sciences. The research has been carried out between May 2017 and December 2017 at the request of Deltares & Rijkswaterstaat, who also offered me a workplace, data and daily supervision.

During my master i got fascinated about the possibilities and limitations of optical remote sensing. In a very short time it is possible to monitor processes on Earth, but first the signal has to travel through the atmosphere to reach the satellite. On this path all kind of particles interfere with or even disturb the satellite signal. In this research project I found out what the possibilities and limitations are in monitoring North Sea water quality using remote sensing.

I would like to thank Dr. Marieke Eleveld for supervising and supporting through my whole graduation process. She provided me with many opportunities to learn and ask critical questions. It was a great and interesting experience to attend the HIGHROC conference in Brussels to present my thesis work with her. Also, I would like to thank Anneleen Oyen for her help as a supervisor from the Rijkswaterstaat team. I appreciate her useful feedback on my work and giving me the opportunity to board one of the Rijkswaterstaat measurement cruises. I also thank the Rijkswaterstaat team, Andries Knotters, Jos Kokke, and Marc Hartogs for all their help and support. I would like to thank Dr. Roderik Lindenbergh for his critical view on my thesis report as supervisor at the TU Delft. Furthermore I would to show my appreciation to Julien Chimot for supporting me with the interpretation of the atmospheric results in this project. I thank Prof. Dr. Pieternel Levelt, and Dr. Pepijn Veefkind for the assistance during the process. Finally, I would like to thank Anouk Blauw and Annette Zijderveld for giving me the opportunity to work on this thesis at Deltares.

E.M.J. Stierman
Delft, January 2013

Contents

List of Figures

List of Tables

1 Introduction

In 2000, the European Water Framework Directive (WFD) was realised. The aim was and is, to improve the water quality in the European Union (EU) by protecting all forms of water, restoring ecosystems, reducing pollution, and guaranteeing sustainable water usage by individuals and businesses [26]. In the Netherlands the implementation of the WFD is managed by the Dutch Ministry of Infrastructure and the Environment (Rijkswaterstaat). One of the issues that should be addressed on a national level is basic monitoring of water quality. Rijkswaterstaat (RWS) is responsible for monitoring water quality of the North Sea in the Netherlands [48].

Typically, RWS monitors water quality by taking in-situ samples in the North Sea. Taking in-situ measurements is labour intensive and expensive. Satellite data products could improve geographical and temporal coverage in water quality monitoring. After the successful launch of the Sentinel-3A satellite in February 2016 and subsequent testing of instruments and data, water quality data products are becoming available. Sentinel-3A data products can be used in order to monitor the North Sea's water quality once they have been validated, which is the main topic of this thesis. This raises the main research question:

What are the possibilities and limitations of Sentinel-3A Level-2 reduced resolution data products for monitoring water quality of the Dutch North Sea?

1.1. Water quality

The first question to be raised is: *"What is water quality?"*. Water can be used in many ways, for example as drinking water, or as a habitat for fish and other aquatic life. The suitability of water for a particular purpose is described by water quality. Water quality is based on physical, chemical, and biological characteristics. Scientists measure and analyse characteristics of water such as the temperature, dissolved mineral content, and number of bacteria [13]. Guidelines and standards such as the WFD are established to maintain the water quality for its different purposes.

Water quality can change through time by natural or human induced processes. Natural processes that change water quality are seasonal variations, climate change, or different types of minerals flowing through a stream. Human induced processes that directly influence water quality are for example farming, burning fossil fuels, and channel broadening. Especially the use of plant fertilisers can change water quality. Fertilisers contain nutrients that make plants grow. When nutrients end up in water they can cause algae to grow extensively which causes a lack of oxygen in the water when decaying and the possibility of fish kills [13]. Phytoplankton are microscopic, single celled algae [9] containing chlorophyll, which account for half of the world's primary productivity [8]. Primary production is the synthesis of organic compounds from carbon dioxide through photosynthesis. Photosynthesis is the process in which chlorophyll transforms carbon dioxide, water, and certain inorganic salts into energy by using light. Primary productivity is important because it forms the foundation of food webs in most ecosystems [6]. Changes in the amount of phytoplankton causes changes in ecosystems.

Ocean colour remote sensing have provided interesting information about the colour of ocean surface water. The colour of the ocean is a good indicator for the amount of phytoplankton. The pigment of phytoplankton is called chlorophyll-a and is of green colour [47]. This green colour is observed by the satellite and can be converted to a concentration of phytoplankton and then to algae. The amount of algae can support the measure of water quality since these are closely related. In this study, chlorophyll-a in-situ measurements will be compared with chlorophyll-a (Chl) satellite data products to see how well satellites can determine the Chl content.

Total Suspended Matter (TSM) is another important water quality parameter. TSM is also known as Suspended Particulate Matter (SPM) and can be defined as all matter suspended in a litre of water [19]. The optical properties of TSM in the North Sea are dominated by the mineral fraction [5]. TSM has a large influence on the amount of light penetrating the water and thus on the primary production and ecology since light is used for the photosynthesis process of chlorophyll [19]. Furthermore, it can transport chemicals and suspend pollutants into the water.

1.2. Ocean Colour Remote Sensing

The Copernicus programme aims to develop a European information service based on satellite earth observation and in-situ (non-space) data [12]. The Sentinel satellite mission is part of this programme. Each Sentinel satellite carries instruments such as radar or multi-spectral imaging instruments for land, ocean and atmospheric monitoring. This master thesis project makes use of data obtained from the Sentinel-3 satellite more specifically from the Ocean Land Colour Instrument (OLCI). The main objective of this instrument is to determine ocean surface colour for the support of marine environment studies [12]. Ocean surface colour products include chlorophyll-a and TSM products.

Ocean colour remote sensing is a passive way of satellite remote sensing. Passive remote sensing is observing emitted sun light reflected from the Earth. Ocean colour remote sensing mostly uses the visible (400 to 700 nm) and near-IR (wavelengths from 700 to less than 2000 nm) parts of the electromagnetic spectrum to obtain the colour of the ocean [36]. When sunlight enters the water its spectral characteristic gets altered by the absorption and scattering properties of the water body as is shown in Figure 1.1. The absorption and scattering properties depend on various constituents in the water such as chlorophyll and TSM. A fraction of the altered sunlight leaves the water and is observed by the satellite, we call this the water-leaving radiance (L_w). Water constituents in the OLCI Level-2 data products are derived from the water-leaving radiance. Therefore the water-leaving radiance will be evaluated By comparing it to AERONET-OC measurements. AERONET-OC stations are ground-based stations measuring water-leaving radiance just above the sea surface. Before this light reaches satellite it has to travel through the atmosphere. This process is shown in Figure 1.1.

1.2.1. Atmospheric influence

The atmosphere has a large influence on radiance measured by satellite instruments. Atmospheric molecules and aerosols scatter and absorb solar radiance indicated in Figure 1.1. Aerosols are suspensions in air (or in a gas) of solid or liquid particles which can scatter or absorb light when large enough [31]. The amount of the solar beam's extinction by aerosols is expressed as aerosol optical thickness (AOT). The AOT is also data products of OLCI Level-2 which will be verified in this thesis by comparing it to AERONET-OC measurements and MODIS satellite products. MODIS is a spectroradiometer on board of the AQUA satellite. MODIS has very specific aerosol data products and is therefore used for the verification of OLCI's AOT product. The AERONET-OC station and MODIS satellite are also shown in Figure 1.1.

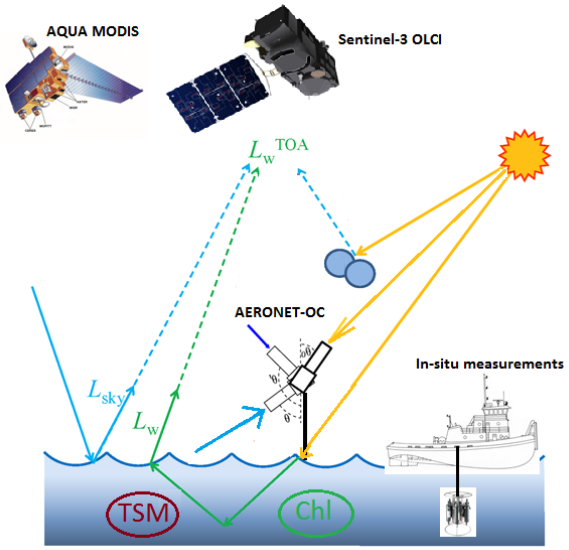

Figure 1.1: Various contributions to the measured TOA radiance. The blue N-N symbols represent NO_2 or any other atmospheric gas molecule, the brown blob represents an aerosol particle [36]

The total radiance (L_t^{TOA}) measured at the top of atmosphere (TOA) by the satellite has different origins. Atmospheric radiance (L_{atm}^{TOA}), reflectance from the sea surface (L_{surf}^{TOA}), and water-leaving radiance (L_w^{TOA}) all contribute to the total radiance. For the atmospheric effects an atmospheric correction is applied. The atmospheric correction and aerosol optical thickness product will be explained in more detail in chapter 3.

1.3. Research area

This research focusses on the Dutch part of the North Sea. This area was chosen because RWS is responsible and can provide chlorophyll and TSM in-situ data for this area. Figure 1.2 gives an overview of the research area with the used in-situ measurements locations of RWS.

The Dutch North Sea can be divided into 2 water types, the Case-1 and Case-2 waters. Case-1 waters are described as natural waters without TSM particles. According to Antoine(2010) Case-1 waters are usually offshore where optical properties are determined by water itself and phytoplankton, microscopic algae containing chlorophyll. The optical properties of Case-1 waters are mostly influenced by Chl concentrations. Case-2 waters are usually coastal waters which are turbid and influenced by river run-off and re-suspension of TSM. The presence of dissolved and suspended particles increases absorption and scattering of light [39]. The dissolved particles are occasionally called as Coloured Dissolved Organic Matter (CDOM) or gelbstoff. CDOM are small organic compounds but are not studied in this thesis. The multiple combinations of particles in Case-2 waters make their optical characteristics very complex. Prieur (1981) created a triangular representation for the division of Case-1 and Case-2 water according to the influence of phytoplankton (P), CDOM (Coloured Dissolved Organic Matter Y), and sediments (S). In Figure 1.3 this representation is shown.

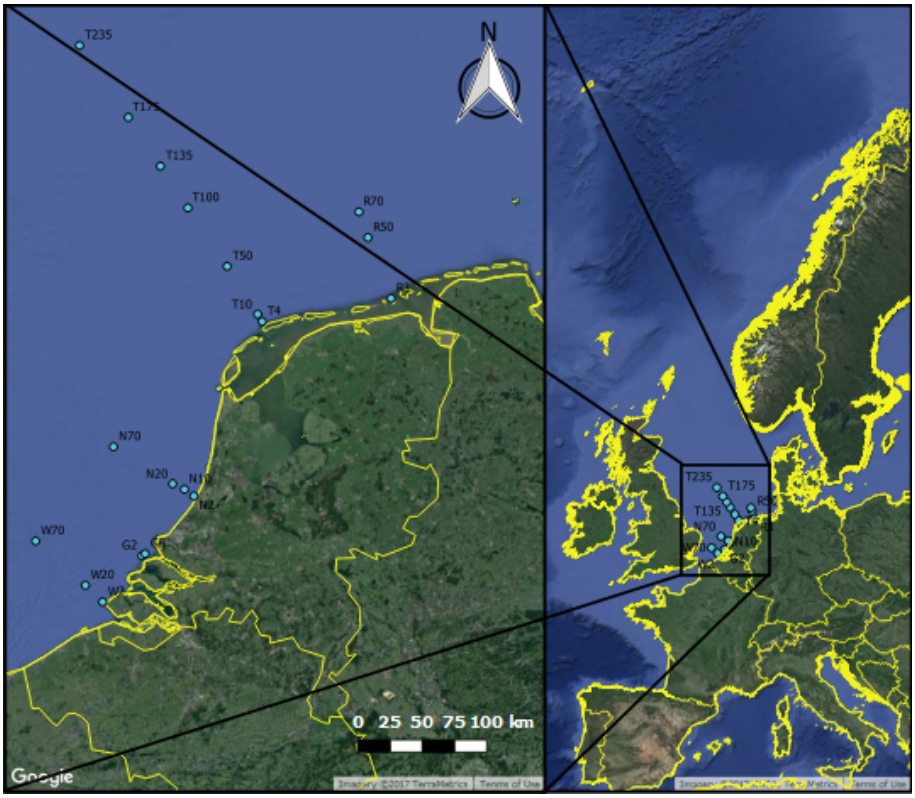

Figure 1.2: Overview of the Dutch part of the North Sea. The in-situ measurement locations of RWS are indicated with dots. The letters in the names indicate on which transect the measurement location is, R = Rottum transect, T = Terschelling transect, N = Noordwijk transect, and W = Walcheren transect. The numbers correspond to the distance the measurements locations are from the coast.

Figure 1.3: Triangular representation of Case-1 and Case-2 waters by Prieur and Sathyendranath (1981) [46]. The corners indicate the dominance by phytoplankton (P), CDOM (Y), and sediments (S). Case-1 waters are located in the upper triangle and Case-2 waters in the lower triangle [2]. It is clear that Case-1 waters are dominated by chlorophyll (P) content, whereas Case-2 waters depend more on TSM (S) and CDOM (Y).

1.4. Project description

Rijkswaterstaat would like know the possibilities for using satellite data for monitoring water quality. Sentinel-3 OLCI data products would be suitable for this purpose, but have to be validated first. Therefore the main topic of this master thesis is to explore the possibilities and limitations in using Sentinel-3A OLCI data for monitoring chlorophyll and Total Suspended Matter products in the Dutch North Sea. The chlorophyll and TSM products of OLCI will be compared to in-situ measurements in order to find out their suitability for water quality monitoring.

In the second part of this thesis the water-leaving radiance from OLCI will be compared with AERONET-OC data. This is done because the chlorophyll and TSM products are derived from the water-leaving radiance products. An atmospheric correction is applied to the top of atmosphere (TOA) measurements of the satellite. One of the by-products of the atmospheric correction is the aerosol optical thickness product. To find out if the suitable atmospheric correction has taken place the aerosol optical thickness product will be validated by comparing it to the aerosol optical thickness product of AERONET-OC and MODIS.

The main question and the sub-questions for this research project are described below. The sub-questions are divided into initial questions and elaborate questions. The initial research question ae formulated to gain knowledge on water quality monitoring using remote sensing. Research questions which will be further investigated in this thesis are called the elaborated research questions. In the report these sub-questions will be discussed in the different chapters.

Main question: What are the possibilities and limitations of Sentinel-3A Level-2 reduced resolution data products for monitoring water quality of the Dutch North Sea?

1.4.1. Initial research questions

Part 1: Evaluation of the chlorophyll and TSM product:

- *What is water quality?*
- *What are chlorophyll and TSM and why are those products important?*
- *How are the Sentinel-3 Level-2 chlorophyll, and TSM products created?*
- *What is the precision and accuracy of the in-situ measurements taken by Rijkswaterstaat?*

Phase 2: Verification of the normalised water-leaving reflectance and the aerosol optical thickness:

- *What is normalised water-leaving radiance and why it is important to verify this?*
- *What is aerosol optical thickness and what is its importance?*
- *How is the aerosol optical thickness Sentinel-3A Level-2 data product created?*

1.4.2. Elaborate research questions

Part 1: Evaluation of the chlorophyll and TSM product:

- *What is the precision and accuracy of the Sentinel-3A Level-2 reduced resolution data products?*
- *What is the correlation between the chlorophyll and TSM Level-2 products and the in-situ measurements of chlorophyll and TSM?*
- *What is the spatial variability of the chlorophyll and TSM Sentinel-3A Level-2 reduced resolution data product?*

Phase 2: Verification of the normalised water-leaving reflectance and the aerosol optical thickness:

- *What is the quality of the normalised water-leaving radiance product?*

- *What is the correlation between the aerosol optical thickness Sentinel-3A Level-2 OLCI data product and aerosol optical thickness measured at AERONET-OC?*
- *What is the correlation between the aerosol optical thickness Sentinel-3A Level-2 OLCI data products and the aerosol optical thickness product of MODIS?*
- *What is the spatial variability of Sentinel-3A's Level-2 reduced resolution OLCI aerosol optical thickness data product?*

1.5. Thesis overview

This thesis contains 7 chapters. Chapter 2 gives insight in the (previous) existing water quality measuring methods and in what range chlorophyll and TSM values are expected. Chapter 3 explains how Sentinel-3 OLCI Level-2 products are derived. Furthermore it gives a brief introduction to AERONET-OC and MODIS. Chapter 4 describes the methodology followed in this research project. Chapter 5 gives the results of the comparisons done between the different measurement techniques. These findings will be discussed in Chapter 6. The final conclusions and further research recommendations are described in Chapter 7.

2

Monitoring Water Quality

The aim of this graduation project is to validate Sentinel-3A data products. These data products can complement Rijkswaterstaat's monitoring of the Dutch North Sea once they are validated. In this chapter, the water quality parameters used in the validation will be described together with their measuring procedures. Furthermore, the climatologies of chlorophyll and TSM will be discussed in order to know what values are expected in this research.

2.1. Water quality parameters

In this research water quality parameters chlorophyll (Chl) and total suspended matter (TSM) will be compared. The chlorophyll and TSM in-situ measurements are taken with a sampler as will be shown in this chapter. The chlorophyll and TSM data products from Sentinel are obtained at top of atmosphere. These two parameters will be described together with their measuring methods.

2.1.1. Chlorophyll

Chlorophyll is responsible for the absorption of light to provide energy for photosynthesis. Chlorophyll is the green pigment of plants and algae. Photosynthesis is the process in which chlorophyll transforms carbon dioxide, water, and certain inorganic salts into energy. Satellites can observe the presence of plants and algae in the sea because of the distinctive chlorophyll absorption spectrum in the visible part of the electromagnetic spectrum. Figure 2.1 shows the absorption spectrum of chlorophyll-a, which is used in this research project. As can be seen in the figure, chlorophyll-a absorbs energy at wavelengths of the blue-violet and orange-red part of the spectrum. Chlorophyll-b absorbs energy from in the blue-green part of the spectrum. The absorption spectrum of carotenoids is shown as well. Carotenoids are pigments in plants which cause an orange or yellow colour, but are not studied in this thesis.

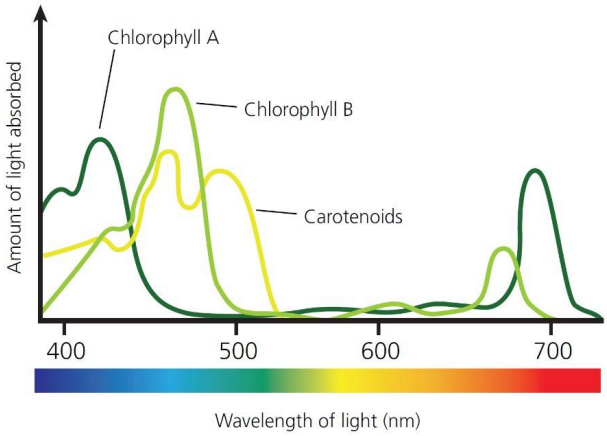

Figure 2.1: The absorption spectra of extracted chlorophyll and carotenoids. Chlorophyll-a and chlorophyll-b absorb most of the light in the blue and red part of the spectrum ([30]). Carotenoids are not used in this research.

2.1.2. Total Suspended Matter (TSM)

TSM stands for total suspended matter which are matter suspended in ocean waters particularly in coastal waters. TSM causes scattering and absorption in the blue-green spectral part of the spectrum. This causes less light to penetrate the water and to be absorbed by chlorophyll. It is difficult to distinguish between TSM and Chl in these waters because they absorb also in the same part of the spectrum [7]. TSM can also transport chemicals into the water which can change the water quality as well.

2.2. Existing measurement techniques

Chlorophyll and TSM are measured in different ways. In this research, Sentinel-3 OLCI remote sensing data is compared with in-situ measurements of Rijkswaterstaat. The preceder of Sentinel-3 was the ENVISAT satellite. ENVISAT had a similar imaging spectrometer on board called MERIS. MERIS used to monitor Chl and TSM content before OLCI did. In this section the different measurement techniques and MERIS climatologies are discussed.

2.2.1. In-situ measurements of Rijkswaterstaat

RWS created a measurement plan called "Monitoring Waterstaatkundige Toestand des Lands" (MWTL), which describes the measurement locations and the activities to monitor water quality of the Dutch waters. An overview of the measurement locations used in this study is shown in Figure 1.2. Water quality of the North Sea is monitored in bi-weekly cruises during summers and monthly cruises during winters. For this project Rijkswaterstaat has taken extra measurements at time of satellite overpass. These extra measurements will be referred to as ADHOC measurements.

At the measurement locations a sampler is let into the water and takes water samples at different depths. These samples are analysed in the lab and results are stored. Another instrument called "Meetvis" is let into the water and measures continuously between the MWTL locations at an approximate depth of 3 m. A picture of the sampler and meetvis is shown in Figure 2.2 and Figure 2.3 respectively. In this research the sampled data at a depth of 3.5 m will be used only. The TSM concentrations are determined during the cruise. Water samples are filtered. The filtrate is then dried and weighted. This filtrate is considered as TSM. The chlorophyll content is determined in a laboratory. The water samples are stored in a cool-box and transported to a lab where they get examined. The derived Chl and TSM results will be compared with OLCI Level-2 Chl and TSM products.

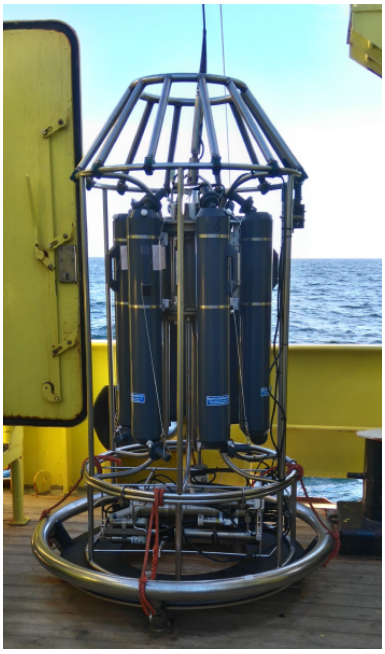

Figure 2.2: Picture of the sampler. The bottles are filled with water and closed at different depths to get samples of the whole water column. From these water samples the chlorophyll and TSM content are determined.

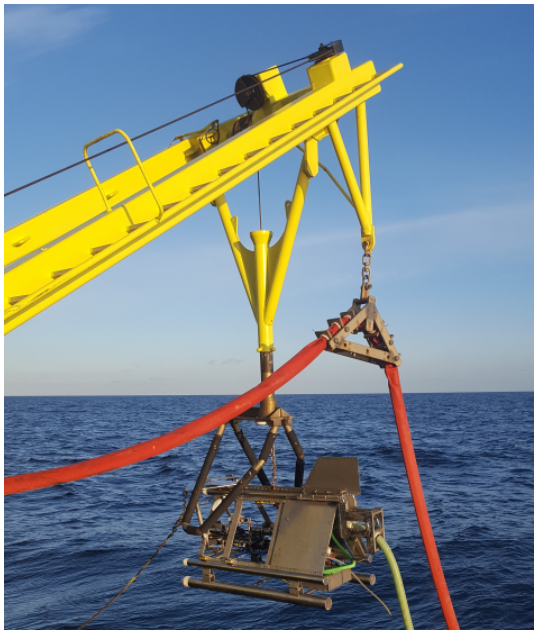

Figure 2.3: Picture of the meetvis. The meetvis is let into the water and measures continuously water quality parameters. In this research the measurements of the meetvis are not taken into account.

2.2.2. ENVISAT MERIS

MERIS stands for MEdium-spectral Resolution Imaging Spectrometer and preceded the OLCI instrument and monitored the Earth between 30 April 2002 and 8 April 2012. MERIS was one of the instruments on board of the ENVISAT satellite. The chlorophyll and TSM data products of MERIS have been used in many research projects and have been proved to be good estimators of chlorophyll and TSM content especially over open ocean areas [17, 43, 49]. Therefore MERIS climatologies can be used in this research to see whether or not OLCI's chlorophyll and TSM values fall in the same range as MERIS chlorophyll and TSM products keeping in

mind the time difference between the two instruments.

MERIS was primary designed for ocean colour purposes and had 15 distinct spectral bands in the visible and near-infra-red part of the spectrum (390 nm to 1040 nm). Its spatial resolution for ocean products was 1040m x 1200 m. MERIS was designed to acquire data over the Earth whenever illumination conditions were suitable. The instrument's 68.5° field of view around nadir covered a swath width of 1150 km. In Figure 2.4 the bands of MERIS are shown with respect to a reflectance curve made with a hand-held radiometer [50]. MERIS preceded OLCI and therefore OLCI has the same measuring bands as MERIS plus 6 extra bands at 400nm, 673.75 nm, 764.375 nm, 767.5 nm, 940 nm and 1020 nm. Some of those extra bands are indicated with black boxes in the figure.

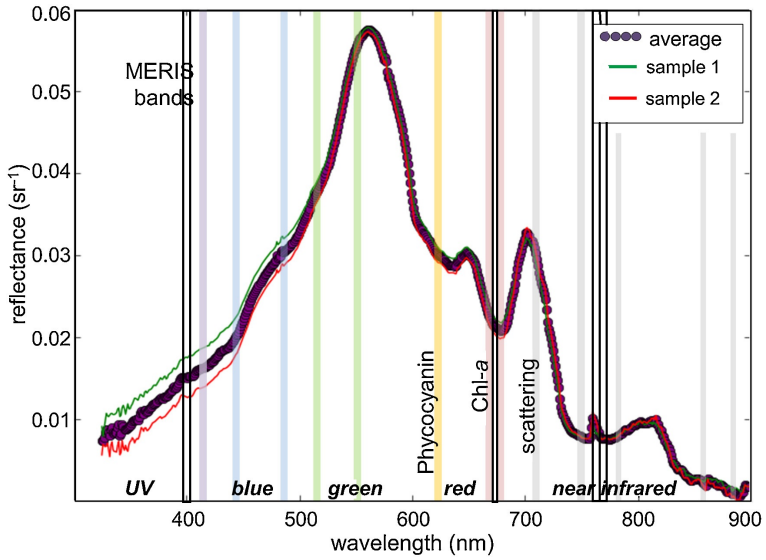

Figure 2.4: Example remote sensing reflectance compared to wavelength obtained by hand-held radiometer. The coloured bands represent the MERIS spectral bands. The black boxes indicate the extra OLCI bands. One of the chlorophyll absorption peaks is indicated as well as one scattering reflection peak occurring due to sediments[50].

MERIS Algal-1 OC4Me

MERIS has two chlorophyll products which will be compared with OLCI's chlorophyll products. The first one is called Algal-1 and is derived by the direct relationship between the maximum band ratio of the blue and green band water-leaving reflectances and the concentration of chlorophyll [22]. This algorithm is called the OC4Me algorithm. The equation for the OC4Me algorithm is the following [38]:

$$\begin{aligned} log_{10}[Chl] &= \sum_{x=0}^{4} (A_x * (log_{10}(R_j^i))^x) \\ R_j^i &= \frac{\rho(\lambda i)}{\rho(\lambda j)} \end{aligned} \tag{2.1}$$

The ratio of the reflectances of band i, among 443, 490, and 510 nm, over that of band j at 560nm are compared with each other and the maximum ratio is used to derive the Chl concentration. The A_i values are 5 coefficients, 0.4502748, -3.259491, 3.522731, -3.359422, and 0.949586 [38].

MERIS Neural Network

The second chlorophyll product of MERIS is called Algal-2. This product is derived by inverting a model of optical properties of the ocean by the use of a neural network [23]. From the same neural network the total suspended matter (TSM) product of MERIS is obtained. An overview of the neural network is given in Figure 2.5 [16]. This figure is divided in two parts, the preparation part and the operation part. In the preparation part the training of the neural network is visualised. Atmospheric parameters, water constituents and angles are implemented as input of the neural network. The atmospheric parameters include an atmosphere divided into 50 layers containing ozone absorption and scattering and absorption by three different aerosols.

The water constituents are chlorophyll, TSM and gelbstoff. Gelbstoff is also known as CDOM and is dissolved organic matter. Gelbstoff is not used in this study but is used as training input of the neural network. The angles describe the zenith angle of the observation angle, the observation azimuth relative to the sun azimuth, and the solar zenith angle. These three input parameters are used to obtain water-leaving reflectances corrected for atmospheric effects using a Monte Carlo simulation. These derived water-leaving reflectances are split up in two parts. One part is used as test variables to train the neural network, the other part is used in the operation part of the neural network.

The actual operation part of the picture shows the retrieval of chlorophyll, TSM, and gelbstoff from the observed water-leaving reflectances. Together with ancillary data such as wind speed, navigation data and water depth reflectances at 8 different bands are used. The water-leaving reflectances are corrected for the atmospheric effects using an atmospheric correction. These atmosphere corrected water-leaving reflectances are then compared to the trained water-leaving reflectances in the "global subroutine". At this point it is also possible to implement a regional subroutine in order to take regional effects into account. In the subroutines the water constituents chlorophyll, TSM and gelbstoff are obtained. An overview of the input and output parameters of the operational part is given in Figure 2.6.

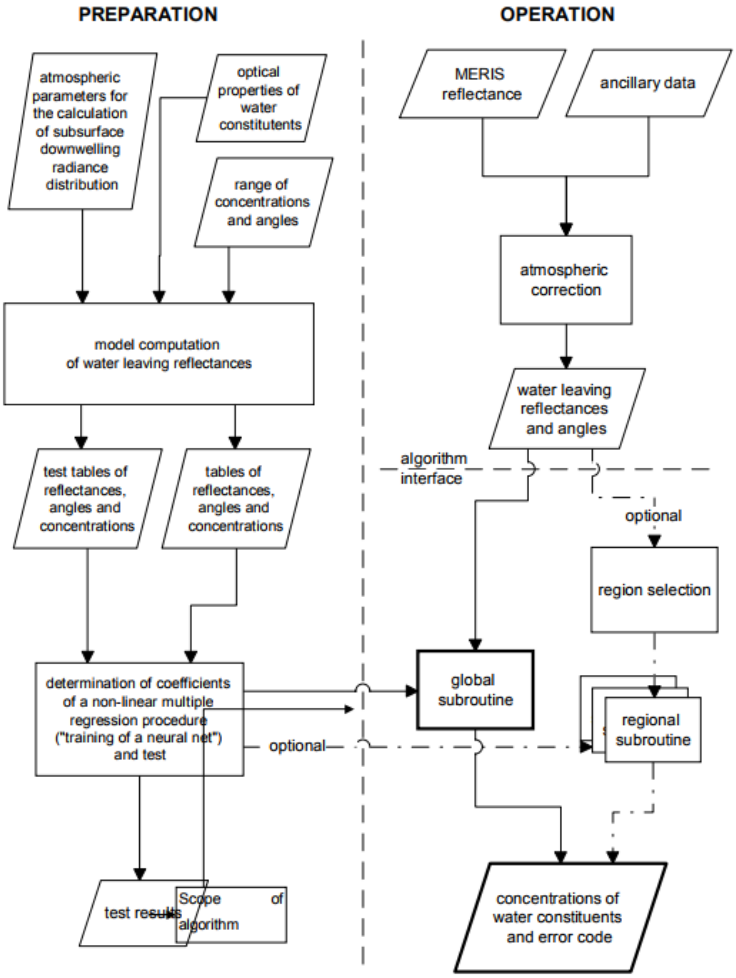

Figure 2.5: Scheme of the neural network. On the left side the training of the neural network is visualised, the right side shows the operational part from which the water constituents are determined. The scheme includes the option of different training sets for different coastal regions [16].

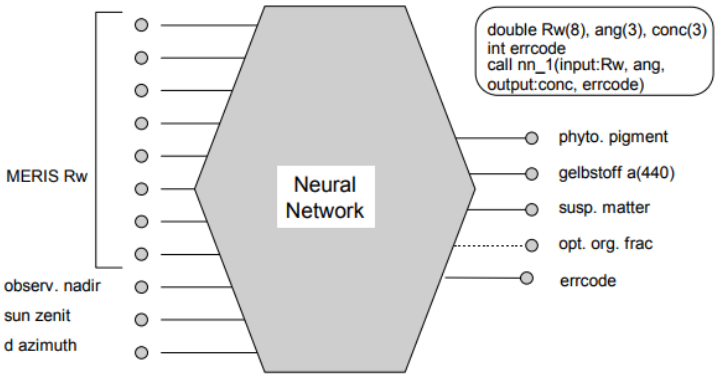

Figure 2.6: Overview of the input and output parameters of the operational part of the neural network [16].

2.3. Chlorophyll climatologies

In order to gain knowledge on the range of chlorophyll values MERIS climatologies and maps will be discussed in this section of the report. The REVAMP atlas contains maps of chlorophyll concentrations based on MERIS data for the North Sea area for 2003 [45]. Monthly, seasonal and yearly maximums and medians are used to present the chlorophyll concentration for the year of 2003.

In Figure 2.7 the seasonal medians are presented from the REVAMP atlas [45]. All of the 3 panels show that chlorophyll values along the Dutch coasts are higher than in open waters approximately 30 km from the coast. The values range between 10 mg/m^3 to 30 mg/m^3 in this area. Another interesting pattern observed in the 3 panels is the higher values of chlorophyll concentrations approximately 100 km from the coast indicated with a black circle. These high chlorophyll values probably originate from the blooms in the Thames estuary and English coast from where these flow North-eastward onto the Dutch continental shelf [45].

Temporal variations are be observed in these maps as well. Higher values of chlorophyll are observed during the spring months. Then during the summer months the chlorophyll content decreases rapidly and starts to increase in autumn again. This temporal variation is caused by variations in solar irradiance. During spring time high nutrient concentrations cause a bloom of algae during the spring months with a peak in April [45]. During the summer months turbulence of the water is very low and increasing solar irradiance heats up water which causes stratification, layering of the water column, to occur. Chlorophyll sinks to a lower water layer and leaves the water surface layer with not much chlorophyll. Satellites can penetrate water for a few meters only and therefore not much chlorophyll is detected during summer months. During autumn solar irradiance decreases and wind causes an increase of water turbulence again. The chlorophyll particles are driven to the water surface again and an increase in chlorophyll is observed during the autumn months. Due to clouds not much data is available for the winter months and is therefore left out. The atlas also does not take these months into account.

For the years after 2003 monthly median maps were created to see if the same pattern occurred in other years. These monthly maps are shown in Appendix A. The spatial and temporal patterns are very similar. Higher values on the coasts and lower values in open waters with a spring bloom. The peak of the spring bloom varies per year but mostly occurring in April. The higher chlorophyll values originating from the Thames outlet are also visible especially in the spring months.

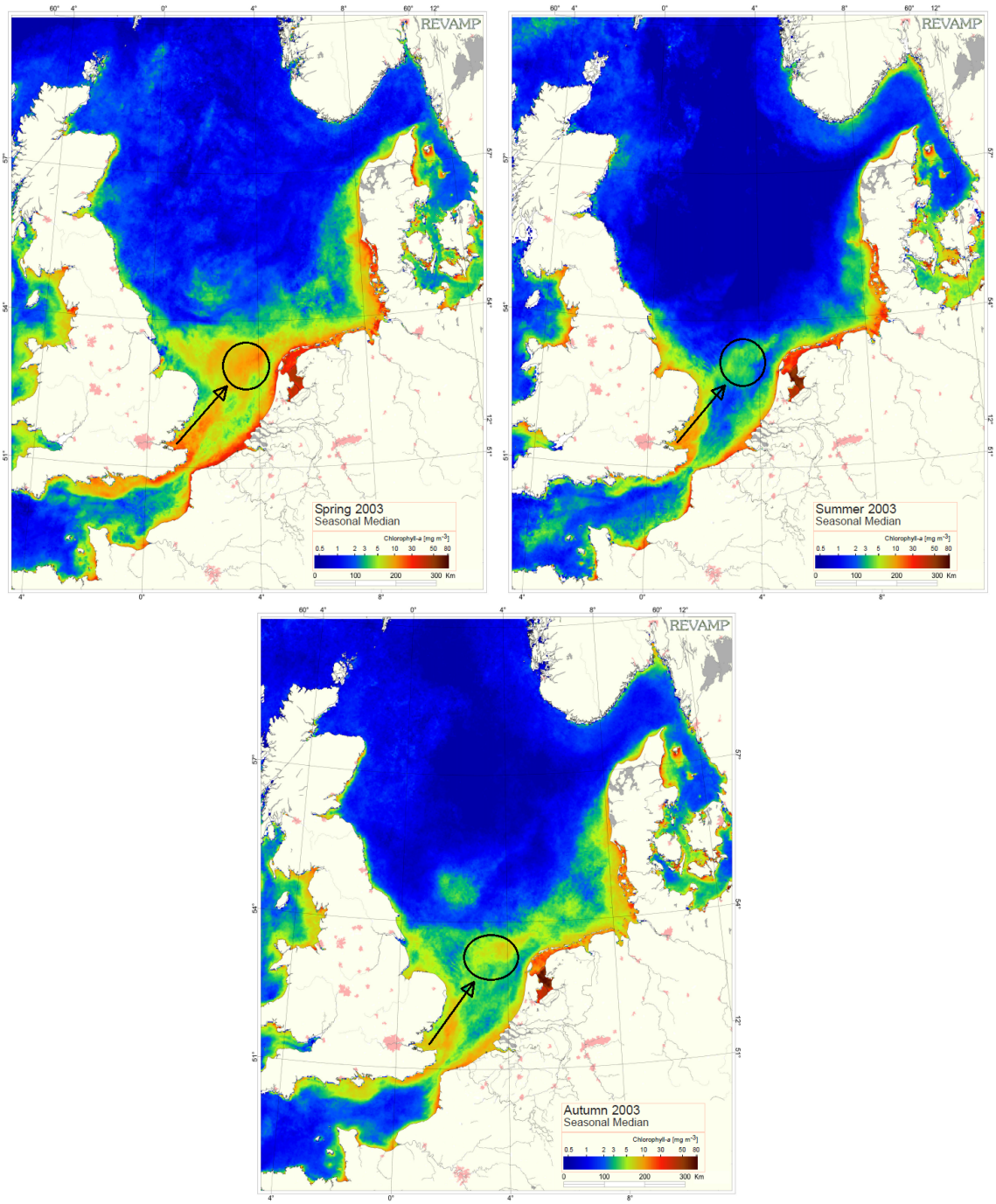

Figure 2.7: Seasonal median chlorophyll values for the North Sea[45]. The top left panel represents the median of the spring months from 15 February - 15 May 2013. the top right panel represents the median of the summer months ranging from 15 May - 15 August 2013. The lower panel represents the median chlorophyll values of the autumn months ranging from 15 August - 15 November 2003 [45]. The circle indicates the higher chlorophyll values originating from blooms in the Thames and the English coast.

2.4. TSM climatologies

To understand the spatial and temporal variabilities in TSM values climatologies and maps are discussed in this section. Unfortunately, there is a lot less data available of TSM observations than of chlorophyll observations. A TSM concentration atlas based on satellite images of 2001 was created by Rijkswaterstaat in 2002 [44]. The satellite data used in this atlas originates from the SeaWIFS. SeaWIFS was a spectrometer on board of the SeaStar satellite developed by NASA. This sensor was particularly developed to monitor ocean surface radiance [27]. One of the products is the TSM product of SeaWIFS. In the atlas 2-monthly average maps are created which are presented in Figure 2.8.

As is shown in the maps the wind is very important for the TSM concentrations. A graph on the right sides of the maps indicates what the wind speed was for the period of the map. In all for the maps a spatial pattern similar to that of chlorophyll is observed. In coastal areas especially near river outlets the TSM concentrations are higher than in the open ocean waters. The TSM maps also show the plume which was observed in the chlorophyll maps originating from the English coast and Thames river discharge. Values in this area are higher than in other areas. Especially in the maps of March-April and September-October this is observed.

Also the temporal pattern of TSM is similar to that of chlorophyll. High concentrations appear in spring and autumn time. During the summer months the TSM values decrease rapidly. This increase in TSM concentrations during spring and autumn time is very dependent on the wind speed. In those months wind speeds are on average higher than in the summer months and cause turbulence of the water [44]. This turbulence drives the TSM to the surface by which it can be observed by satellites.

Overall we can say that the spatial and temporal patterns of TSM are similar to those of chlorophyll. Wind is a major factor in the transport of TSM. TSM values range between less than 5 g/m^3 in off-shore water to >28 g/m^3 in coastal waters.

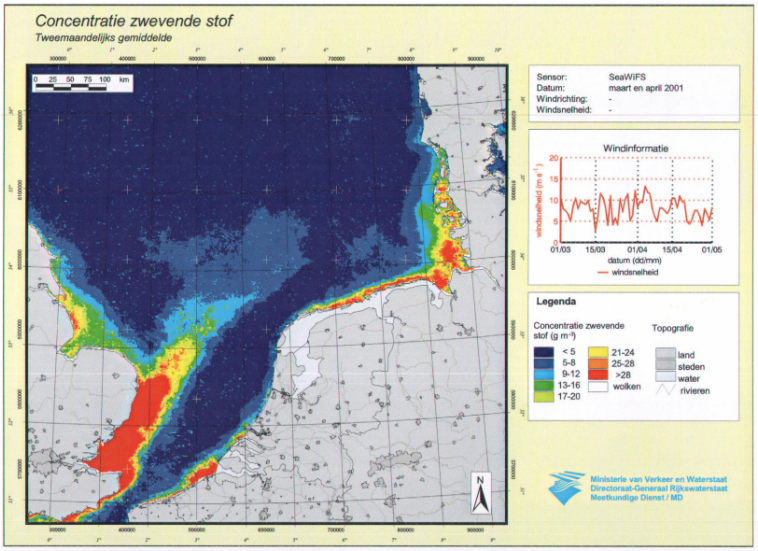

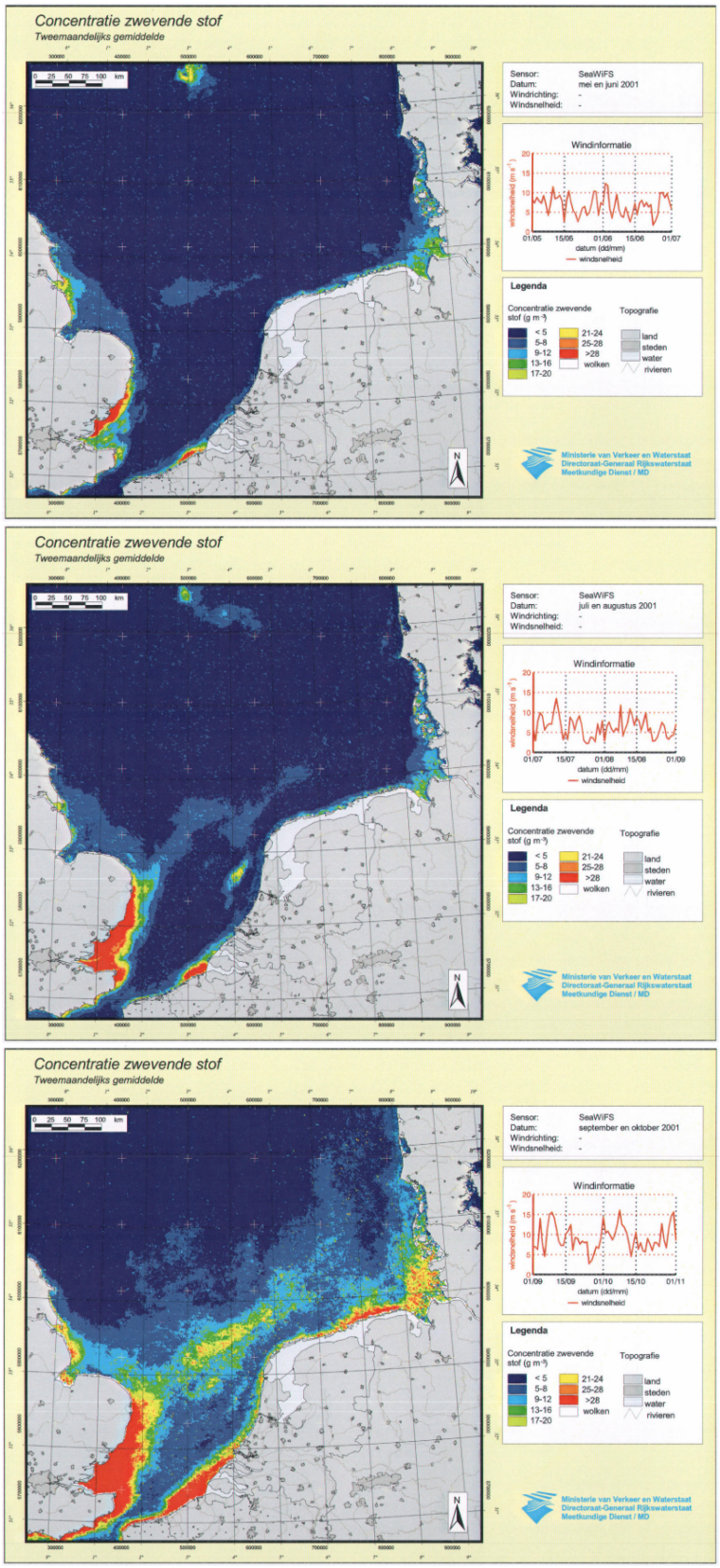

Figure 2.8: Mean TSM values for 2 monthly periods in 2001. The first image represents the mean TSM for the months March and April, the second image for May and June, followed for an image based on July and August. The last image represents September and October. The data originates from the SeaWIFS satellite instrument [44].

2.5. Conclusions

This chapter discussed the different measurement techniques used to observe chlorophyll and TSM concentrations in the North Sea. The in-situ measurements were discussed together with MERIS chlorophyll and TSM data products. Furthermore we looked at the spatial and temporal variability of chlorophyll and TSM. The conclusion of this chapter are answers to some of the sub-questions and will be presented here.

- The term water quality was explained as the suitability of water for a particular purpose. In this thesis we will particularly look at the North Sea and therefore water quality can be seen as the status of North Sea ecosystem. When major changes occur certain types of flora and fauna can become extinct.
- In this research chlorophyll and TSM are two particular parameters to be looked at. Chlorophyll is the pigment of phytoplankton which are micro algae. A change in chlorophyll means a change in algae which means a changes in water quality. Also TSM is an important parameter since a change in TSM causes a change in solar irradiance to penetrate the water and less light for chlorophyll to perform photosynthesis.
- MERIS preceded OLCI and therefore it has similar products to those of OLCI. MERIS contains two chlorophyll products, a OC4Me product and a neural network product. It has only one TSM product based on a neural network.
- MERIS climatologies and maps gave insight in the spatial and temporal variability of chlorophyll and TSM. Along the coasts and during spring and autumn chlorophyll values are high when they range between 10 mg/m^3 and 30 mg/m^3. The chlorophyll originating from the Thames discharge was another interesting pattern to observe. The TSM values where observed to be very high in the coastal areas but very soon became close to 0 in the off-shore waters. It also seemed that wind, river discharge and tide played an important role in the spatial variability.
- SeaWIFS climatology maps gave insight in the TSM concentrations in the Dutch North Sea. Similar spatial and temporal patterns were found for TSM as for chlorophyll concentrations. Values of TSM can range between less than 5 g/m^3 in off-shore water to >28 g/m^3 in coastal waters. The wind is an important factor in the transport of TSM. During spring and autumn months these winds are stronger which cause higher TSM values for these periods.
- The main difference found between in-situ measurements and remote sensing measurements was the depth at which the parameters were observed. The in-situ measurements are taken underwater while the remote sensing chlorophyll and TSM data products are derived from water-leaving reflectances measured at top of atmosphere (TOA).

3

Sentinel-3 satellite mission

The Sentinel-3 satellite mission will consist of a pair of identical satellites. Sentinel-3A was launched on 16 February 2016 and Sentinel-3B will follow in 2018 [21]. These satellites will orbit in constellation for optimal global coverage and data delivery. This chapter explains the Sentinel-3 satellite in more detail. Furthermore a brief overview of the satellite products will be given and how they are obtained.

3.1. Ocean Colour Land Instrument (OLCI)

The Sentinel-3 satellites have an Ocean Land Colour Instrument (OLCI) on board which is a spectrometer with five cameras. The OLCI instrument is the successor to ENVISAT's Medium Resolution Imaging Spectrometer (MERIS) having additional spectral channels.

The spectrometer measures reflectance from Earth in 21 bands. The 21 distinct bands are in the 400 nm - 1020 nm spectral region chosen to specifically measure ocean colour and atmospheric parameters. An overview of those bands is given in Table 3.1.

The swath width of the Ocean and Land Colour Instrument (OLCI) is 1270 km. The Earth's perimeter at 52° is approximately $6371 * cos(52°) \approx 24500$ km which means that the North Sea is fully covered within 24500/1270 = 19 cycles. The duration of 1 cycle is approximately 100 minutes, thus the Dutch coastal area should be covered within 2 days ([21]). These specifications are visualised in Figure 3.1. The full spatial resolution of the OLCI is approximately 300 m x 300 m. But the reduced resolution data products , which are used in this research, are converted to a 1.1 km x 1.1 km grid.

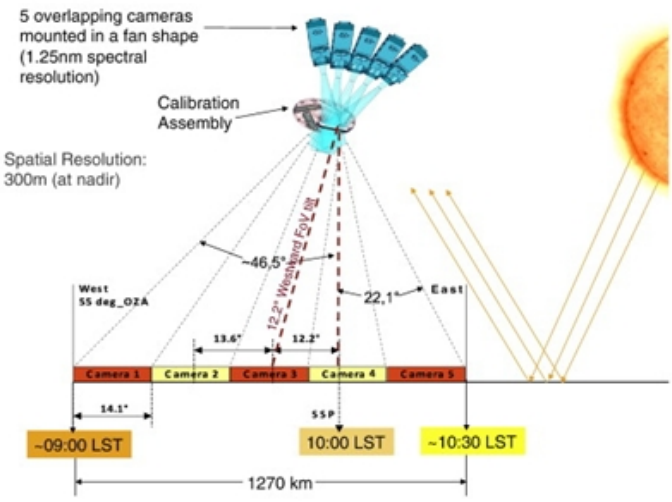

Figure 3.1: Geometry of the OLCI instrument with its coverage. The 5 cameras viewing the Earth have a swath width of 1270 km. The observation zenith angle is 55°. The local solar time (LST) is indicated at the bottom of the Figure [21]).

Table 3.1: OLCI measurement bands with details, in cyan MERIS heritage bands, in yellow additional bands [18]. The 8th column gives the function of each band.

Band	λ centre nm	Width nm	Function
Oa1	400	15	Aerosol correction, improved water constituent retrieval
Oa2	412.5	10	Yellow substance and detrital pigments (Turbidity).
Oa3	442.5	10	Chl absorption max., Biogeochemistry, vegetation
Oa4	442	10	High Chl, other pigments
Oa5	510	10	Chl, sediment, turbidity, red tide.
Oa6	560	10	Chlorophyll reference (Chl minimum)
Oa7	620	10	Sediment loading
Oa8	665	10	Chl (2nd Chl abs. max.), sediment, yellow substance/vegetation
Oa9	673.75	7.5	For improved fluorescence retrieval and to better account for smile together with the bands 665 and 680 nm
Oa10	681.25	7.5	Chl fluorescence peak, red edge
Oa11	708.75	10	Chl fluorescence baseline, red edge transition.
Oa12	753.75	7.5	O2 absorption/clouds, vegetation
Oa13	761.25	2.5	O2 absorption band/aerosol corr.
Oa14	764.375	3.75	Atmospheric correction
Oa15	767.5	2.5	O2A used for cloud top pressure, fluorescence over land.
Oa16	778.75	15	Atmos. corr./aerosol corr.
Oa17	865	20	Atmos. corr./aerosol corr., clouds, pixel co-registration.
Oa18	885	10	Water vapour absorption reference band. Common reference band with SLST instrument. Vegetation monitoring.
Oa19	900	10	Water vapour absorption/vegetation monitoring (max. reflectance)
Oa20	940	20	Water vapour absorption, atmos./aerosol corr.
Oa21	1020	40	Atmos./aerosol corr.

Ocean colour instruments are designed to derive the up-welling radiance just above the water surface. This is called the water-leaving radiance. The chlorophyll (Chl) and total suspended matter (TSM) content can be derived from the water-leaving radiance through bio-optical algorithms like the OC4Me algorithm (section 2.2.2). An atmospheric correction is applied to the radiances observed by the satellite in order to get a reliable water-leaving radiance product. This is challenging since only 10% of the radiation measured originates from the water surface.

3.1.1. Atmospheric influence

The total radiance (L_t^{TOA}) measured at the top of atmosphere (TOA) by the satellite has different origins. Atmospheric radiance (L_{atm}^{TOA}), reflectance from the sea surface (L_{surf}^{TOA}), and water-leaving radiance (L_w^{TOA}) all contribute to the total radiance. This is shown in Figure **??**.

The atmospheric radiance originates from scattering by atmospheric gases and aerosols. Scattering from gases is called Rayleigh radiance (L_R). Rayleigh radiance is defined as the mathematical model of scattering by particles which are smaller than the wavelength of the light [36]. If there were no aerosols in the atmosphere, the atmospheric radiance would be equal to the Rayleigh radiance. The aerosol contribution to the atmospheric radiance is denoted as (L_a). Last, the radiance occurring between aerosols and gases is denoted as (L_{aR}).

The radiance originating from the reflectance of the sea surface can be divided into Sun glint (L_g^{TOA}); background sky radiance reflected by the surface (L_{sky}^{TOA}); and by Sun and sky radiance reflected by whitecaps and foam (L_{wc}^{TOA}). Whitecaps and foam are particles on the sea surface causing extensive scattering. When filling in all those variables, the equation for the total radiance at top of atmosphere(TOA) becomes:

$$L_t = L_R + [L_a + L_{aR}] + L_g^{TOA} + L_{sky}^{TOA} + L_{wc}^{TOA} + L_w^{TOA} \tag{3.1}$$

Equation 3.1 is the equation considering TOA measured radiances. It can be rewritten to obtain radiances just above the water surface also known as water-leaving radiance. Equation 3.1 then becomes:

$$L_t = L_R + [L_a + L_{aR}] + TL_g + tL_{wc} + tL_w \tag{3.2}$$

L_w, L_{wc}, and L_g are converted to values measured at sea level. T is the direct transmittance between the sea surface and the TOA along the viewing direction, t is the diffuse transmittance in the viewing direction of the satellite.

Figure 3.3 shows all the contributions to total radiance measured at the top of atmosphere. The symbols correspond to the variables mentioned before. L_u represents the water-leaving radiance in upward direction, the L_{gs} and L_{gs2} are the sun glints in different directions. Figure 3.3 shows the fraction of contribution for some of the processes. The colours correspond to the colours used in Figure 3.2. This figure shows that the water-leaving radiance contributes at most 10% of the measured TOA radiance. The atmospheric path radiance contributes for 70 to 90% of the L_t. Figure 3.3 is modelled under circumstances that are not realistic for the Dutch part of the North Sea but shows the basic concept of signal loss because of atmospheric influences.

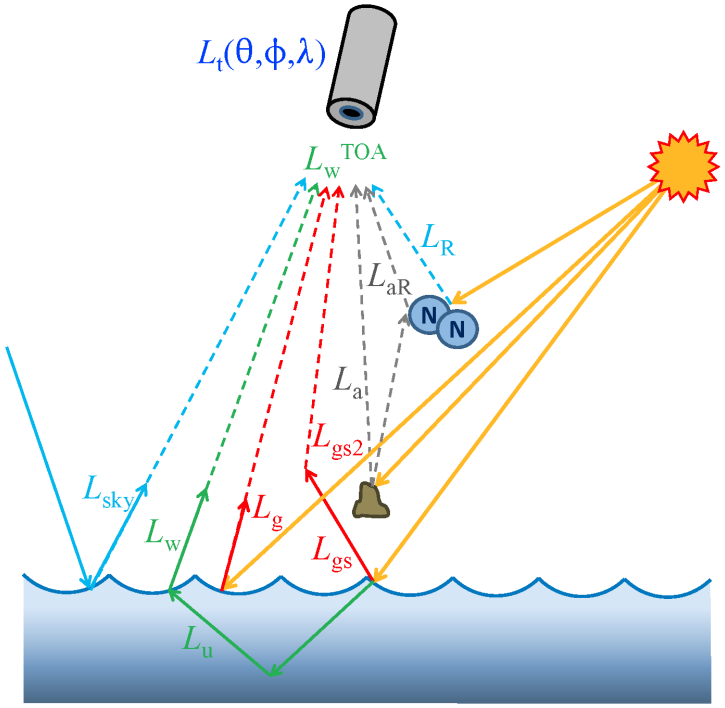

Figure 3.2: Various contributions to the measured TOA radiance. The blue N-N symbols represent NO_2 or any other atmospheric gas molecule, the brown blob represents an aerosol particle [36]

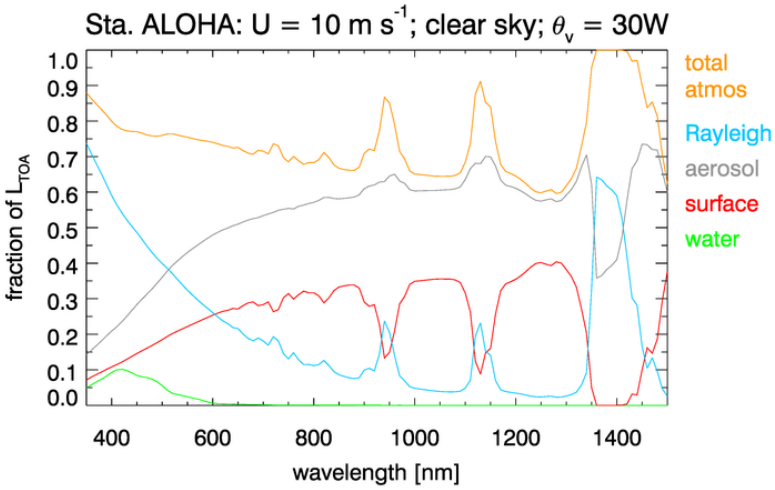

Figure 3.3: Fractional contribution of the various processes to the total measured TOA radiance. The figure shows radiances for clear sky conditions, which means no clouds, a viewing angle of 30^o, and a wind speed of 10 m/s. The results were obtained for station ALOHA (A Long-term Oligotrophic Habitat Assessment) located north of the island of Oahu, Hawaii [36]. For the Netherlands these conditions are not realistic but this picture shows the basic concept of the influence of the atmosphere on the measured radiance by the satellite.

Chlorophyll and TSM satellite data products are derived from the water-leaving radiance measured by the satellite after atmospheric correction has been applied. Therefore the quality of the water-leaving radiance product has to be know as well. The quality of the water-leaving radiance product will be investigated by comparing it with the water-leaving radiance product of AERONET-OC. The atmospheric correction is

very important in the derivation of the water-leaving reflectance since it contributes for 70 to 90% to the total radiance measured by the satellite. This atmospheric correction will also be validated by comparing the aerosol optical thickness by-product of Sentinel-3 with the aerosol optical thickness products of AERONET-OC and MODIS. AERONET-OC is a radiometer measuring water-leaving radiance directly and aerosol optical thickness at the ground-level just above the water surface. MODIS is another imaging spectroradiometer on board of the AQUA satellite developed by NASA. AERONET-OC and MODIS are discussed in more detail in paragraph 3.7. The processing chain to derive chlorophyll and TSM through the water-leaving radiance after atmospheric correction is applied is briefly discussed in the next paragraph.

3.2. Processing steps OLCI

In this section a summary is given of the available OLCI data products and their process to obtaining those. There are three main products types distributed to OLCI product users.

1. The Level-1B product, provides radiances for each pixel in the instrument grid. Level-1 data products can be seen as the measured top of atmosphere radiances.
2. The Level-2 land product, provides land and atmospheric geophysical parameters. These products are obtained after atmospheric correction.
3. The Level-2 water product, provides water and atmospheric geophysical parameters. Also these products are obtained after atmospheric correction.

In this research the Level-2 water products will be used. OLCI's Level-2 water product contains many products such as the chlorophyll and TSM content. An overview of those products is given in Table 3.2.

Table 3.2: Overview of OLCI L2 water products

Variables	Description	Units	Input Bands
Rxxx	Surface directional reflectance, corrected for atmosphere and sun specular reflection.	dimensionless	all except Oa13, Oa14, Oa15, Oa19 and Oa20
CHL_OC4ME and CHL_NN	Chlorophyll-a concentration, computed using "OC4Me" or Neural Network algorithms.	mg (Chl a) m-3	- Oa3 and Oa6- Oa1-Oa12, Oa16, Oa17 and Oa21
TSM_NN	Total suspended matter concentration.	g.m-3	Oa1-Oa12, Oa16, Oa17 and Oa21
KD490_M07	Diffuse attenuation coefficient for down-welling irradiance, at 490 nm.	m-1	Oa4 and Oa6
ADG_443_NN	Absorption of coloured detrital and dissolved material at 443 nm.	m-1	Oa1, Oa12, Oa16, Oa17, Oa21
PAR	Quantum energy flux from the sun in the spectral range 400-700 nm.	µEinstein.m-2. s-1	-
T865 and A865	Aerosol load, expressed in optical depth at a given wavelength (865 nm) and spectral dependency of the aerosol optical depth, between 779 and 865 nm.	dimensionless	Oa5, Oa16 and Oa17
IWV	Integrated Water Vapour column	kg.m-2	Oa18, Oa19

In this research we will be mainly interested in the OLCI Level-2 water quality products (CHL_oc4me, CHL_NN, and TSM_NN) , the water-leaving reflectances (Rxxx), and the aerosol optical thickness product (T865). Various steps are taken to arrive at the final data products including some atmospheric corrections. In the following paragraphs these steps are discussed in more detail. An overview of the processing steps is given in Figure 3.4.

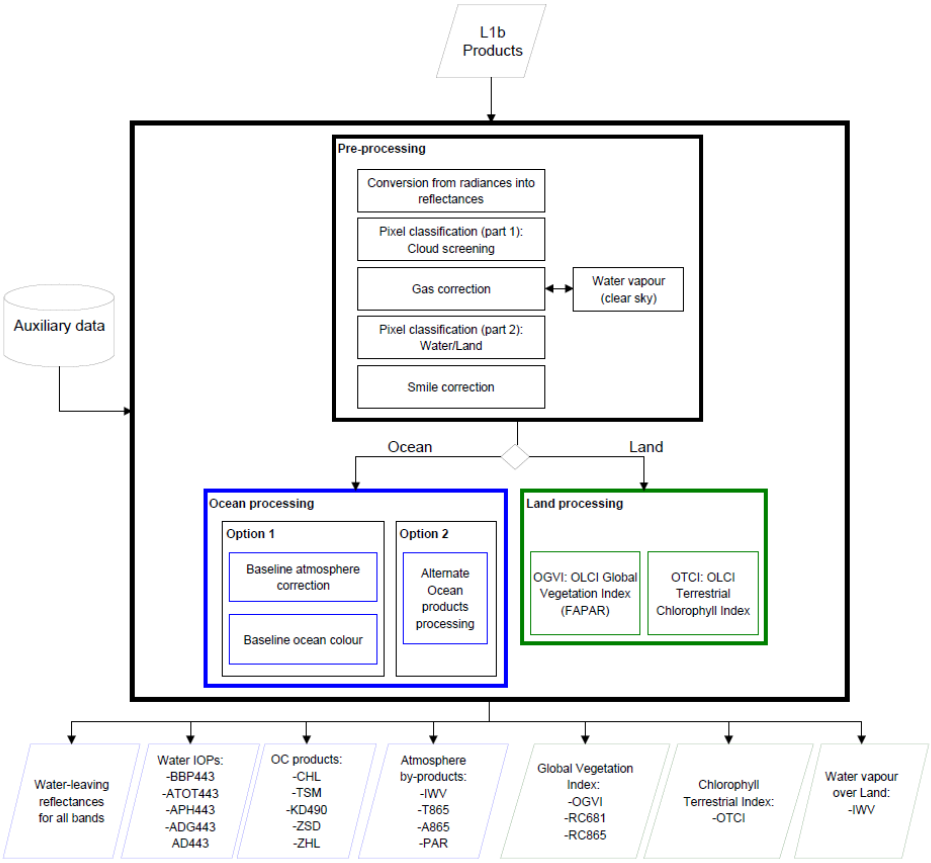

Figure 3.4: Overview of the applied processing steps to get from OLCI Level-1B to the Level-2 data products ([20]).

From the Level-1B data products, which are Top Of Atmosphere (TOA), several processing steps are taken to derive the Level-2 products. The photons originating from the Sun, make their way towards the Earth's surface by travelling through the atmosphere. In this journey, many processes occur such as absorption, scattering and reflection. The magnitude and spectral dependence of the solar radiation reaching the Earth is a function of the solar zenith angle and atmospheric conditions [36].

Three atmospheric corrections (AC) are applied to the Level-1B data products in order to obtain the Level-2 water-leaving reflectance products. These ACs should be verified in order to see if the suitable atmospheric correction has been applied. One of the by products of the atmospheric correction is the aerosol optical thickness (AOT) product. Therefore the AC will verified with the AOT product.

3.3. Preprocessing

Several steps are taken in the pre-processing of Level-1 data towards Level-2 data and are also shown in Figure 3.4.

1. Radiance to reflectance conversion. The satellite measures top of atmosphere radiance which are converted to reflectance first.

2. Pixel classification. Pixels are classified as cloud, land, ocean, or invalid. This is done to select which processing steps are taken afterwards. This is different for land and water pixels.

3. Gaseous correction, corrects for gaseous absorption (O_2, H_2O and O_3). This gas correction is a process of finding the right radiative transfer function using the amount of atmospheric gas in the atmosphere. This radiative transfer function is then multiplied with the TOA reflectance to remove the effect of atmospheric gas. The radiative transfer functions originate from the HITRAN2008 database [28].

4. Second pixel classification, estimates glint reflectance and completes pixel classification starting at the second step by consolidating the classification land and water pixels.

5. Smile correction. The smile effect occurs on a line of pixels. OLCI is measuring the TOA radiance using 5 cameras. Each pixel has its own setting to measure this radiance using the 5 cameras. This causes variations in the spectral wavelength called the smile effect.

6. Water vapour retrieval, retrieves atmospheric water vapour content from clear sky pixels.

3.4. Ocean processing atmospheric corrections

The pixels classified as water (ocean) are treated differently than the pixels classified as land, this is also shown in Figure 3.4. The ocean and land pixels have different processing lines after pre-processing has been applied. For the ocean pixels the atmospheric correction starts from here. The ocean atmospheric corrections can be divided into two approaches, the baseline approach and the alternative approach. In the following paragraphs the two approaches will be briefly described.

3.4.1. Baseline approach

The baseline AC removes all non ocean colour top of atmosphere reflectance. This means glint and white caps are corrected for, an estimation of Near Infra-Red (NIR) reflectances is carried out, and an aerosol and Rayleigh correction is applied (paragraph 1.2.1).

The estimation of the NIR reflectance is only applied to coastal turbid (Case-2) waters because it is caused by TSM particles. The TSM causes backscatter in the NIR [37]. This correction is called Bright Water Atmospheric Correction (BWAC). Once BWAC is applied the Clear Water Atmospheric Correction (CWAC) is applied. The CWAC atmospheric correction is meant for oceanic (Case-1) waters. But since the BWAC atmospheric correction is applied first, this CWAC is also applied to Case-2 waters. The principal of the CWAC is to obtain information about the aerosol content due to the radiances measured in the NIR bands. This knowledge can then be interpolated towards the visible domain where the AC is applied [4]. This process is explained in more detail in paragraph 3.5. From the CWAC also the aerosol optical thickness is estimated for pixels having the baseline atmospheric correction.

After the baseline atmospheric correction is applied the chlorophyll is determined through the baseline ocean colour procedure which is explained by the OC4Me algorithm (section 2.1).

3.4.2. Alternative atmospheric correction

The purpose of the alternative atmospheric correction is to improve the atmospheric correction over turbid and highly absorbing Case-2 waters. Furthermore, it improves the AC for areas which are contaminated by Sun glint [15]. This correction is based on the same artificial neural network as the chlorophyll and TSM product are. The neural network of the chlorophyll and TSM data products is described below in paragraph 3.8.2.

3.5. Aerosol Optical Thickness (AOT) & Ångström exponent

The aerosol optical thickness (AOT) and the Ångström exponent are obtained during the CWAC or during the alternative atmospheric correction. The aerosol type and load are estimated from the NIR bands at 779 and 865 nm once contributions from the water at those channels is known. This paragraph describes the procedure to find the AOT and Ångström exponent. According to *Antoine2010* the total reflectance at TOA is estimated from the atmospheric path reflectance and the diffuse transmittance along the pixel to sensor path. Equation 3.3 shows this.

$$\rho_t(\lambda) = \rho_{path}(\lambda) + t_d(\lambda) * \rho_w(\lambda) \tag{3.3}$$

in which $\rho_t(\lambda)$ is the total TOA reflectance observed by OLCI, $\rho_{path}(\lambda)$ is the atmospheric path reflectance, $t_d(\lambda)$ is the diffuse transmittance, and $\rho_w(\lambda)$ is the water-leaving reflectance. Usually the reflectance by aerosols and by Rayleigh scattering are taken separately, but to find the right AOT and Ångström exponent these components are taken together now as $\rho_{path}(\lambda)$. In 1998, *Antoine1998* showed that the ratios $\rho_{path}(\lambda)/\rho_r$ never change and that there are unique functions for the AOT for a given aerosol geometry [3]. In which ρ_r

is the Rayleigh reflectance. These functions allow to find the right aerosol type from predefined models. The Rayleigh (molecular scattering) contribution is determined from tabulated results of radiative transfer computations, corrected for local variations in atmospheric pressure [1, 3]. The following steps explain better how the AOT and Ångström exponent are found [3].

1. The ratio ρ_{path}/ρ_r is formed at 775 and 865 nm in which $\rho_t = \rho_{path}$ because the water-leaving reflectance is 0 in the NIR. ρ_r is the reflectance for an aerosol-free atmosphere, precomputed and stored in look-up tables.
2. Several values of AOT(865) are compatible with the ratio because multiple scattering effects depend on the aerosol type. Each of these values belong to an aerosol model of which the Ångström exponent can be obtained.
3. The several values of AOT(865) are converted into the equivalent set at 775nm, making use of spectral attenuation coefficients of each aerosol.

$$AOT(775) = AOT(865) * \frac{c(775)}{c(865)} \tag{3.4}$$

4. To these AOT(775) values correspond several values of the ratio ρ_{path}/ρ_r at 775nm, which differ according to the aerosol type.
5. Now, comparing these ratios to the actual ratio at 775nm will give the best fitted two aerosol models and thus the best fitting AOT and Ångström exponent.

These steps are also shown in Figure 3.5. The numbers correspond to the arrows.

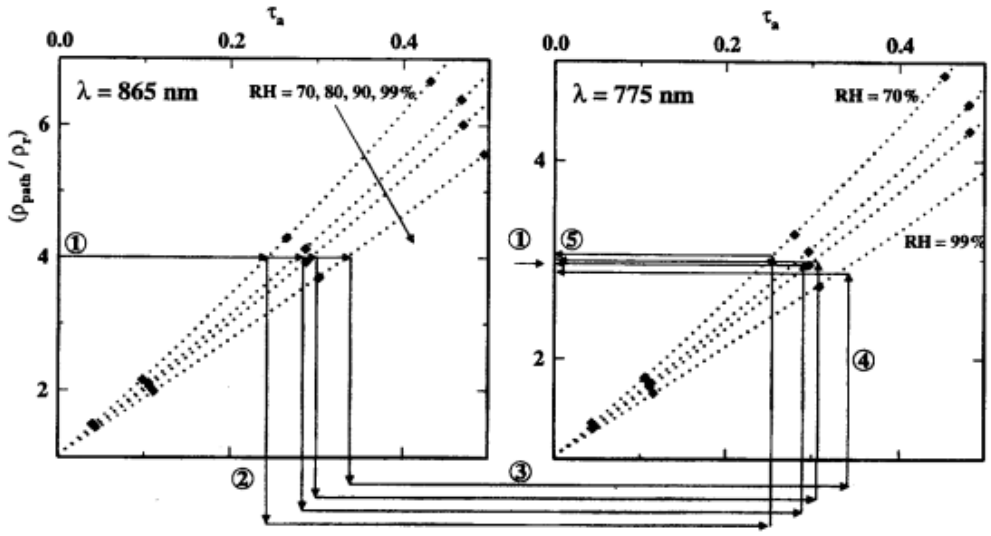

Figure 3.5: Visualisation of the AOT and and Ångström exponent finding process [3]. The dotted lines represent the different aerosol models for different relative humidities.

Since the aerosol optical thickness model is the basis on which atmospheric correction is applied, the AOT product of OLCI was chosen to be researched as well. In order to do so, it will be compared to AERONET-OC station Thornton and MODIS AOT data product. These measuring techniques will be briefly discussed in section 3.7. Due to time limitations the Ångström exponent is not taken into consideration.

3.6. Normalised Water-Leaving Radiance

Once the atmospheric correction is applied, we are left with the water-leaving reflectance. One of the main OLCI Level-2 products is the water-leaving reflectance. It is determined for all the bands except those dedicated to measurement of atmospheric gas (Band 13, 14, 15, 19 and 20). An overview of the OLCI's bands can

be found in Table 3.1. To compare the normalised water-leaving reflectance with normalised water-leaving radiance products, a conversion from reflectance to radiance has to be applied. The following equation is used for this [51].

$$L_w(\lambda)_N = \frac{\rho_w(\lambda)_N}{\pi} * f_0(\lambda) \tag{3.5}$$

in which $L_w(\lambda)_N$ is the normalised water-leaving radiance, $\rho_w(\lambda)_N$ is the normalised water-leaving reflectance, and $f_0(\lambda)$ is the mean solar flux above Earth's atmosphere. The $f_0(\lambda)$ is also provided in the OLCI Level-2 product.

3.7. Monitoring the aerosol optical thickness and normalised water-leaving radiance

The aerosol optical thickness (AOT) has a large influence on the water-leaving radiance from which the water quality products are derived (section 1.2.1). The AOT is a by-product of the atmospheric correction. The AOT of OLCI will be compared with the AOT of AERONET-OC Thornton and of MODIS in order to evaluate the atmospheric correction. AERONET-OC and MODIS will be briefly discussed in this paragraph.

3.7.1. AERONET-OC

The data for the verification of the OLCI AOT data product and water-leaving radiance products come from AERONET-OC station Thornton shown in Figure 3.7. There are two AERONET-OC stations in the Belgian part of the North Sea, Thornton and Zeebrugge. In this research data from the Thornton station is used because data from the Zeebrugge station were unavailable. There is currently no AERONET-OC station in the Dutch North Sea.

AERONET stands for AErosol RObotic NETwork, the OC stands for Ocean Colour. AERONET is managed by the National Aeronautics and Space Administration (NASA). AERONET provides a long-term and continuous data of aerosol optical and radiative properties of the atmosphere. One of the data products retrieved by NASA from the AERONET, is the Aerosol Optical Depth (AOD). The AOD is a measure of the extinction of a solar beam by aerosols. AOD can be used to compute columnar water vapour (Precipitable Water) and estimate the aerosol size. AERONET stations determine the AOD using sun photometers. Sun photometers measure the direct solar radiation [29]. The concept of AERONET-OC is shown in Figure 3.6. AERONET-OC contains two photometers, one to measure the direct irradiance from the Sun and another one to measure the sky radiance and water-leaving radiance.

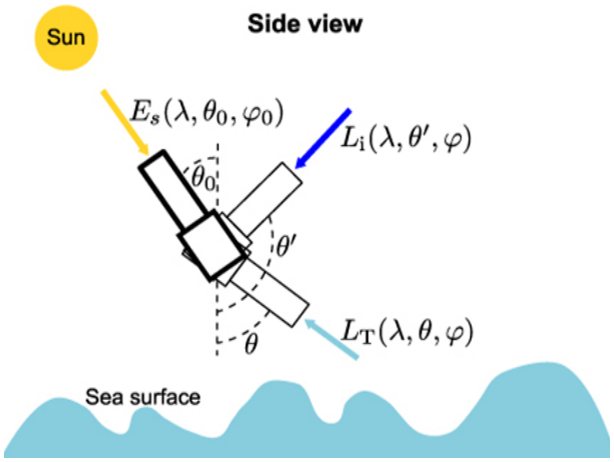

Figure 3.6: Picture of an AERONET-OC station. Two photometers measure the irradiance from the Sun and the radiance just above the water surface (water-leaving radiance) [29].

Figure 3.7: Map of The Netherlands and Belgium with AERONET-OC stations Thornton and Zeebrugge indicated with yellow pins. (Source: 'Netherlands', 51°53'07.65"N and 4°23'30.51"E. Google Earth. 14 December 2015. 29 August 2017.)

Besides the AOD AERONET estimates the normalised water-leaving radiance as well. The normalized water-leaving radiance is determined for all AERONET-OC measurement bands. AERONET-OC's normalised water-leaving radiance will be compared with OLCI's normalised water-leaving radiance (after conversion (3.6)). Since the AERONET-OC bands and the OLCI bands are not exactly the same, only the water-leaving radiance for the overlapping bands will be compared using AERONET-OC data. A table of the comparing bands with their wavelengths is given in Table 3.3. The AOT is determined at all the measurement wavelengths of the instrument, but OLCI only determines the AOT at a wavelength of 865nm. The AERONET-OC AOT estimation at band 869 nm is closest to that of OLCI and will therefore be used for comparison.

Compared AERONET-OC and OLCI bands						
AERONET-OC band wavelengths [nm]	413	441	488	668	869	1020
OLCI band wavelengths [nm]	412.5	442.5	490	665	865	1020

Table 3.3: Matching AERONET-OC and OLCI bands

The biggest difference between OLCI and AERONET-OC is that AERONET-OC is a ground-based station whereas OLCI is the Sentinel-3 satellite. AERONET-OC can therefore directly measure the water-leaving radiance without having to correct the signal for atmospheric effects. Furthermore, the AOT of AERONET is determined directly and is not a by-product of the atmospheric correction as for OLCI. Many studies have been performed using AERONET's AOT measurements to validate satellite AOT products [29, 33]. It is therefore believed to be a good measure for the verification of OLCI's AOT.

3.7.2. AQUA MODIS data

The AERONET-OC station Thornton is located in the Belgian North Sea and therefore might not be suitable for the research area of this thesis. Furthermore, it is a point measurement and can therefore not say much about the spatial distribution of the AOT. To verify OLCI's AOT product for the Dutch North Sea it is compared to MODIS' AOT. MODIS is another imaging spectroradiometer on board of the AQUA and TERRA satellites

developed by NASA. MODIS stands for MODerate resolution Imaging Spectroradiometer [34]. The swath width of MODIS is 2330 km and monitors the entire world in 1 to 2 days. MODIS has 36 spectral bands ranging from 405 nm to 14385 nm and a spatial resolution of 250 m, 500 m, and 1000 m. An overview of MODIS's bands with their purpose is given in Table 3.4. MODIS is an passive remote sensing instrument for the first 19 bands and an active remote sensing instrument for the other bands. The AOT determined at band 2 (841 - 876 nm) is used in this research for comparison with OLCI.

Table 3.4: Overview of MODIS spectral bands [42].

BAND #	RANGE nm	RANGE um	KEY USE
	Reflected	Emitted	
1	620–670		Absolute Land Cover Transformation, Vegetation Chlorophyll
2	841–876		Cloud Amount, Vegetation Land Cover Transformation
3	459–479		Soil/Vegetation Differences
4	545–565		Green Vegetation
5	1230–1250		Leaf/Canopy Differences
6	1628–1652		Snow/Cloud Differences
7	2105–2155		Cloud Properties, Land Properties
8	405–420		Chlorophyll
9	438–448		Chlorophyll
10	483–493		Chlorophyll
11	526–536		Chlorophyll
12	546–556		Sediments
13h	662–672		Atmosphere, Sediments
13l	662–672		Atmosphere, Sediments
14h	673–683		Chlorophyll Fluorescence
14l	673–683		Chlorophyll Fluorescence
15	743–753		Aerosol Properties
16	862–877		Aerosol Properties, Atmospheric Properties
17	890–920		Atmospheric Properties, Cloud Properties
18	931–941		Atmospheric Properties, Cloud Properties
19	915–965		Atmospheric Properties, Cloud Properties
20		3.660–3.840	Sea Surface Temperature
21		3.929–3.989	Forest Fires & Volcanoes
22		3.929–3.989	Cloud Temperature, Surface Temperature
23		4.020–4.080	Cloud Temperature, Surface Temperature
24		4.433–4.498	Cloud Fraction, Troposphere Temperature
25		4.482–4.549	Cloud Fraction, Troposphere Temperature
26	1360–1390		Cloud Fraction (Thin Cirrus), Troposphere Temperature
27		6.535–6.895	Mid Troposphere Humidity
28		7.175–7.475	Upper Troposphere Humidity
29		8.400–8.700	Surface Temperature
30		9.580–9.880	Total Ozone
31		10.780–11.280	Cloud Temperature, Forest Fires & Volcanoes, Surface Temp.
32		11.770–12.270	Cloud Height, Forest Fires & Volcanoes, Surface Temperature
33		13.185–13.485	Cloud Fraction, Cloud Height
34		13.485–13.785	Cloud Fraction, Cloud Height
35		13.785–14.085	Cloud Fraction, Cloud Height
36		14.085–14.385	Cloud Fraction, Cloud Height

There are two MODIS aerosol products, one which has a pixel size of 10 km x 10 km and one that has a pixel size of 3 km x 3 km [42]. The 3 km x 3 km product will be used in this research because it is closest to the pixel size of OLCI's AOT data product (1 km x 1 km). The aerosol products of MODIS have been extensively validated by AERONET data [42].

3.8. Chlorophyll & TSM

The chlorophyll (Chl) and total suspended matter (TSM) products are derived from the water-leaving reflectance products. In total there are 2 chlorophyll products and 1 TSM product in the Level-2 datasets of OLCI. These products will be discussed in the following sections.

3.8.1. OC4Me algorithm

One of the Chl products is determined through the Maximum Band Ratio (MBR) semi-analytical algorithm developed by Morel [40] called the OC4Me algorithm. The same algorithm was used to determine chlorophyll in the Algal-1 product of MERIS (paragraph 2.1). The difference between the OLCI and MERIS product is the used water-leaving reflectance bands in the algorithm. For OLCI bands 443, 490, 510nm, and band 560nm. Throughout this report we will refer to this product as CHL_OC4Me. CHL_OC4Me will be compared to the MERIS Algal-1 product, since they are derived in the same way.

3.8.2. Neural Network

The neural network of OLCI has followed the heritage of MERIS by chosing an artificial neural network as a multiple non-linear regression technique. This means that the neural network translates water-leaving radiances into inherent optical properties. Inherent optical properties are properties of a medium not depending on other light fields in its surrounding. Water has well defined absorption and scattering properties even if there is no light to be absorbed or scattered. These inherent optical properties can be obtained in a lab from a water sample but also from in-situ measurements in the ocean [35]. The absorption coefficient and scattering coefficient are two examples of inherent optical properties. From the inherent optical properties the water constituents chlorophyll and TSM are determined by a regression method [14].

The neural network of OLCI works in a similar way as that of MERIS. An overview is shown in Figure 3.8. On the left hand side of this figure the training of the neural network starts. Bio-optical data is used as input, these are absorption by particulate organic matter, absorption by dissolved organic matter, absorption by chlorophyll, scattering by TSM, and scattering by white particles. For the chlorophyll pigment 221 different absorption spectra have been compiled from measurements in the North-Sea, Skagerrak, and the Norwegian Sea throughout spring until autumn season. The ATBD does not specify from which database the TSM measurements are taken [14]. A bio-optical model is chosen for these bio-optical data. The bio-optical model is used to simulate water-leaving radiances using Hydrolight [14]. Hydrolight is a numerical model to obtain water-leaving radiances from bio-optical properties [35]. A standard atmosphere is defined to apply an atmospheric correction. A part of the simulated water-leaving radiances is used for training and another part for testing. The same was done in the MERIS neural network. The selection criteria to divide the training and testing data are based on measurements taken in the German Bight (North Sea North of Germany, West of Denmark). A consequence of this selection is a constraint in the selected water-leaving reflectances used as test data.

At this point we arrive at the right hand side of Figure 3.8 where the neural network is applied. The neural network consists of two smaller neural networks, the inverse neural network and the forward neural network. A zoomed-in overview of this part is given in Figure 3.9. The inverse neural network obtains inherent optical properties from the input water-leaving radiances. The forward neural network derives water-leaving radiances from inherent optical properties. The water-leaving radiances of the input of the inverse neural network and the output of the forward neural network are compared to test how far the determined water-leaving radiance is apart from the training data set. An invalid flag is raised for pixels which have a difference above a certain threshold. If this flag is not raised, the inherent optical properties are used to determine the Chl and TSM content of the pixel using the following equations:

$$\begin{aligned} Chl(mg/m^3) &= 22 * a\_pig(443)^{1.04} \\ TSM(g/m^3) &= 1.7 * b\_part(443) \end{aligned} \tag{3.6}$$

in which a_pig is the absorption coefficient for chlorophyll, and b_part is the scattering coefficient of TSM.

The ATBD states some assumptions and limitations for this algorithm [14]. The relevant limitations for this project are stated below:

- The neural network is only valid a a certain range of inherent optical properties which means exceptional values during bloom time are not taken into account.
- The uncertainty of the inherent optical properties increases with a decreasing concentration of the constituents.
- The model does not take water depth into account which means that bottom reflections can be seen as water inherent optical properties as well.

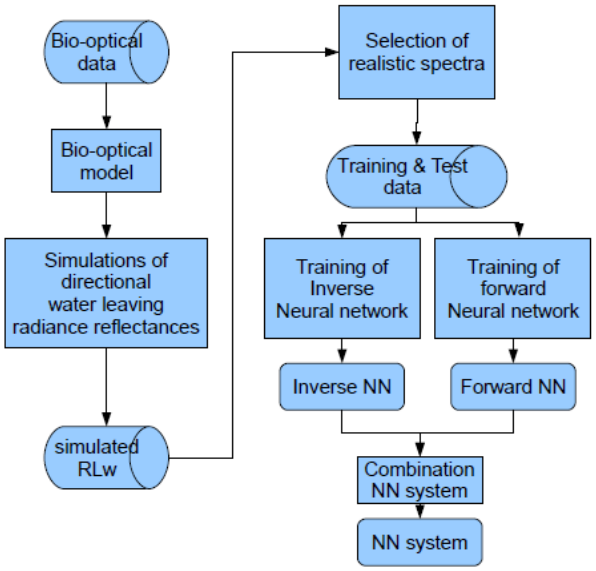

Figure 3.8: Overview of the steps to take to build OLCI's neural network [14].

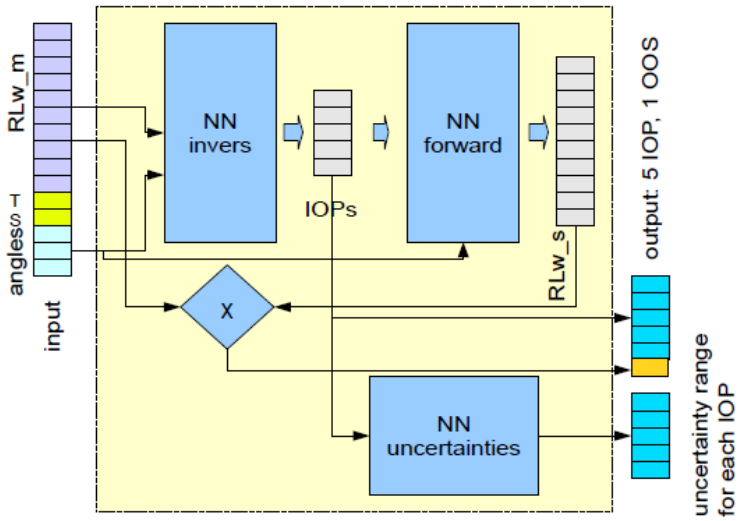

Figure 3.9: Zoomed in on the two neural networks [14].

3.9. Conclusions

This chapter showed specifications of Sentinel-3 OLCI ad its Level-2 data products. The retrieval of those data products was explained as well. Furthermore, AERONET-OC and MODIS were briefly discussed which will be used in the verification of the water-leaving reflectance and aerosol optical thickness products. The following conclusions were drawn from chapter 3.

- In this chapter we saw how important the atmospheric correction is for the retrieval of water-leaving reflectance and eventually the water constituents chlorophyll and TSM. It is therefore important to verify the water-leaving reflectance and atmospheric correction as well. The water-leaving reflectance will be compared with water-leaving radiance of AERONET-OC. The atmospheric correction has aerosol optical thickness as by-product. The AOT product of OLCI will be compared to AOT AERONET-OC and MODIS to verify the atmospheric correction.
- OLCI contains 2 chlorophyll products similar to the chlorophyll products of MERIS. One of those is obtained by the OC4Me algorithm and one by a neural network. TSM is obtained from the same neural network. The origin of the chlorophyll and TSM products lay in the water-leaving reflectance. To conclude on the quality of the chlorophyll and TSM products it is important to know the quality of the water-leaving reflectance product.
- The AOT is a by-product of the atmospheric correction and will therefore be verified as well. It will work as the verification of the atmospheric correction. The aerosol optical thickness is obtained through a method developed by Antoine and Morel in 1998. It originates from the Clear Water Atmospheric Correction (CWAC).
- The AOT will be verified by comparing it to the AERONET-OC station Thornton. This station is located in the Belgian part of the North Sea. AERONET-OC obtains the water-leaving radiance and will therefore be used to verify the OLCI water-leaving radiance product also. The difference between AERONET-OC and OLCI is the measurement level. AERONET-OC is a ground-based station and measures the AOT and water-leaving reflectance directly at ground-level while OLCI obtains these products from the Top of atmosphere radiance (TOA) by applying algorithms and functions as described in this chapter.
- AERONET-OC is a point measurement and not available in the research area of this thesis. AOT OLCI is compared to AOT MODIS to verify the AOT for the Dutch part of the North Sea. Furthermore the spatial variability can be researched in this manner.

4

Data description & Methodology

This chapter describes the methodology and the working procedures followed in this research project. A supporting flowchart was created and is presented in Figure 4.4.In this research 5 different types of data were used. Three types of satellite data were used, Sentinel-3A OLCI Level-2 reduced resolution data, ENVISAT MERIS Level-2 reduced resolution, and AQUA (EOS PM) MODIS Level-2 3 km resolution data of the aerosol optical thickness. In-situ measurement data of chlorophyll and TSM were used to compare OLCI's water quality products with. AERONET-OC data from the Thornton station were used to compare OLCI's normalised water-leaving reflectance and aerosol optical thickness products with. These 5 different data types will be described. The acquisition and processing of these data types will be discussed in the following paragraphs.

4.1. Data selection and pixel extraction

As can be seen in the flowchart the first step was to select data including the Dutch North Sea for all data types except the AERONET-OC data. The AERONET-OC station used in this research is located in the Belgian part of the North Sea, data at this location was selected. For the in-situ data this was done by selecting the MWTL locations in the North Sea. For OLCI and MERIS data a script was created that defined a bounding box which had the following coordinates: upper left corner (51.00, 8.00), upper right corner (56.00, 8.00), lower right corner (56.00, 8.00), lower left corner (51.00, 2.00). Data within this bounding box were extracted. This bounding box is shown in Figure 4.1. For MODIS data only the data tiles including a part of the Dutch North Sea were downloaded.

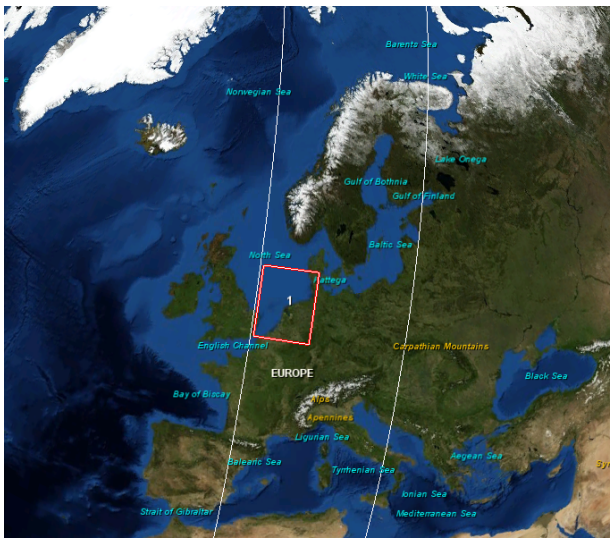

Figure 4.1: Overview of the selected area. The red box represents the bounding box used in this research. The white box represents a full data strip.

Pixel extraction was performed on the selected remote sensing data using the open-source SNAP software [10]. Pixels at the MWTL locations and AERONET-OC Thornton location were extracted for all data products and all data sets. At the locations of the ADHOC measurements (extra RWS measurements, paragraph 4.1.4) pixels were extracted from the OLCI data. To investigate the spatial variability 3x3 pixels around the Rijkswaterstaat measurement locations were extracted as well.

4.1.1. Sentinel-3A OLCI data

Sentinel-3A OLCI Level-2 reduced resolution data were collected through Deltares' EUMETCAST system receiving OLCI data products near real-time as described in paragraph 3.2. Data were collected from 5 May 2017 until 15 October 2017 to fulfil this research. On 6 July 2017 EUMETSAT updated the neural networks for the OLCI processing line and therefore the OLCI data were split into two sets, one called the old processing line and one the new processing line. The results of the new processing line will be discussed in chapter 5, the results of the old processing line will be included in the Appendix C.

Another aspect taken into consideration were the 'invalid' pixels in the satellite data. ESA and EUMETSAT classify data pixels into cloud, land, water or invalid (paragraph 3.3). The invalid and cloudy pixels were filtered out before the validation process was applied. Many quality and science flags are provided for the OLCI data products, which give more information about a certain pixel. The available flags are shown in Table 4.1. For each data product different flags can be applied according to EUMETSAT's product notice of 5 July 2017 [25]. In this project these recommended flags were applied. An overview of flags used for the different products is given in Figure 4.2. For example for TSM_NN the Common flags were applied and the Product flag "not OCNN_FAIL". For the CHL_OC4ME data product extra Processing chain flags were applied.

Product names	Products	Common flags	Processing chain flags	Product flags
Water leaving reflectances	Oa**_reflectance → Oa**_reflectance	**Ocean Colour Products** (WATER *or* INLAND_WATER) *and not* (CLOUD CLOUD_AMBIGUOUS CLOUD_MARGIN INVALID COSMETIC SATURATED SUSPECT HISOLZEN HIGHGLINT SNOW_ICE)	**Open Water products** *not* (AC_FAIL WHITECAPS ANNOT_ABSO_D ANNOT_MIXR1 ANNOT_DROUT ANNOT_TAU06 RWNEG_O2 RWNEG_O3 RWNEG_O4 RWNEG_O5 RWNEG_O6 RWNEG_O7 RWNEG_O8)	*none*
Algal pigment concentration in open waters	chl_oc4me → CHL_OC4ME			*not* OC4ME_ FAIL
Diffuse attenuation coefficient	trsp → KD490_M07			*not* KDM_FAIL
Photosynthetically Active Radiation	par → PAR			*not* PAR_ FAIL
Aerosol Optical Thickness and Ångström exponent	w_aer → T865, A865			*none*
Algal pigment concentration in complex waters	chl_nn → CHL_NN		**Complex Water Products** *no specific flags to be applied*	*not* OCNN_FAIL
Total suspended matter concentration	tsm_nn → TSM_NN			*not* OCNN_FAIL
Coloured Detrital and Dissolved Material absorption	iop_nn → ADG443_NN			*not* OCNN_FAIL
Integrated Water Vapour Column	iwv → IWV	**Atmospheric Products**	**Water Vapour** over WATER *not* MEGLINT	*not* WV_FAIL

Figure 4.2: Recommended OLCI Level 2 flag combinations for masking of cloudy or unreliable pixels for the individual Level-2 data products [25].

Table 4.1: Overview of the the different characteristics provided by the water quality and science flags [24].

Flag Name	Water Classification, Quality and Science Flags Flag Description
Classification and Quality Flags	
INVALID	Invalid flag: instrument data missing or invalid
WATER	Clear sky water
LAND	Clear sky land
CLOUD	Cloudy pixel
SNOW_ICE	Possible sea-ice or snow contamination
INLAND_WATER	Fresh inland waters flag: based on Level-1 land_water flag
TIDAL	Pixel is in shallow water: based on Level-1 land_water flag
COSMETIC	Cosmetic flag (from Level-1B): missing data filled in by interpolation
SUSPECT	Suspect flag (from Level-1B): transmission errors means measurements may be unreliable
HISOLZEN	High solar zenith: >70°
SATURATED	Saturation flag: saturated within any band from 400 to 754 nm or in bands 779, 865, 885 and 1020 nm
MEGLINT	Flag for pixels corrected for glint
RISKGLINT	Flag for pixels for which the glint correction is not reliable
WHITECAPS	Whitecaps flag
ADJAC	Meaningless - reserved for future use
WVFAIL	The water vapour retrieval algorithm failed
PAR_FAIL	PAR calculation failed. Internal flag is OC_PAR_FAIL
ACFAIL	Atmospheric correction is suspect
OC4ME_FAIL	OC4Me algorithm failed
OCNN_FAIL	IMT NN algorithm failed
KDM_ FAIL	KDM07 algorithm failed
KDL_ FAIL	KDL05 algorithm failed
Science Flags	
BPAC_ON	BWAC was switched on and attempted
WHITE_SCATT	"White" scatterer flag within the water
LOWRW	(p'w(b, j, f) <R560MIN) or HIINLD_F raised
HIGHRW	High RW at 560nm or CASE2_F raised
ANNOT	Annotation flag for the quality of the atmospheric correction
RWNEG	Provides a "negative water-leaving reflectance" flag for each water-leaving reflectance band

4.1.2. ENVISAT MERIS data

MERIS Level-2 reduced resolution data were collected from 30 April 2002 until 8 April 2012. For MERIS data the same area was extracted as for OLCI using the bounding box presented in Figure 4.1. For the first part of this project algal and TSM products were used. MERIS has two algal products which were compared with OLCI's chlorophyll products. Algal-1 is derived through the OC4Me algorithm (3.8) and thus compared with the Chl OC4Me OLCI data product. The Algal-2 data product is derived with a neural network and was compared with OLCI's chlorophyll product obtained through the neural network. MERIS' TSM product is also based on a neural network. Similar to OLCI MERIS also has some quality flags. It was advised to used the PCD-13 flag as check-up to filter out invalid pixels.

4.1.3. AQUA MODIS data

MODIS Level-2 3 km resolution data of the aerosol optical thickness were collected for the period 6 July 2017 until 19 September 2017. The data were obtained through NASA's Level 1 and Atmosphere Archive and Distribution System Distributed Active Archive Center (LAADS DAAC) archive (https://ladsweb.modaps.eosdis.nasa.gov). OLCI's reduced resolution data products has a spatial resolution of 1.1 km and therefore the finest 3 km resolution of MODIS data were chosen. MODIS's data product has many varieties of AOT products, but in this research was chosen for the Effective Optical Depth Average for ocean band 2, which has a central wavelength of 859nm.

4.1.4. In-situ data of Rijkswaterstaat

RWS created a measurement plan called "Monitoring Waterstaatkundige Toestand des Lands" (MWTL), which describes the measurement locations and the activities to monitor water quality of the Dutch waters. An overview of the measurement locations can be found in Figure 1.2. Water quality of the North Sea is monitored by RWS 2-weekly during summers and monthly cruises during winters. For this research historical MWTL data from 1 January 2002 until now was used to plot time series. Depending on the MWTL location availability of data differs. Furthermore, in-situ data for the period 8 May 2017 until 28 August 2017 was used to create regressions with OLCI data. For this project RWS took extra measurements during the time of satellite overpass. These measurements were called ADHOC measurements and will be discussed separately in the results chapter.

4.1.5. AERONET-OC

The data for the validation of the OLCI AOT data product and the normalised water-leaving reflectance products came from AERONET-OC station Thornton shown in Figure 3.7. The Thornton station was chosen because it is closest to the area or interest. Historical data were obtained from 9 April 2015 until now to create time series of the AOT. Data from the period 7 July 2017 until 19 October were used to create regression plots with OLCI's AOT and normalised water-leaving reflectance. For the same period of data normalised water-leaving radiance spectra were created. The data were downloaded from NASA's AERONET-OC website (https://aeronet.gsfc.nasa.gov).

4.2. Part 1 Verification chlorophyll and TSM data products

First of all, maps were created of the OLCI CHL_NN, CHL_OC4ME, and TSM data products to visually explore the Chl and TSM values in the selected area. In this way interesting areas were observed such as the coastal and cloudy areas. Immediate differences between the MWTL locations and Chl products were noticed. The difference in Chl and TSM values occuring due to the different processing lines was noticed as well.

Time series were created of MERIS, in-situ and OLCI data in one plot per MWTL station in order to see if the range of OLCI values and new in-situ measurements were comparable with historical values. CHL_OC4ME was compared to MERIS Algal-1 historical data and CHL_NN was compared to MERIS Algal-2 historical data. The time series also showed the seasonal patterns through the year for historical MERIS and in-situ data. Last but not least, the differences between the different MWTL locations were confirmed.

Regressions between OLCI and in-situ measurements were created to compare the pixels 1 by 1. Match-up constraints applied to the data to create the regressions were: location, time and OLCI flags. It is important to have match-up data points closely together in time since wind, river discharge, and tide can quickly change the Chl or TSM concentration at a certain location, especially for the MWTL locations near the coast. The idea was to use the ADHOC measurements for this, since they are approximately taken at the time of Sentinel-3A overpass. In order to obtain more match-up data than just the ADHOC measurements, the time difference between the measurements was increased to 1 day, 2 days, 5 days, 10 days, and no time constraint. Match-ups were found for those time constraints and regressions were created between in-situ and OLCI data products for each of the time constraints. These regressions were generated for the OLCI CHL_OC4ME, CHL_NN, and TSM data products. From these regressions statistics were calculated such as the intercept, slope, r-value, p-value, and standard deviation. These statistics quantify the quality of the regressions. The OLCI 3x3 pixel extractions were used to create boxplots of OLCI CHL_OC4ME, CHL_NN, and TSM products. The spatial variability of OLCI was investigated at all MWTL locations.

4.3. Part 2 Verification of water-leaving radiance and aerosol optical thickness

In the second part of this project, the normalised water-leaving reflectance and aerosol optical thickness (AOT) products of OLCI were verified. OLCI's normalised water-leaving reflectance is available for all bands except band 13, band 14, band 15, band 19, and band 20 (Table 3.1). OLCI's AOT product is estimated for band 17 (865 nm) only.

4.3.1. Normalised water-leaving radiance verification

OLCI's normalised water-leaving reflectance was converted to normalised water-leaving radiance (nL_w) in order to compare it with the nL_w obtained at the Thornton AERONET-OC station (section 3.6). OLCI's nL_w bands do not exactly coincide with the AERONET-OC station bands. Regressions between OLCI and AERONET were created for each of the coinciding bands (paragraph 3.7.1). Match-up constraints applied to the data were: Thornton location, time and OLCI flags. The only AERONET-OC station available close to the research area was the Thornton station, therefore no other data was used to verify OLCI's nLw. The nL_w is dependent on the solar angle, therefore the time constraint is very important is this research. The regressions were created for match-ups which had a maximum time difference of 2 hours. The erroneous OLCI pixels were filtered using the suggested flags.

nL_w spectra were created of all OLCI bands and AERONET-OC bands to investigate if the shape of the whole spectrum was similar. Spectra were created for measurements at the Thornton location only which had a maximum time difference of 2 hours. The flagged OLCI pixels were filtered.

4.3.2. Aerosol optical thickness verification

OLCI's AOT data product was verified by comparing it with the AOT from the AERONET station and the AOT product of MODIS. Maps were created to see the spatial differences in the area of interest. Spatial variations were noticed from these maps.

Time series of the AOT were created for all MWTL stations including the AERONET-OC Thornton station. These time series were used to investigate if the range of OLCI's AOT values matched the AERONET and MODIS AOT values. AERONET AOT data were only available at the Thornton location therefore the AERONET data is not used for the time series of the other MWTL locations.

Regressions between OLCI and AERONET AOT values and OLCI and MODIS AOT values to quantify the quality of OLCI's AOT product. The time difference between the AERONET-OC data and OLCI data was maximum 2 hours, because the AOT estimated at the AERONET station is dependent on the solar angle. This regression was created using 1 pixel of OLCI only.

OLCI and MODIS have similar overpass times therefore match-ups with a time difference of a few hours was applied. The daily difference of OLCI and MODIS AOT values was investigated using time difference constraints of maximum 2 hours, 12 hours and 2 days in the same manner as was done for the Chlorophyll and TSM regression plots. To compensate for the difference in spatial resolution between MODIS and OLCI, not only 1 pixel of OLCI was compared with 1 pixels of MODIS data, but the mean of a 3x3 area of OLCI pixels was taken to compare with a single MODIS pixel at the location of a MWTL location. A detailed regression plot for the match-ups with a maximum time difference of 2 hours was created to investigate the spatial variability. In this detailed plot the spatial variability is visualised as well by showing error bars representing the standard deviation within in 3x3 pixel area. Statistics of the regressions were calculated such as the slope, intercept, r-value, p-value and standard deviation. The spatial variability of OLCI's AOT values was also investigated by creating boxplots for each of the MWTL points.

4.4. Statistics

In this research different types of statistics were used. These statistics are discussed in this paragraph.

4.4.1. Regressions

Various regression between OLCI, in-situ measurements, AERONET-OC, and MODIS were created. The quality of the regressions were defined by the intercept, slope, r-value (correlation coefficient), and the standard deviation. The ideal intercepting value for a perfect regression would be 0,0. The further the intercept is from 0,0 the more offset a dataset has. The best possible slope would be a value of 1. This means that the data would exactly change with the same value as the reference dataset. An offset factor can be obtained if the slope value is larger or smaller than 1. A larger value would mean an overestimation of the data, and smaller values would mean an underestimation. The r-value shows the correlation between two different datasets. A correlation of 1 means the datasets are perfectly related to each other whereas an r-value of 0 would mean there is no correlation at all. The standard deviation explains the range of values a dataset contains. A high standard deviation means a large variability within a dataset. All the regressions are based on a linear least squares fit method.

4.4.2. Boxplots

Boxplots were used to investigate the spatial variability of the OLCI data products. An example boxplot is shown in Figure 4.3. As is shown in the figure a median value, also called the 50th percentile value, is determined first. From this median value the interquartile range (IQR) is calculated. The IQR consists of 25% of data points below and above the median value. The lower limit of the IQR is called the 25th percentile or 1st quartile, the upper limit is called the 75th percentile or 3rd quartile. The whiskers indicated as blue dashed lines are calculated by getting the 25th of 75th percentile value plus 1.5 * IQR. All data points outside the whiskers are considered as outliers. In this research the boxplots are created of 3x3 pixels around a Rijkswaterstaat measurement location for each day of valid OLCI data. The number of boxplots created in one plot tells us how many times the pixels at a certain location had 3x3 valid pixels and thus how often a algorithm fails. The different medians of the boxplots within one plot tells us the temporal variability of the pixel values at a certain location. When the median values differ a lot at one location, the temporal variability is large. The size of a boxplot represents the variability of values within the 3x3 pixel area. The larger the box is, the larger the spatial variability. A large spatial variability within 3x3 pixels (area of 3 km x 3 km) is not very realistic in most of the satellite products.

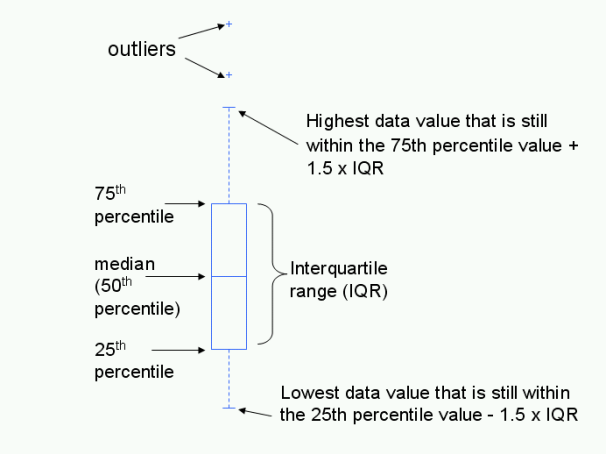

Figure 4.3: Example boxplot to explain the principles of the statistics in a boxplot.

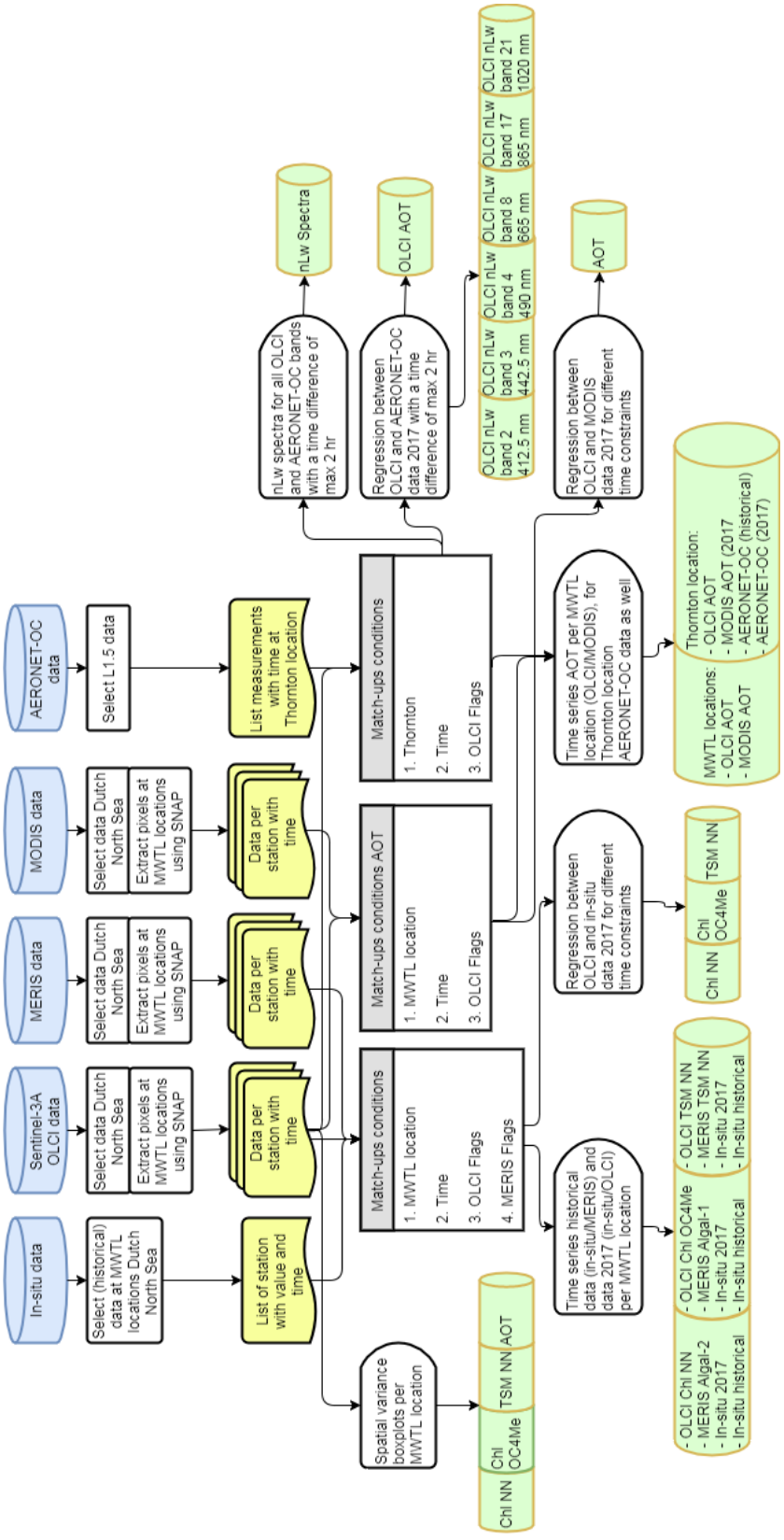

Figure 4.4: Flowchart of the methodology. Indicated in blue are the used data sources. The white square boxes represent the selection and pixel extraction procedures applied to obtain the datasets which were verified, represented in yellow. Match-up conditions are given in the middle of the flowchart. The white one-side-rounded boxes represent the measure applied to obtain results. The results are indicated by the green tubes.

4.5. Conclusions

This chapter described the data that was used in this project. Furthermore the different comparison methods were explained in more detail. The statistics used to investigate the quality of the different data products has been explained as well. The following conclusions are drawn from this chapter.

- A standard processing is to select data from the different data sources. First, the full data products are obtained and sub-setted for the study area of this thesis. Using SNAP, data at Rijkswaterstaat's measurement locations are extracted from the sub-setted data. The data products compared with AERONET-OC data were extracted at Thornton location. The extracted pixels are then filtered using recommended Sentinel-3 Validation Team flags in order to leave invalid or erroneous pixels out.
- Several data products will be used in the verification of the Sentinel-3 OLCI Level-2 reduced resolution data products. For the evaluation of the chlorophyll and TSM products in-situ measurements of Rijkswaterstaat will be used. Also time series of MERIS, in-situ measurements, and OLCI will be compared in order to see if OLCI's value range is correct. For the verification of the water-leaving radiance and the aerosol optical thickness (AOT) data products AERONET-OC and MODIS will be used. Time series of the AOT will show the value ranges.
- Different constraints will be applied in the comparison of the data products. The Rijkswaterstaat measurement locations will be used as location constraint. The comparisons of chlorophyll, TSM and AOT will be done at those locations. The comparisons done for the water-leaving radiance and the AOT from AERONET-OC will use the coordinates of the Thornton station as location constraint. Furthermore time constraints are applied. For the water-leaving radiance and AOT it is important that the time difference between the different measurements is as small as possible since these measurements are very dependent on the solar angles. A maximum time difference of 2 hours will be applied for those comparisons. To increase the number of match-up data for the chlorophyll and TSM measurements different time constraints will be used ranging from a few hours to a few days.
- To quantify the quality of the OLCI data products regressions between the different data types will be created using a linear least squares fit. Statics from these fits include the intercept, slope, correlation coefficient and the standard deviation. Furthermore, boxplots will be created to quantify the temporal and spatial variability of the OLCI data products at the Rijkswaterstaat measurement locations.
- An important thing to mention is the change in the processing line of OLCI. From the 6th of July a new processing line was applied. For this reason the verifcation study was divided into two sections. The verification results of the most recent processing line will be shown in the results chapter. The comparisons results obtained with the data using the old processing line are included in Appendix C.

5
Results

In this chapter the derived results are presented and described. First the Chlorophyll (Chl) and Total Suspended Matter (TSM) comparisons are shown followed by the verification results of the normalised water-leaving radiance (nL_w), and aerosol optical thickness (AOT).

5.1. Chlorophyll (Chl) & Total Suspended Matter (TSM) results

This section is divided into four parts. The first part describes the created maps of Chl and TSM. Then the time series are presented, followed by the regression plots between in-situ and OLCI measurements. Boxplots were created of the Chl and TSM data products at each of the MWTL locations to look into the spatial variability. Three standard OLCI data products were verified in this part, chlorophyll neural network (CHL_NN), chlorophyll OC4Me (CHL_OC4Me), and total suspended matter (TSM_NN).

5.1.1. Overview maps

Maps of the research area containing Chl and TSM OLCI data products were presented for 9 July 2017 because it was a clear day with very few clouds. Figure 5.1 presents Sentinel-3 maps of the Chl content for the Dutch part of the North Sea. On the left side the resulting map for CHL_NN is presented for 9 July 2017, on the right the map of CHL_OC4Me. For both data products the Chl is higher along the coasts compared to the open waters. Chl is also a lot higher around clouds than in the rest of the maps, especially for the CHL_NN data product. This could imply a bias in the Chl products for pixel values close to clouds/cloud boundaries. The Chl values of the CHL_NN are in general lower than of the CHL_OC4Me product. An interesting pattern to notice in the CHL_NN products are the high Chl values at the Maas drainage near Rotterdam and Westerschelde drainage. A remarkable thing to notice in the CHL_OC4Me algorithm is that it always fails at the IJsselmeer part of the map. Besides the IJsselmeer failures it occurs often that the algorithm fails in coastal areas as is also visible in this map. These failures are indicated with purple. The CHL_NN product rarely fails in obtaining the Chl content.

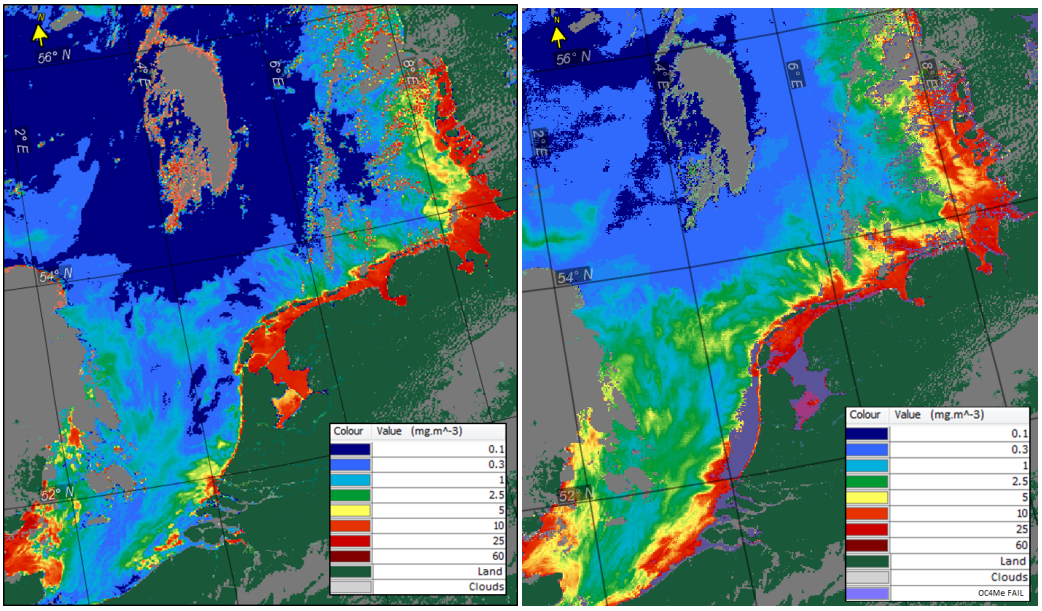

Figure 5.1: OLCI Chl content maps created using SNAP for 9 July 2017. On the left hand side the CHL_NN is presented, on the right CHL_OC4Me. The colours represent chlorophyll values as shown in the legends. OLCI's land mask is presented in green, the cloud mask in grey. These maps show that the Chl values of the neural network product are significantly lower than the OC4Me product. Both maps show high Chl values in coastal areas and around clouds. This could imply that the cloud mask is not strict enough yet. The map of OC4Me shows many failing pixels along the coast, this means that the algorithm is not performing well in this area. This was also seen in maps of other days. (Copyright 2017 EUMETSAT)

Figure 5.2 presents the OLCI TSM content for the Dutch part of the North Sea on 9 July 2017. Interesting to note is that the same patterns as were observed for the Chl maps are also noticed in this maps, high TSM values for coastal pixels and pixels close to clouds. Values for TSM are high for the area of the Maas and Westerschelde drainage, which was observed in the CHL_NN map as well. Another remarkable thing to notice in the three maps is the abrupt decrease of Chl in the CHL_NN and CHL_OC4Me maps and TSM in the TSM_NN map just below the 54° latitude line. This has most probably to do with the Doggersbank located in this area.

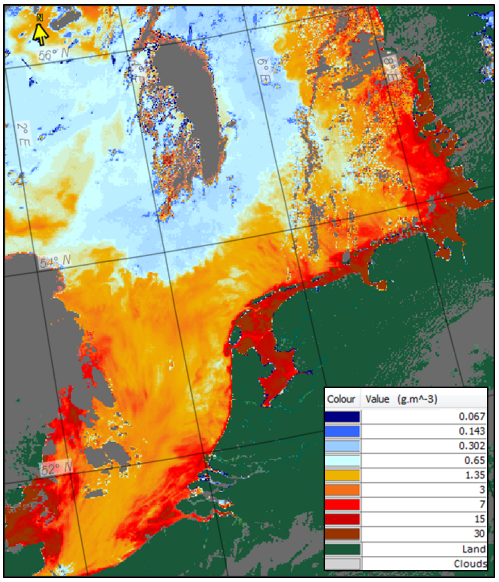

Figure 5.2: OLCI TSM map created using SNAP for 9 July 2017. The colours in the legend represent TSm values in g/m^3. This map shows that coastal areas show higher values of TSM than offshore areas. Another noticeable point are the high TSM values around clouds. This implies that OLCI's cloud mask might not be strict enough. (Copyright 2017 EUMETSAT)

5.1.2. Timeseries

For each Rijkswaterstaat measurement location a time series is plotted. In appendix B time series of all the MWTL locations can be found. The three most interesting time series are discussed in more detail below. The time series were based on in-situ measurements and remote sensing data. The Sentinel-3 data obtained through pixel extraction based on the coordinates of the in-situ measurements. Pixels which were flagged out were not taken into account.

Time series chlorophyll based on OLCI neural network

Figure 5.3 shows chlorophyll time series of three MWTL locations. The N20 and T10 locations are considered as coastal stations and therefore Case-2 water types as mentioned in section 1.3. The T175 location is an open water station and therefore a Case-1 water type station. The main difference between the Case-1 station and the Case-2 stations is the chlorophyll content. The figure clearly shows that the Case-1 station has low chlorophyll content throughout the year. The N20 and T10 station show an increase in chlorophyll constant in the warmer/lighter months of the year. Especially the T10 station shows a peak concentration during spring time in the months April, May and June (Day 90 until day 160). This is most probably caused by the spring bloom, which occurs in those months. The Chl contents from OLCI are neural network values. The Chl values of OLCI seem to slightly underestimate when comparing those to the in-situ measurements. This is especially clear for the Case-2 water stations.

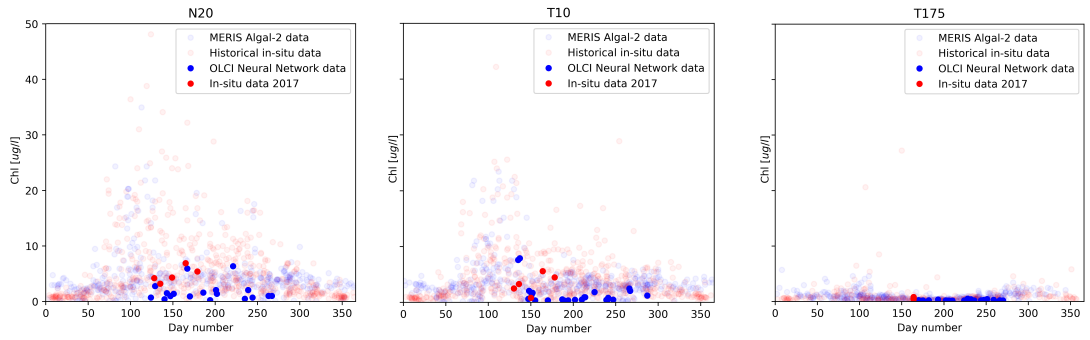

Figure 5.3: Time series of the chlorophyll content at Rijkswaterstaat measurement locations N20, T10 and T175 respectively (Figure 1.2). The red markers represent the in-situ data of which the bright red markers are the in-situ measurements of 2017, the transparent red markers represent historical in-situ data. The blue markers represent remote sensing data of OLCI based on the neural network.

Time series chlorophyll based on OLCI OC4Me algorithm

Figure 5.4 shows chlorophyll content time series of the same three MWTL locations. The main difference between the Case-1 and Case-2 stations is the Chl content, which is much higher for the Case-2 water stations. The OC4Me plot do not show an underestimation as was noticed in the measurements of the neural network data (Figure 5.3). The OC4Me algorithm seem to fit the in-situ data better than the neural network data did.

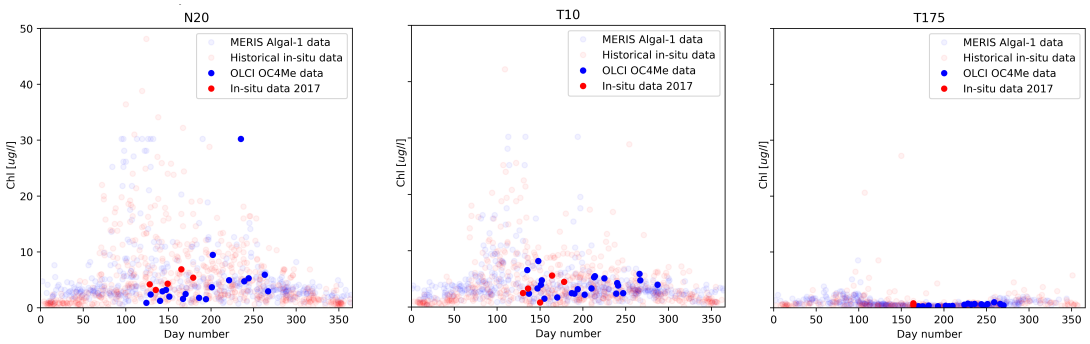

Figure 5.4: Time series of the chlorophyll content at Rijkswaterstaat measurement locations N20, T10 and T175 respectively (Figure 1.2). The red markers represent the in-situ data of which the bright red markers are the in-situ measurements of 2017, the transparent red markers represent historical in-situ data. The blue markers represent remote sensing data of OLCI based on the OC4Me algorithm

Table 5.1: Table of match-up data with a maximum time difference of 2 hours. The in-situ measurements were approximately taken at the time of satellite overpass.

In-situ CHL (μg/l)	OLCI CHL_NN (μg/l)	OLCI CHL_OC4Me (μg/l)	In-situ TSM (mg/l)	OLCI TSM (mg/l)
0.575	0.834	3.825	2.390	2.476
0.690	0.502	6.129	6.940	0.865
0.644	1.115	7.348	3.160	3.077

Time series TSM based on OLCI neural network

Figure 5.5 shows Total Suspended Matter time series of three MWTL locations, N2, T10 and T100. The N2 and T10 locations are considered as coastal stations and therefore Case-2 water types. The T100 location is an open water station and therefore a Case-1 water type station. For the Case-1 station we would not expect TSM at all, since it is dominated by Chl. The plot of T100 shows small amounts of TSM.

In all of the Case-2 stations increase when decreasing the distance to the coast (G2, N2, R3, T4, W2 Figure 1.2). This is logical since the sea depth decreases and therefore particles get easily closer to the water surface. Another interesting thing to notice is the increasing TSM towards the colder darker months (Days 300 until day 70). This is especially visible in the plots of the coastal stations (G6, N2, T4, W20). The reason for this could be the frequency of storms in these months. Especially during autumn more storms occur which creates currents transporting sand to the water surface. Stations R3 and W2 show a very random distribution of TSM throughout the year which probably has to do with the fact that these points are located on sand benches where TSM is always very high.

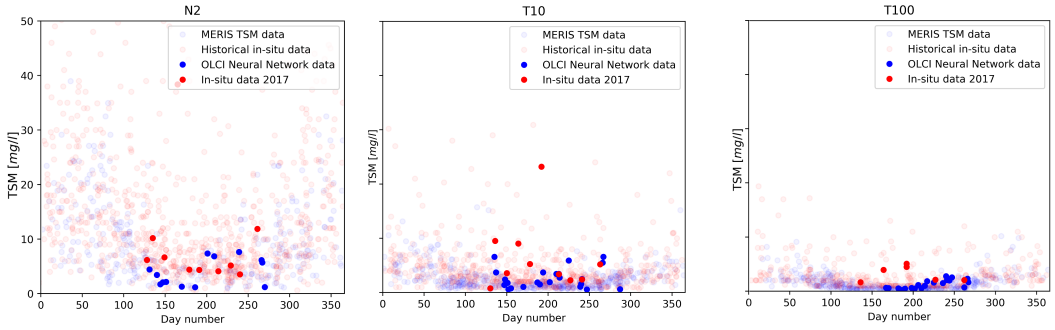

Figure 5.5: Time series of the TSM content at Rijkswaterstaat measurement locations N2, T10 and T100 respectively (Figure 1.2). The red markers represent the in-situ data of which the bright red markers are the in-situ measurements of 2017, the transparent red markers represent historical in-situ data. The blue markers represent remote sensing data of OLCI based on the neural network

5.1.3. ADHOC data

For this project extra in-situ measurements were taken during satellite overpass. The time difference between the in-situ measurement and satellite data pixel is therefore minimal. For optimal comparison between OLCI and in-situ data the time difference between in-situ measurement and satellite overpass should be kept as small as possible (section 4.2). During the period of research, 17 extra in-situ observations were taken for chlorophyll and 21 for TSM. Three valid match-ups were found with a maximum time difference of 2 hours between the in-situ measurement and satellite overpass. Of these three match-ups, 2 were ADHOC measurements and 1 match-up was taken at T10, one of the regular MWTL points. The match-up data are presented in the table below, Table 5.1.

The CHL_OC4Me data product massively overestimates the Chl content at all 3 ADHOC measurement points. The CHL_NN products overestimates the Chl as well except of the second measurement. The TSM_NN data product of OLCI shows similar values of TSM for the first and third measurement. The second OLCI TSM observation underestimates TSM a lot. The 3 match-ups found are located very close to the coast, T10 (measurement 1 in able 5.1), near Vlieland (measurement 2 in able 5.1), and near Alkmaar (measurement 3 in table 5.1) respectively as shown in Figure 5.6. These measurements were taken on 1 August, 16 August, and 29 August 2017 respectively. 1 August 2017 was a very cloudy day in which some surrounding pixels of T10

are marked as clouds. For the first ADHOC measurement taken on 16 August 2017 counts that it is located near the boundary of the cloud mask. The second ADHOC measurements taken on 29 August 2017 was taken during a cloud free period.

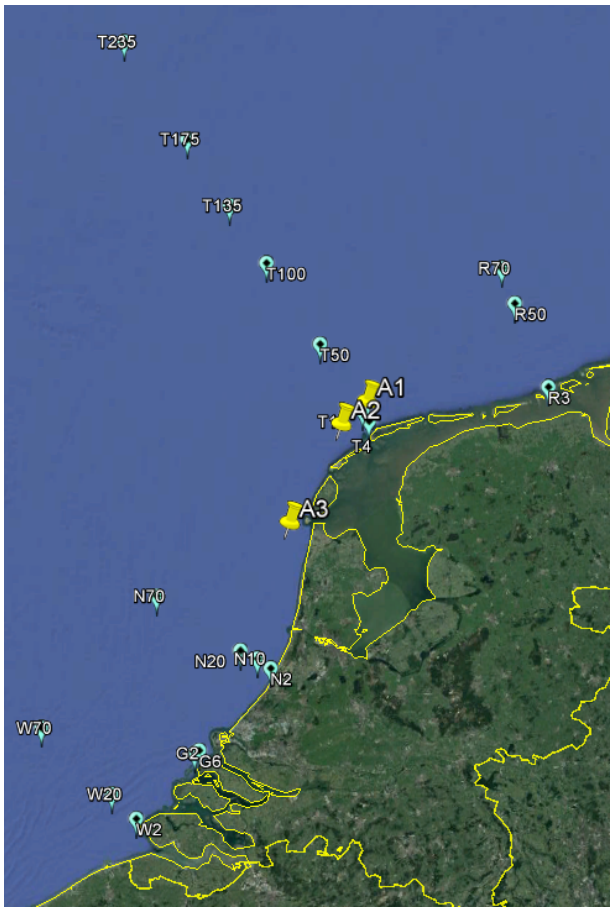

Figure 5.6: Overview of the ADHOC locations. The yellow pins indicated ADHOC location 1, 2 and 3 which correspond to table 5.1. The blue pins indicate Rijkwaterstaat's measurement locations.

5.1.4. Regression plots

To quantify the comparisons made in the previous parts, regression plots were created and analysed. These regressions are discussed in this paragraph. To create the regression plots, it was of utmost importance to find data points at the same location and time, because the tide, wind and river run-off have a large influence on the Chl and TSM concentrations. The idea was to use the ADHOC data for this study but only 3 match-ups were found with a time difference of maximum 2 hours. To increase the number of match-up data points, the time difference between the in-situ measurements and satellite overpass was increased. Match-ups were found for different time constraints to see the influence of time on the regressions. In-situ data were available for the months May until August. OLCI data were available for those months as well, but on the 7th of July EUMETSAT updated the processing line and therefore these two different processing lines were compared separately. The results of the most recent processing line are shown in this paragraph. The results of the previous processing line are shown in Appendix C.

Regression Chl based on OLCI neural network

Figure 5.7 shows the regression plots of chlorophyll based on the neural network of OLCI versus in-situ measurements. The plot shows that the OLCI data fits the in-situ data less when the time difference between the match-ups increases. From these regression plots statistics were calculated which are shown in table 5.2. It can be concluded that the smaller the time difference between the match-ups is the better the OLCI data fits the in-situ measurements. The overall best fit is the fit of the second processing line when the match-ups are maximum 1 day apart. An improvement is seen between the first and second processing line. The error

bars used in this plot are obtained from OLCI's data products. The average error found is approximately 21%. Although the error product is used here, it is not recommended to be used because the error products of OLCI are not calibrated and validated yet. The error bars for the in-situ measurements imply an error of 23%. This error is reported from the lab where the chlorophyll samples were analysed. From the error bars we can say that the error in the in-situ measurements is similar to the error in the OLCI product.

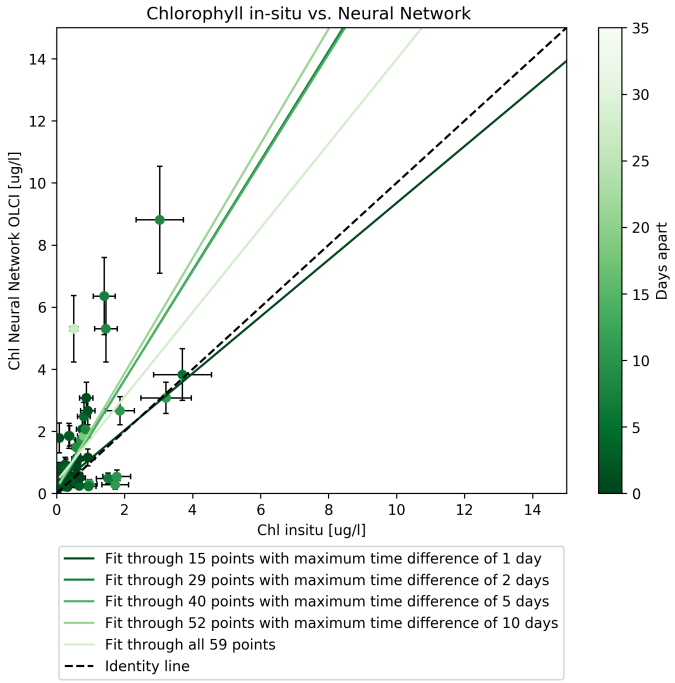

Figure 5.7: Regression plot for the chlorophyll content of OLCI based on the neural network. The black line represents the identity line. The greenness of the markers represents the time difference between the match-up data points. The darker green the dot is, the smaller the time difference was between the time of the in-situ measurement and the satellite overpass. The green lines represent linear least square fits to the points based on time constraints specified in the legend.

Table 5.2: Statistics of the regressions estimated in Figure 5.7. The best values for the different statistics are marked green.

CHL_NN	Slope	Intercept	r-value	p-value	std-dev
Line 1 day apart	0.9149	0.2040	0.7693	0.0008	0.2107
Line 2 days apart	1.7647	0.1238	0.6414	0.0001	0.3989
Line 5 days apart	1.7489	0.1576	0.5912	0.0001	0.3871
Line 10 days apart	1.8484	0.1710	0.7461	0.0000	0.2333
Line through all points	1.3590	0.3916	0.6148	0.0000	0.2309

Regression Chl based on OLCI OC4Me algorithm

Figure 5.8 shows regressions between in-situ data and OLCI Chl contents obtained with the OC4Me algorithm. The regression plot shows a large overestimation of approximately a factor 2 of the chlorophyll content estimated by the OC4Me algorithm. The statistics of those regressions are presented in table 5.3. These statistics show the same as the plots, an overestimation of a factor 2 for Chl by the OC4Me algorithm is shown with the slope of approximately and a large variance between the different fits. Not much difference was seen between the first and second processing line shown in Appendix C. The error bars of OLCI originate from the error product which is included in the level-2 data. The average error of the chlorophyll OC4Me algorithm is 13%. This means that the error of the OC4Me data product is smaller than the error of the in-situ measurements.

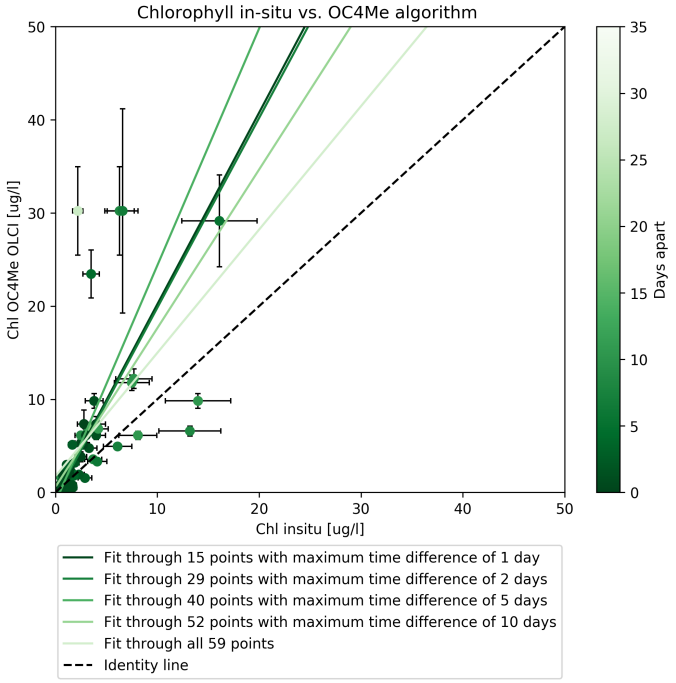

Figure 5.8: Regression plots for the chlorophyll content of OLCI based on the OC4Me algorithm. The black line represents the identity line. The greenness of the markers represents the time difference between the match-up data points. The darker green the dot is, the smaller the time difference was between the time of the in-situ measurement and the satellite overpass. The green lines represent linear least square fits to the points based on time constraints specified in the legend.

Table 5.3: Statistics of the regressions estimated in Figure 5.8. The best values for the different statistics are marked green.

CHL_OC4Me	Slope	Intercept	r-value	p-value	std-dev
Line 1 day apart	2.0582	-0.3868	0.9270	0.0000	0.2310
Line 2 days apart	2.0383	-0.5636	0.9040	0.0000	0.1855
Line 5 days apart	2.5446	-1.0854	0.6843	0.0000	0.4399
Line 10 days apart	1.7040	0.5906	0.6846	0.0000	0.2566
Line through all points	1.3240	1.7413	0.5715	0.0000	0.2518

Regression TSM based on OLCI neural network

Figure 5.9 shows the regression plot for TSM estimated by the neural network of OLCI versus the in-situ measurements. Table 5.4 presents the statistics of those regressions. The plot shows a large underestimation of OLCI's TSM estimations based on the neural network. Another noticeable point is the fact that the plot shows a large variance in the in-situ measurements whereas the variance of the OLCI estimations is small. The statistics confirm the massive underestimation of the OLCI TSM neural network product, because all slopes are approximately 0. All the r-values are less than 0.5 which means that the correlation between the in-situ measurements and the OLCI observations is low. Not much difference or improvement was found between the first and second processing line (appendix C). The error bars shown in this plot come from the Level-2 error data product. The average error for OLCI TSM was found to be 13%. There was no error product available for the TSM in-situ measurements and therefore there is no error bar shown in the x-direction.

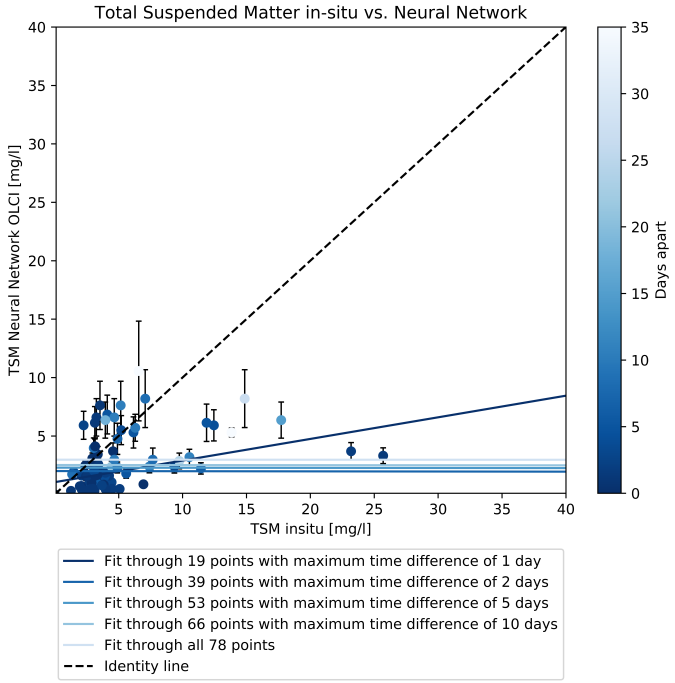

Figure 5.9: Regression plots for TSM of OLCI based on the neural network. The black line represents the identity line. The blueness of the markers represents the time difference between the match-up data points. The darker blue the dot is, the smaller the time difference was between the time of the in-situ measurement and the satellite overpass. The blue lines represent linear least square fits to the points based on time constraints specified in the legend.

Table 5.4: Statistics of the regressions estimated in Figure 5.8. The best values for the different statistics are marked blue.

TSM_NN	Slope	Intercept	r-value	p-value	std-dev
Line 1 day apart	0.1850	1.0460	0.1761	0.4644	0.2472
Line 2 days apart	-0.0033	1.9969	-0.1595	0.3322	0.0013
Line 5 days apart	-0.0010	2.2881	-0.0959	0.4945	0.0014
Line 10 days apart	-0.0007	2.5146	-0.0613	0.6244	0.0015
Line through all points	-0.0002	2.9697	-0.0136	0.9060	0.0017

5.1.5. Boxplots

To investigate the spatial variability of the standard OLCI products, boxplots were created for a 3x3 pixels area. Pixels of OLCI were extracted for all of the MWTL locations. These boxplots can be found in Appendix E. The orange line indicates the mean value within a box, the box is defined by the first and third quartile. The whiskers indicate value of 3x standard deviation. The points that are outside the whiskers can be considered as outliers. The sample number indicated on the x-axis is the number of times valid pixels were found and a boxplot was made. This number is very dependent on the flags used to filter the erroneous pixels. For all of the three data products not enough observations were found at W2 location therefore it is left out.

Boxplots Chl neural network

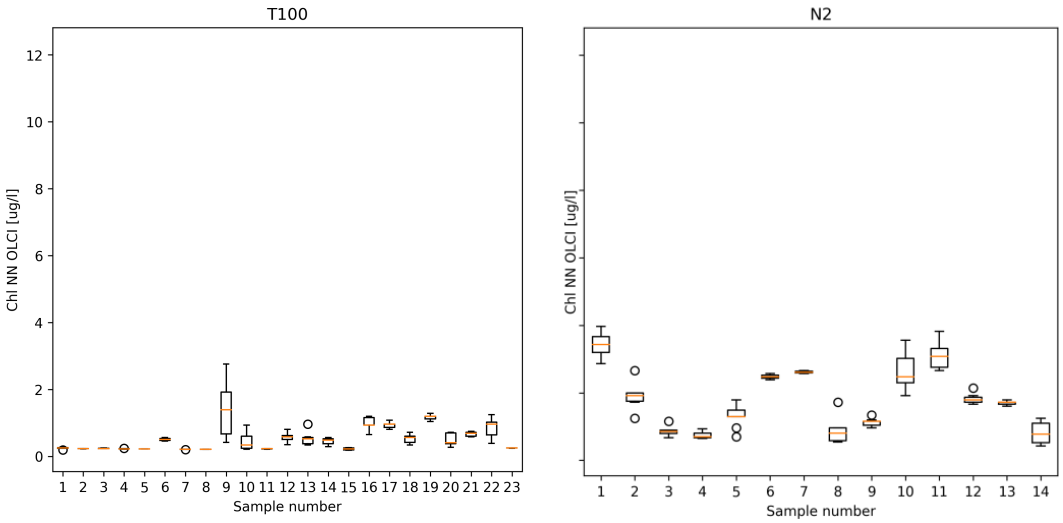

Figure 5.10: Boxplots of chlorophyll neural network for 3x3 pixels around location T100 on the left and for N2 on the right.

The first thing to note when looking at the boxplots for the CHL_NN data product is that there is a very large difference in number of samples that is obtained for each of the stations. The least number of samples found is for station G6, it had 5 samples. The most number of samples found is at station T235, it had 35 samples. This is interesting to note, since it means that certain locations are more often flagged as invalid than others. For CHL_NN this is mostly the case for stations G2, G6, and R3. These stations are coastal stations.

Another point to note is the variability in mean values between the different stations. As noted also before, the offshore stations have lower mean values than the coastal data points. For stations further than 50 km from the coast, the mean values of most boxplots is just above 0. For stations less than 50 km from the coast the mean values of the boxplots is very variable. This mean that some points are more sensitive to temporal differences like tides, winds and river discharge changes.

The length of the boxes determines the variability within the 3x3 pixel area. For some locations this box is often very small or not even visible. This means that all values in the 3x3 box have the same value and that the spatial variability for that point is approximately 0 per kilometre. This is the case for stations N70, T50, T100, T135, T175, T235 and W70. These stations are located more than 50 from the coast. For locations closer to the coast, the boxes are often longer, especially N2, N10, N20, T4 and T20 have this. The stations that have suddenly 1 tall box are considered as exception boxplots. This is seen for N10, T4, T10, T100, and T135.

Boxplots Chl OC4Me algorithm

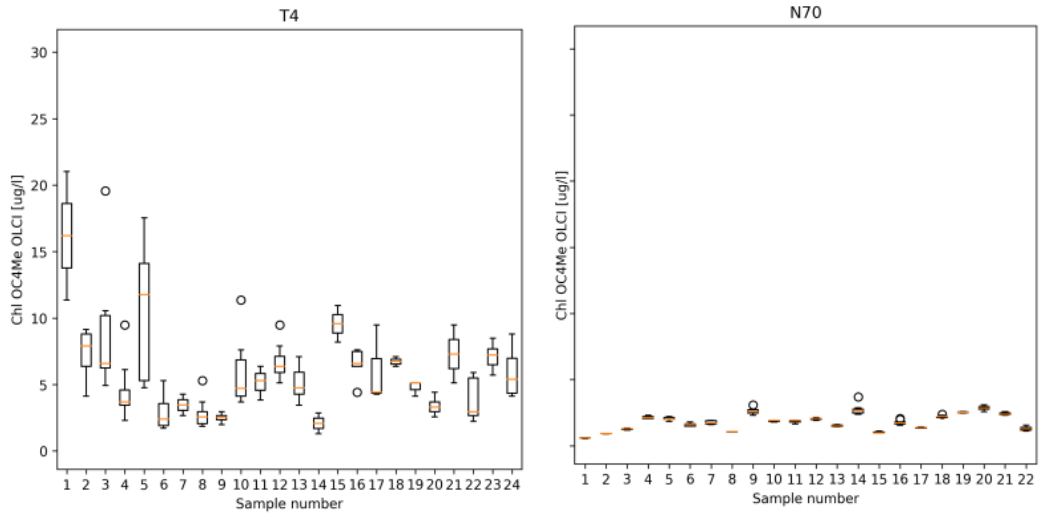

Figure 5.11: Boxplots of chlorophyll OC4Me for 3x3 pixels around location T4 on the left and for N70 on the right.

For the Chl OC4Me data product, boxplots were created at all the MWTL locations except W2 as well. The first thing to notice again is that for the same coastal stations, fewer samples are available. Especially G6 and R3 have only 3 and 6 samples respectively. This means that the pixels at those stations are filtered out more often than pixels at other stations.

It is interesting to see the large difference in boxplot size between the coastal and open water stations for the OC4Me algorithm results. For all stations further than 50 km from the coast the size of the boxes is almost 0. For the stations less than 50km away from the coast the boxplot size is very variable. This means that the OC4Me algorithm gets very variable results for each kilometre (each pixel) at the stations close to the coast.

Comparing the OC4Me boxplots with the boxplots of the CHL_NN products, we see that the neural network produces more outliers at all of the MWTL locations. These outliers are indicated by the circles. This means that the neural network is less stable than the OC4Me data product.

Boxplots TSM neural network

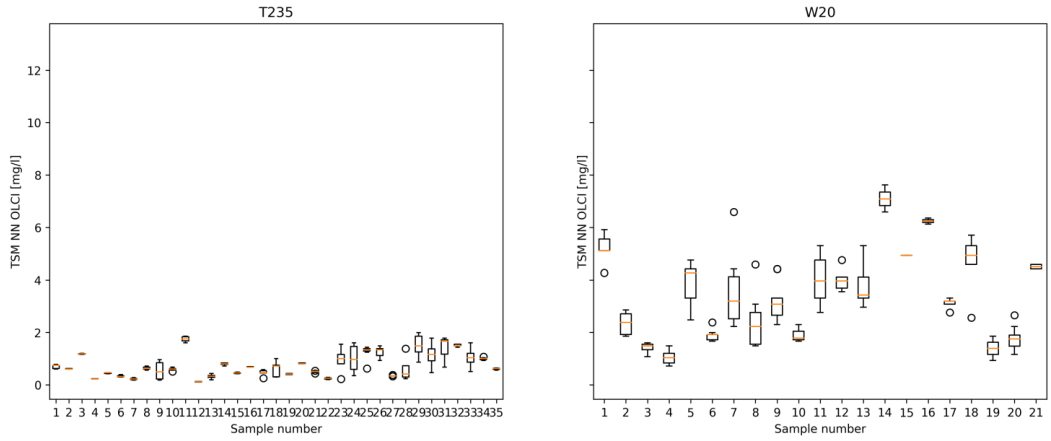

Figure 5.12: Boxplots of TSM for 3x3 pixels around location T235 on the left and for W20 on the right.

Also for the TSM data product boxplots were created of the 3x3 pixels extractions at all of the MWTL locations. Again we can notice that the number of samples at the stations close to the coast is less than the number of samples at stations further away from the coast. This means that for the TSM product also pixels are filtered out faster at the coastal stations.

The TSM concentration are a lot lower for the open water stations (>60km for the coast) then we stations closer to the coast. An average value of approximately 1 g/l is observed for the stations N70, T100, T135, T175, T235, and W70. It is logical that these stations have lower values of TSM since these are further away for river discharges and less influenced by winds or tides because the sea bottom and sediments are most probably deeper. The stations very close to shore (<10km) have average values of 6 g/l.

The spatial variability within the 3x3 pixel boxes is largest for stations T4. At almost all the samples the boxes have a length of approximately 1 g/l. This means that there is a deviation of 1 g/l per kilometre around station T4. For the other stations this is less. Comparing the spatial variabilities of chlorophyll data products with the TSM products, is that the spatial variability of the neural network products (CHL_NN & TSM_NN) is a lot less than of the OC4Me algorithm product but have more outliers. This could mean that the OC4Me data product is more precise than the neural network products and is also more stable.

5.1.6. Conclusions OLCI Chl & TSM

When looking at all the results of the data products CHL_NN, CHL_OC4Me and TSM_NN it can be concluded that the CHL_NN product performed the best when a time limit of maximum 1 day between the in-situ measurement and satellite overpass was applied. Unfortunately, too few match-ups were found to compare in-situ and OLCI data within the 2 hour frame time difference. Interesting to notice is that the data products of OLCI have improved with the second processing line, but more improvements are needed to make the products reliable.

When looking at the maps created in Figure 5.1 and 5.2 it was noticed that areas around the edges of clouds and coasts are most difficult to determine the Chl and TSM content. Especially in the neural network products this was visible. Another interesting point to mention were the filtered pixels in the OC4Me data product. For many maps, a large part of the coastal area was flagged as invalid.

The boxplots of the three data products showed largest spatial variability for stations close to the coast (<50km). The OC4Me dataset shows less outliers than the neural network data products but has a larger spatial variability and can thus be said to be more precise than the neural network datasets.

5.2. Water-leaving reflectance

The chlorophyll and TSM products are created through the water-leaving reflectance products of OLCI. It is therefore important that the water-leaving reflectance is verified as well. In order to do so, the water-leaving reflectance products of OLCI were first converted to water-leaving radiance to make it possible to compare this with the water-leaving radiance measured at the AERONET-OC station. First 1 pixel coinciding with the location of the AERONET-OC station was extracted for the data between 9 July and 20 October. Five match-up pixels were found after filtering the invalid pixels and keeping a time difference of maximum 2 hours.
The results of this study are shown in Figure 5.13. When we look at the match-up data, we see that the spread for OLCI values is very high for the blue and green bands. The water-leaving radiances determined by the AERONET-OC station vary a lot in the green band and one pixel in the blue band (412.5 nm). The NIR infra-red bands (865 nm and 1020 nm) bands correlate well with the AERONET-OC normalised water-leaving radiance. Error bars used for the OLCI data product were not recommended to be used since they are not validated and calibrated yet. This is also visible in the plot. The error bars seem to be unrealistically large. For the AERONET-OC normalised water-leaving radiance product no uncertainty was specified, therefore there are no error bars shown in the x-direction. The AERONET stations are calibrated every 2 years and therefore we can assume that the uncertainty of the AERONET water-leaving radiance is smaller than the errors presented for OLCI in this plot.

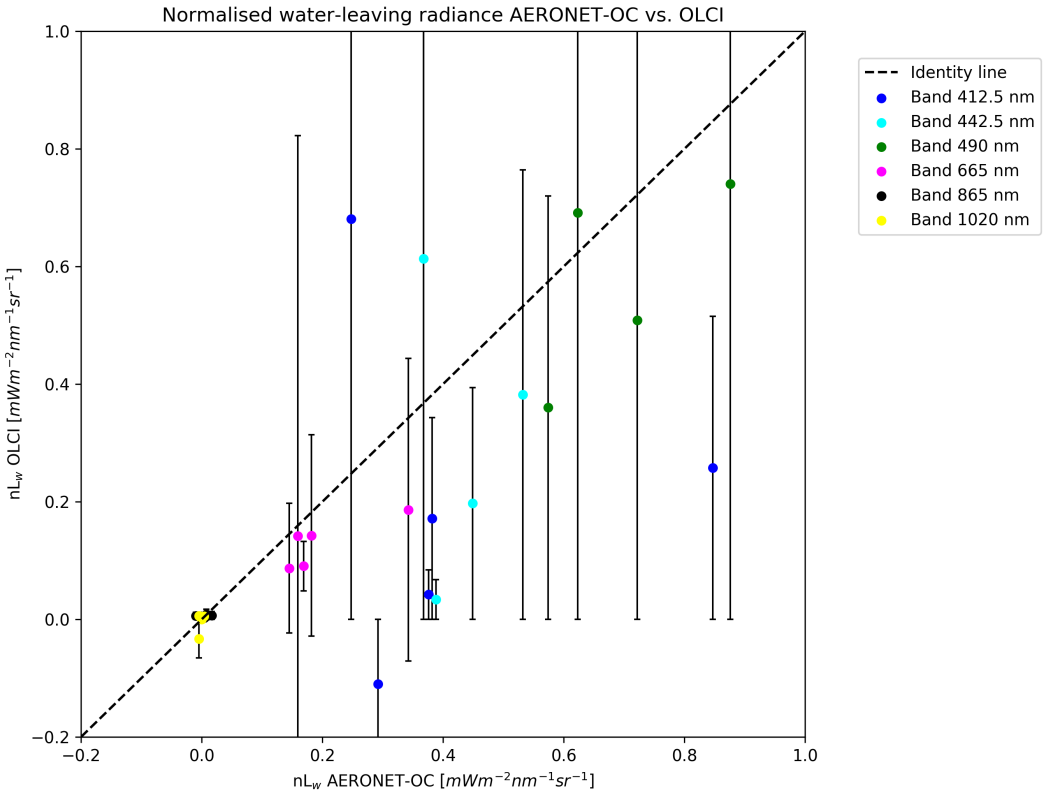

Figure 5.13: Comparison plot of the water-leaving radiances for different wavelengths represented in different colours. On the x-axis the normalised water-leaving radiances determined by the AERONET-OC Thornton station are given. On the y-axis the normalised water-leaving radiances of the matching pixels at the Thornton location of OLCI. The dashed black line represents the identity line. The coloured lines represent the linear least square fit of the data points in colours of the match-up points.

The match-up data spectra were also compared in total. For the single pixel case, just 5 match-us were found. The spectra of these 5 match-ups are found in Figure 5.14. The spectra vary between the different days. Overall the spectra have a promising shape for water-leaving radiance. For almost all days count that OLCI underestimates the normalised water-leaving radiance. This can be seen as a bias in OLCI's . Only for 20 July there is an overestimation in the blue and green bands of OLCI. The plot for 19 September shows the biggest difference between OLCI and AERONET-OC. Comparing this plot to the other plots, it was noticed that the estimated nL_w of AERONET-OC station Thornton measured on this day is very high.

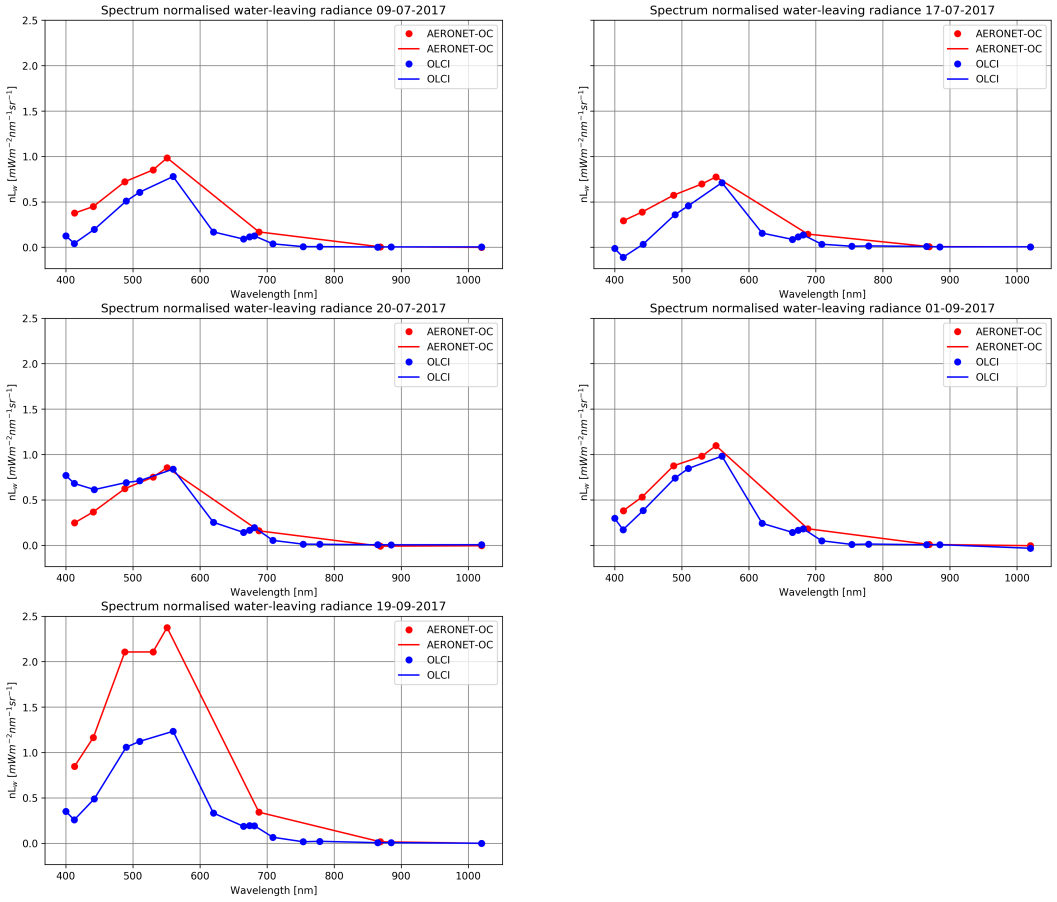

Figure 5.14: Normalised water-leaving radiance spectra for 5 match-up cases. In blue the OLCI is given, in red the AERONET-OC. The dots represent the centre of the measurement bands wavelength. Important to notice is that some of OLCI's bands do not consist as measurement bands for the AERONET-OC instrument and the other way around.

5.2.1. Conclusions nL_w

Concluding from the regression plots in Figure 5.13 we can say that the variability of OLCI data is very high for the blue and green bands. The red and NIR bands of OLCI correlate well with the AERONET-OC values for this band. Since the atmospheric correction (AC) and the AOT estimation of OLCI is based on the NIR bands we expect that the AC has performed well.

5.3. Aerosol Optical Thickness verification

The AOT determined by OLCI was compared with the AOT measured at the AERONET-OC station Thornton, and with MODIS data for the period starting from 7 July 2017 until 20 October 2017. Maps, time series and regression plots were created to compare the different data sets. The flags (section 4.1.1) were applied to the OLCI data. The results are discussed in this section.

5.3.1. Maps

Figure 5.15 presents a map of the OLCI AOT product for 14 June 2017 and 9 July 2017. Interesting to note is the difference in aerosol content between both images. The map of 14 June has values ranging from 0.06 to 0.80 while the map of 9 July shows values ranging between 0.03 to 0.15. According to [32] the values for 14 June are very high and for Dutch coastal waters the AOT is supposed to have values between 0.05 and 0.30.

Another thing to note is the spatial pattern. In all OLCI AOT data products, the AOT value seem to be very high on the coast, near land, and near clouds. Especially in the map of 9 July this is remarkable. The pixels at the Afsluitdijk and Houtribdijk show unrealistic high values. As was also seen in the Chl and TSM maps high values appear near the Maas and Westerschelde drainage area. It seems this area causes problems in the

investigated data products CHL_NN, CHL_OC4Me, TSM_NN, and AOT.

To see if MODIS AOT maps were similar to OLCI's AOT maps a MODIS AOT map was created for 9 July 2017 as well. This map is shown in Figure 5.16. An interesting thing to note is the fact that MODIS leaves out coastal pixels. Therefore there is almost never data available for the coastal measurement locations. This is an interesting point since one of the problem areas of OLCI's AOT was the coastal area. It might be that MODIS has the same difficulties in determining the AOT at coastal locations as OLCI, but that these erroneous pixels are left out in this product. The pixels for which the AOT was determined have similar values to those of the OLCI data products.

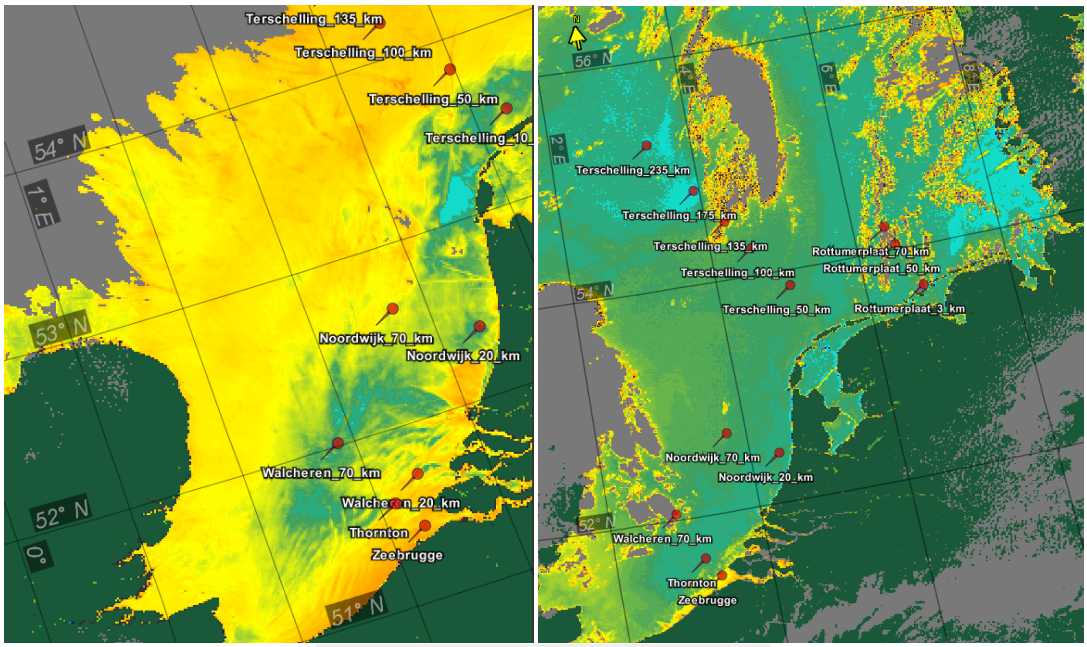

Colour	Value
	0.005
	0.011
	0.027
	0.062
	0.146
	0.341
	0.798
	1.867
	4.368

Figure 5.15: OLCI maps of the aerosol optical thickness for 14 June on the left and 9 July 2017 on the right. Indicated with red pins are some of Rijkswaterstaat's measurement locations and the AERONET-OC station Thornton and Zeebrugge. The colours in the legend represent different values of AOT, grey are clouds, green is land. (Copyright 2017 EUMETSAT)

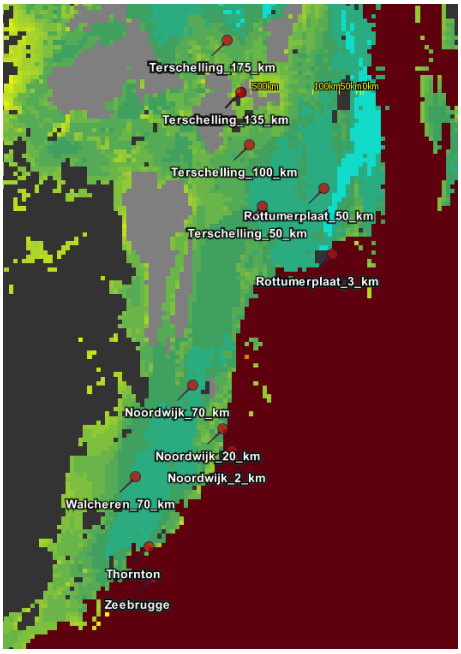

Figure 5.16: MODIS map of the AOT. The same colour scale as for the OLCI AOT maps was used. The MODIS data product does not contain a cloud or land mask and therefore it is very unclear if MODIS detects those differences. In the picture I coloured the Netherlands in maroon and some clouds grey.

5.3.2. Time series AOT

Figure 5.17 shows a time series at the AERONET-OC Thornton station location. Time series of the other MWTL locations are given in appendix B. The time series in the appendix show similar values for AOT of OLCI and MODIS. The AOT is ranging between 0 and 0.6 for both instruments. AOT values ranging between 0.05 and 0.3 is expected for the Dutch coasts, so values above 0.3 seem to be unrealistically high. Figure 5.17 shows that AOT values of OLCI are similar to MODIS' AOT values represented with blue and red dots respectively. But, OLCI seems to overestimate the AOT slightly when comparing it to the AERONET-OC data. Especially the historical AOT data are lower than the OLCI values. The same counts for MODIS data. Regressions between OLCI and AERONET-OC and OLCI and MODIS were created to evaluate this finding in more detail.

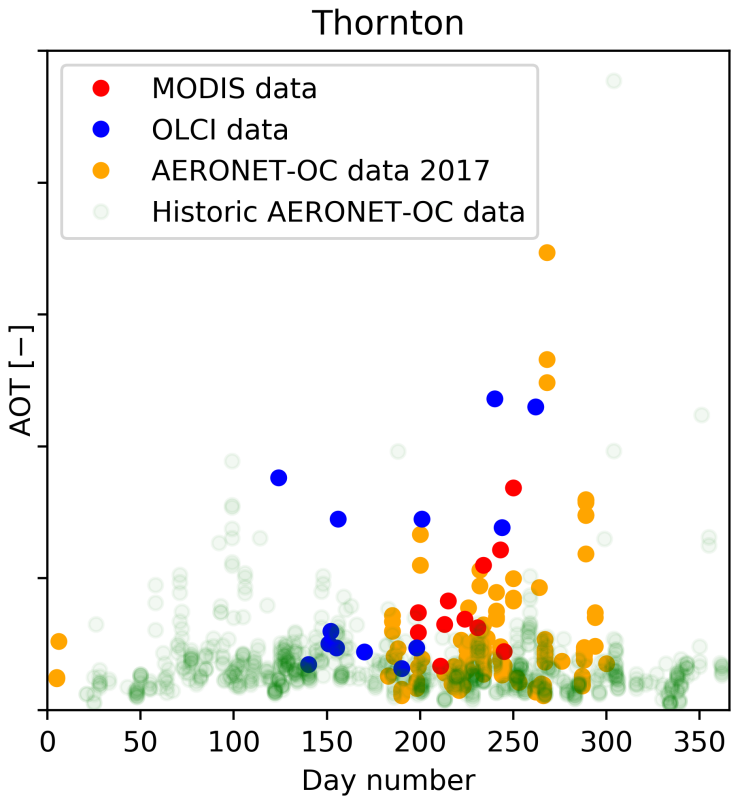

Figure 5.17: Time series of the AOT plotted against the day number for location Thornton. In red MODIS AOT is given, in blue OLCI and in yellow AERONET-OC data of 2017. The historical AERONET-OC data is indicated with green transparent dots.

5.3.3. Regression between OLCI and AERONET-OC station Thornton

OLCI's AOT observations are very high compared to the AERONET values. Figure 5.18 shows a scatter plot. In this scatter plot a box of pixels at the Thornton AERONET-OC station from the OLCI data between 7 July and 20 October were extracted. Comparing the date and time of the OLCI and Thornton station data, match-ups were found. A timeslot of 2 hours was used to find matching data. Invalid or flagged pixels were filtered out. The dashed black line indicates the 1-to-1 line. Only 5 match-ups were found, these were the same match-ups as were found in the water-leaving regression part.

From this plot we can clearly see that the AOT OLCI values are a lot higher than the AOT values determined by the AERONET-OC station. For a clear cloud day the values seem to be lower, but still higher than the value found at the AERONET-OC station. To investigate the spatial variability boxplots were created at the MWTL stations and the Thornton station for a pixel extraction of 3x3 pixels. This is shown in the next part.

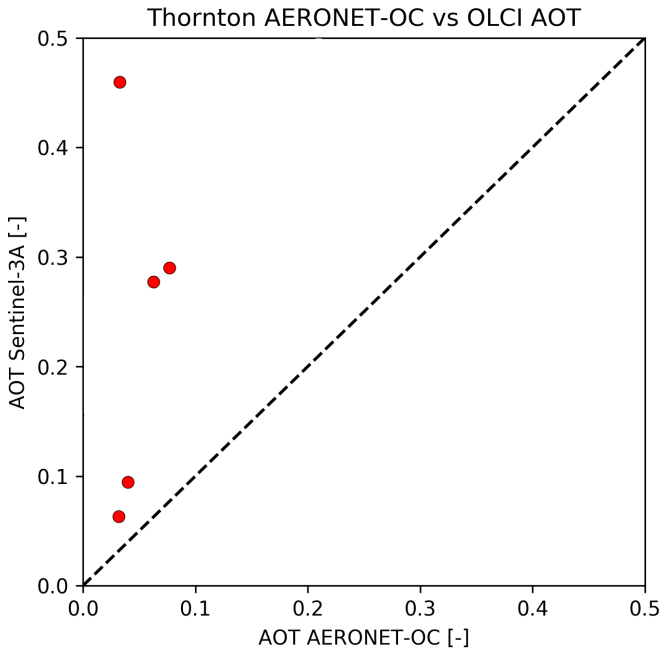

Figure 5.18: Comparison plot of the aerosol optical thickness. On the x-axis the AOT values determined by the AERONET-OC Thornton station are given. On the y-axis the AOT values of the matching pixels around at the Thornton location of OLCI are given.

5.3.4. Regression between OLCI and MODIS

The main idea in this thesis was to compare OLCI AOT values with AERONET-OC measurements only, but the results were very disappointing. To have a second investigation of OLCI's AOT data product, it was compared with MODIS AOT data. This analysis was done at the MWTL locations. The mean of 3x3 pixels was calculated for the OLCI data to compensate for the spatial resolution difference of 1.1 km for OLCI and 3 km for MODIS. Regressions were obtained between OLCI and MODIS using different time constraints between the match-ups to investigate which time difference was most suitable. These regressions are shown in Figure 5.19. This Figure shows that the difference between AOT OLCI and AOT MODIS increases with an increasing time difference and that the best fit is obtained using a time difference of maximum 2.5 hours.

Figure 5.19 also shows that OLCI's AOT values show a large variability for the lower AOT values measured by MODIS, this spread decreases with increasing AOT values of MODIS AOT values. The table in table 5.5 confirms this. The slope of 0.81 and intercept of almost 0 imply a regression line very close to the identity line. The r-value and p-value are very promising as well. The standard deviation of the match-ups with a maximum time difference of 2.5 hours apart appears to be high. The match-ups with a maximum time difference of 2.5 hours apart were investigate further in detail.

Figure 5.20 shows the regression between OLCI and MODIS for the match-ups with a time difference of maximal 2.5 hours apart. To show the difference between the 3x3 pixels extracted from the OLCI data, error bars of the standard deviation within the 3x3 pixels were plotted as well. For some points it is shown that the standard deviation is almost 40%. This means that the AOT of OLCI could differ with 40% within an distance of 1 km. For some match-ups the standard deviation was very small or 0 which means that all pixels within the 3x3 box had the same AOT value. The uncertainty of the MODIS aerosol product was not specified. In the MODIS product there are different levels of AOT products. In this research we used the average AOT data product. In order to get some idea about the uncertainty of MODIS AOT product I subtracted the average AOT product from the best AOT product. This difference I used as error bars for the MODIS product. The uncertainty is very small and therefore the error bars in x-direction are almost invisible.

Table 5.5: Statistics of the regression between OLCI and MODIS AOT. The best statistical results are indicated with orange.

AOT	Slope	Intercept	r-value	p-value	std-dev
Line 2.5 hours apart	0.81	0.02	0.58	0.00	0.26
Line 12 hours apart	0.39	0.09	0.47	0.00	0.11
Line through all points	-0.11	0.25	-0.03	0.69	0.27

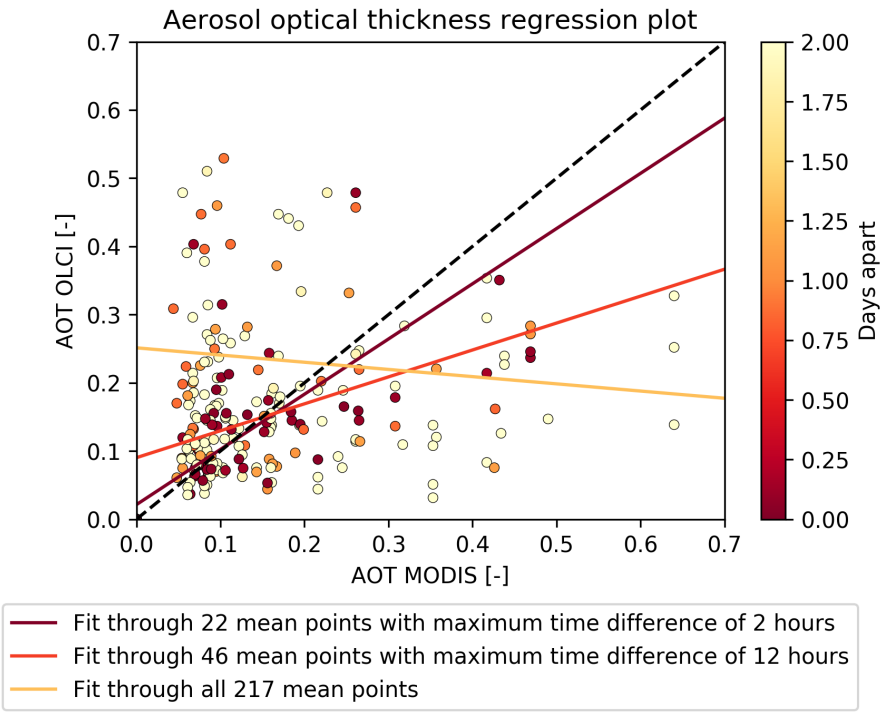

Figure 5.19: Comparison of AOT OLCI on the y-axis with AOT MODIS on the x-axis. The identity line is represented with the black dashed line. The match-up data were represented in different shades of orange to show different time constraints used as explained by the legend at the bottom of the figure. Linear least square error estimation was used to find best fitting lines.

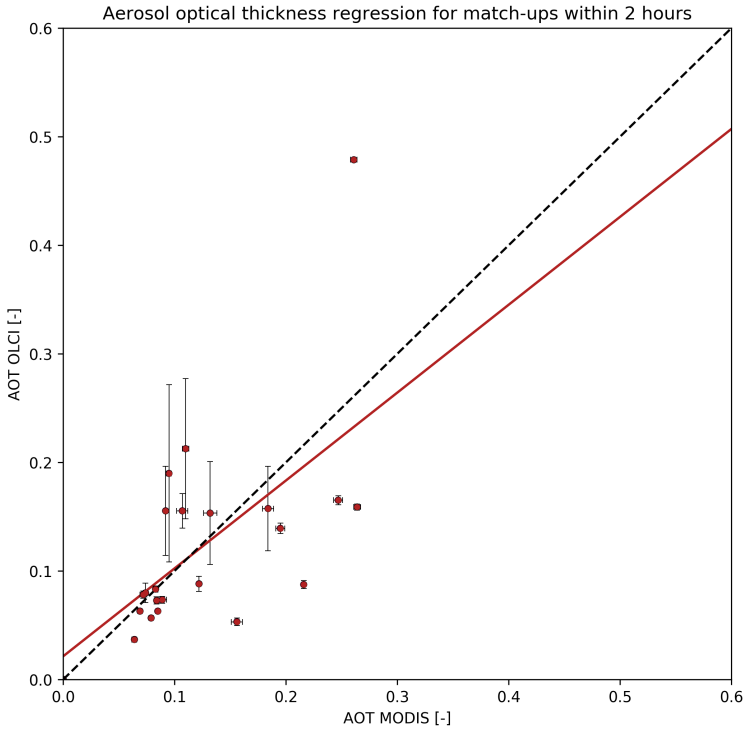

Figure 5.20: Match-up data with a time difference of maximum 2.5 hours. The error bars represent the standard deviation of the 3x3 pixels box. The red line shows the best linear least squares fit, the dashed line represents the identity line.

5.3.5. Boxplots OLCI AOT

To get better insight in the spatial variability of the AOT data product, boxplots were created in the same way as for the Chl and TSM data products (section 5.1.5). These boxplots are presented in Appendix F. In Figure 5.21 two boxplots are shown at two measurement locations.

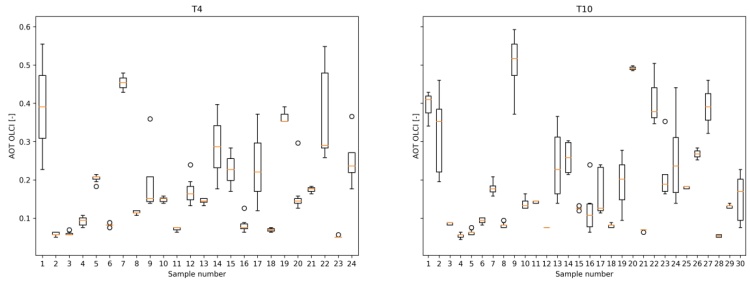

Figure 5.21: Boxplots of the aerosol optical thickness for 3x3 pixels around location T4 on the left and for T10 on the right.

The boxplots confirm that the spatial variability for a 3x3 pixel area is very large for all of the MWTL locations. Fewer samples are found for the coastal stations, G2, G6 and R3. This is an interesting point because it was also observed for the CHL_NN, CHL_OC4ME, and TSM_NN data products.

Another point I would like to mention is the maximum value of 0.6 which is never exceeded, but reached often. A value of 0.6 for the AOT is not realistic for the North Sea when looking at previous researches and literature. The different mean values of AOT at the MWTL locations show that there is a very large temporal variability between the different satellite images as well.

5.3.6. Conclusions OLCI AOT

The resulting maps of OLCI AOT shown in Figure 5.15 presented a large variability in AOT values within the area of research. The regression plots and boxplots confirm this. OLCI's spatial variability seems to be unrealistically large with differences up to 40% per kilometre. What was also noticed in the maps, was the fact of unrealistic values of AOT around cloud edges and coasts. This was earlier observed in the Chl and TSM maps as well.

The regression plot of OLCI and AERONET showed that the values of OLCI are very high. This was also noted in the time series. For clear weather days, with no clouds, OLCI's AOT values are more realistic compared to AERONET, but are still very high.

The regression plots between OLCI and MODIS data show more promising results. When the time difference between overpass times is kept to a maximum of 2.5 hours, a well fitting regression was found with a slope of 0.81 and an intercept of almost 0. The r-value and p-value of this regression were also promising. One thing to note about this regression was the large spatial variability in OLCI data. Error bars of the standard deviation showed this in Figure 5.20. Another thing to mention is the large spread in AOT values for both OLCI and MODIS. OLCI has AOT values up to 0.6 and MODIS up to 0.65 while AERONET showed only values up to 0.1.

6 Discussion

This chapter discusses the results presented in the previous chapters. Points of discussion include improvements in the data processing and comparison manners. Also difficulties are explained which came across during this thesis project.

6.1. Data selection

To obtain the comparison results shown in chapter 5 many choices and decisions on the selecting of valid data were made. Some of these decisions were crucial and are therefore discussed in this paragraph.

6.1.1. Applied filters

Many filters were applied to leave out erroneous and invalid data pixels (paragraph 4.1.1). These filters were recommended by the Sentinel-3 Validation Team. After applying those filters approximately 15% of all OLCI data could be used for the validation. Research of the filters and which one to apply for a certain area could increase the amount of data that can be used to validate the Sentinel-3 data product. This was not done in this research.

6.1.2. Time constraints

Time constraints were applied in order to find match-up data. For chlorophyll this was done per hour to see when a sufficient regression was reached. This point was reaches with a time difference of 1 day maximum. A time difference of 1 day does not seem reasonable taking into account tides, river discharges and winds which have a time frame of a few hours. Figure 6.1 shows modelled tidal ranges for the Dutch North Sea at different measurement locations corresponding to Figure 1.2. The different colours represent tides at a certain measurement location. The Dutch coast has a meso-tidal to macro-tidal environment. For example the plot on the left hand side shows the tidal range at measurement location W2 and W70. Match-up data for OLCI CHL_NN with in-situ measurements were found at these locations indicated in red and green respectively connected with a black line. This representation is shown for 4 days on which match-up data with a maximum time difference of 1 day was found. When the tidal range is very large and has a period of approximately 6 hours it does not seem reasonable to compare data points with a time difference of more than a few hours. Especially when the tidal range is very large as it is for most coastal stations. The same counts for river discharge and wind speeds. More research into the maximum valid time difference between in-situ measurement and satellite overpass could improve verification results.

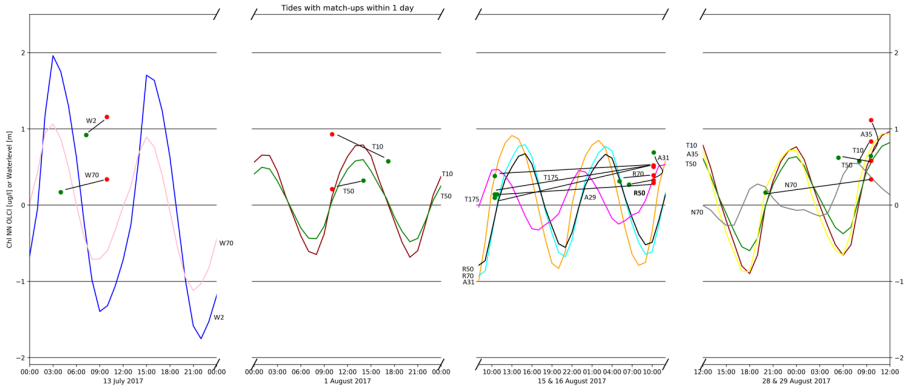

Figure 6.1: Tidal range at certain measurement locations as indicated. The different colours represent water levels dependent on the tide at a certain location. Coastal stations have a larger tidal range than off-shore stations. Points that were found as match up data between OLCI CHL_NN and in-situ measurements are shown in red and green respectively and are connected with a black line. When the time difference between match-up data becomes too large the tide and thus movement of water can have moved Chl or TSM contents. The tide at coastal stations is very strong therefore it is extremely important for these stations to have a small time difference between the match-ups.

6.1.3. Spatial variability

To investigate the spatial variability an area of 3x3 pixels around the Rijkswaterstaat measurement locations was used. A larger area of pixels should be investigated as well in order to say more about the spatial variability and the general spatial patterns in the area of research.

In this research coastal and offshore stations have not been separated in the comparison studies. Therefore it is unclear to say where the offshore stations or coastal stations of OLCI perform better results. More research should be done on the different results of coastal or offshore stations in order to take the Case-1, Case-2 water division into account. Furthermore, the spatial patterns are not further investigated such as the Thames river discharge (paragraph 2.3). This special case should be studied in more detail to investigate the validity of OLCI data products for extreme values.

6.2. Comparison results

Different comparison results were shown. The findings of these results will be discussed in this paragraph.

6.2.1. Number of match-ups

For the verification of chlorophyll and TSM regression plots were created. Chlorophyll and TSM can change quickly through time by tides, river discharge and wind. Therefore it is important to find match-up data with a small time difference. The idea was to use ADHOC data for this which was obtained at satellite overpass. Rijkswaterstaat took 21 ADHOC measurements in the time frame between 8 May 2017 and 21 September 2017. These ADHOC measurements were randomly taken during the regular measurement cruises. At all available OLCI data files the ADHOC measurement locations were extracted. Following to this the cloudy and invalid pixels were removed which ended in 3 valid match-ups. These 3 match-ups were compared in paragraph 5.1.3. In order to create more match-ups the time difference between in-situ measurement and satellite overpass was increased. For the chlorophyll neural network dataset this lead to a very promising regression line between in-situ measurements and OLCI data which were maximally 1 day apart. This regression line was based on 15 points only and therefore we have to mention here if it is reasonable to create a regression between 15 points only. On a longer time scale more Sentinel-3 data and in-situ measurements will be collected to compare. The standard deviation of these points is still very large which imposes that the spread of values is averaged out.

6.2.2. Different measurement techniques

In this research the results of many different measurement techniques have been compared. We have to keep in mind that the data is obtained in different ways. The OLCI chlorophyll and TSM data products are based on atmospheric correction water-leaving radiances whereas the in-situ measurements derive chloro-

phyll and TSM directly from water samples. Other researches compare water-leaving radiance products and not the water constituents. More research should have been done on the water-leaving radiance product of OLCI.

The same counts for the comparison between OLCI and AERONET-OC. AERONET-OC is a ground-based station measuring the water-leaving reflectance and aerosol optical thickness (AOT) directly whereas OLCI derives those products through algorithms and processing techniques. The comparison done between MODIS and OLCI is the only one comparing the same measuring techniques, both remote sensing. This comparison also gave the best results. This could mean that OLCI and MODIS have the same problems in obtaining the AOT. Or it could mean that comparing remote sensing techniques with other measurement techniques is not a sufficient way of verification of remote sensing data.

Another point to mention is the depth at which the water samples were taken. The chlorophyll and TSM products of OLCI were compared to water quality measurements taken at a depth of approximately 3 meters. We could question if chlorophyll and TSM at a water depth of 3 meters is the same as at the water surface from where OLCI obtains the chlorophyll and TSM concentrations.

6.2.3. Uncertainty of the data

To conclude about the validity of OLCI's data products it was important to know the uncertainty of the reference data to which OLCI data products was compared. The uncertainties of some of the datasets were not clear. This caused challenges in this comparison study. Especially for the in-situ measurements of Rijkswaterstaat it was difficult to find the error or uncertainties in the data product. An uncertainty of 23% was found for the chlorophyll measurements obtained in the laboratory. For the TSM measurements no uncertainty could be found for the data products. Besides the laboratory uncertainties there are other error that should have been taken into account such as the sampling water depth, weighing uncertainties and storage uncertainties. These uncertainties could not be found and are therefore not taken into account. Rijkswaterstaat should be more clear about the uncertainties in the data that they provide.

For AERONET-OC Thornton no uncertainties were stated in the normalised water-leaving radiance and AOT product. From literature studies I found out that the uncertainty in AERONET-OC data is very small, because the instrument is calibrated every two years.

The uncertainty of the MODIS data product was determined by determining the difference between the average aerosol optical thickness product and the best aerosol optical thickness product. These differences were very small that error bars were almost invisible in the comparison plots. The reliability of using this difference as uncertainty estimation should be investigated.

For almost all OLCI Level-2 data products an error is included in the dataset. The Sentinel-3 validation team does recommend not to use these error products yet, because they are not calibrated and validated yet. The error product of the water quality constituents showed an uncertainty of approximately 14%. The uncertainty of the water-leaving radiance products was very large and might be unrealistic when comparing it to the standard deviation within the different bands. The uncertainty of the AOT product was determined by taking the standard deviation of 3x3 pixels. This standard deviation was sometimes very large and reached up to 40%.

6.2.4. Processing lines

Two different processing lines took place during the time frame of this research. The data products of the different processing lines are treated separately in this thesis. Every time a new processing has been applied to the Sentinel-3 OLCI data a new validation should take place. The problem is that the amount of data which can be used for validation is decreased again. In the future data products processed with the old processing lines will be reprocessed again. Once this is finished a validation research has to be done again.

6.2.5. Clouds

In this research clouds seemed to have a large influence on the comparison results. Pixels close or near clouds always showed unrealistic high values in the water constituent products and in the aerosol optical thickness product. Especially this seemed to be a problem in the aerosol optical thickness product. This is shown in Figures 6.2, 6.3, and 6.4. This imposes that the cloud mask used in the OLCI data products is not strict enough.

It seemed that when a pixel was not flagged as cloud, it added value to the AOT product. For next researches it might be better to leave pixels close to clouds out of the comparison in order to avoid this error.

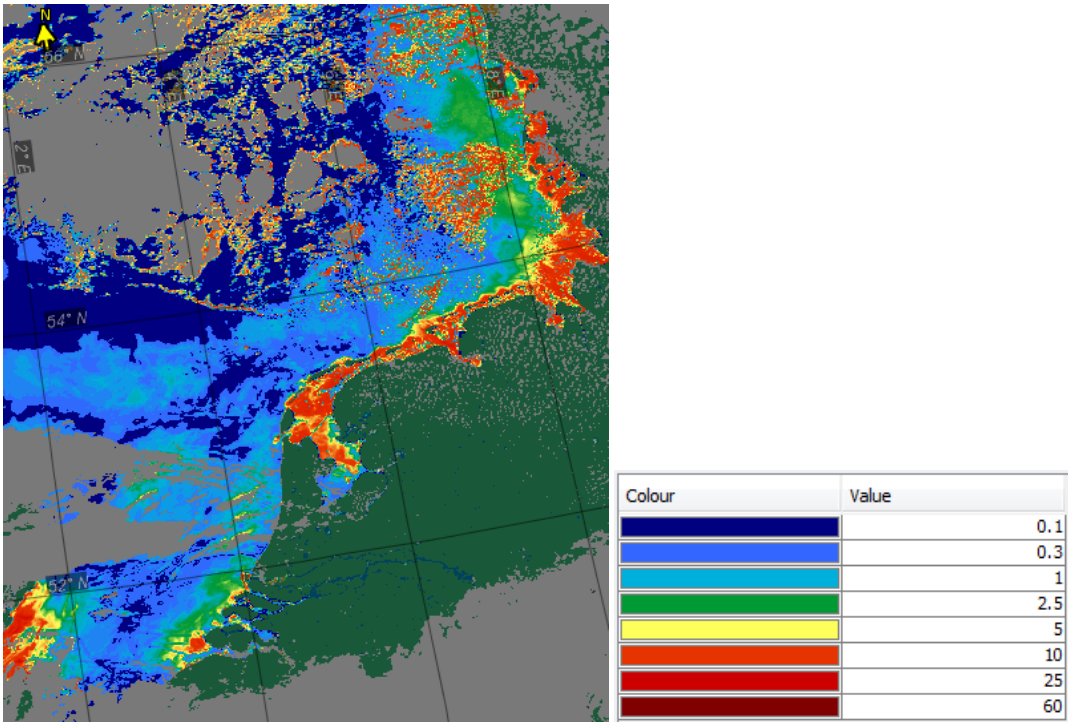

Figure 6.2: Map of the chlorophyll neural network product of OLCI for the Dutch North Sea on 17 July 2017. Colours indicate different chlorophyll contents in μg/l. Red is a high chlorophyll content, blue a low chlorophyll content. The land mask is presented in green, the cloud mask is given in grey. This map was created to show the high chlorophyll value around clouds. Especially in the North of this map at 56° latitude the effect is clearly visible. (Copyright 2017 EUMETSAT)

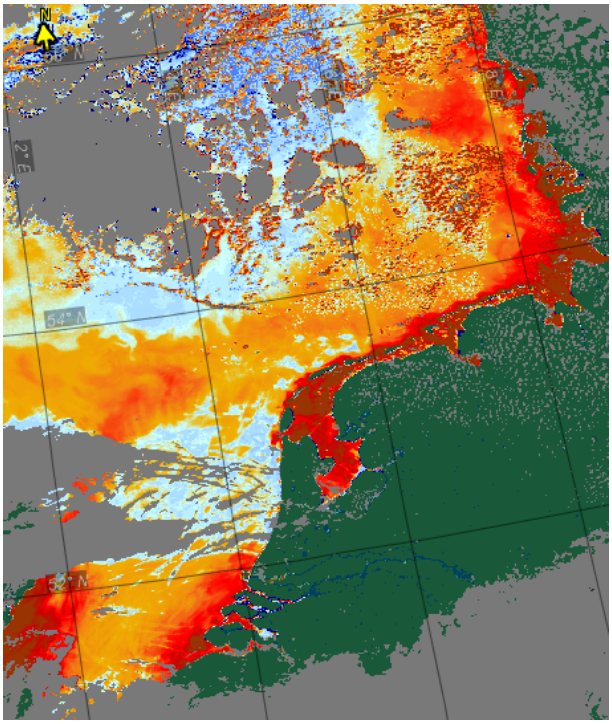

Colour	Value
	0.067
	0.143
	0.302
	0.65
	1.35
	3
	7
	15
	30

Figure 6.3: Map of the TSM neural network product of OLCI for the Dutch North Sea on 17 July 2017. Colours in the legend represent TSM values in mg/l. OLCI's land mask is given in green and the cloud mask in grey. The map shows that TSM values are high around the edges of clouds as was also shown for chlorophyll in the previous figure. It especially seems a problem in areas with very thin clouds such as the area around 56° latitude. (Copyright 2017 EUMETSAT)

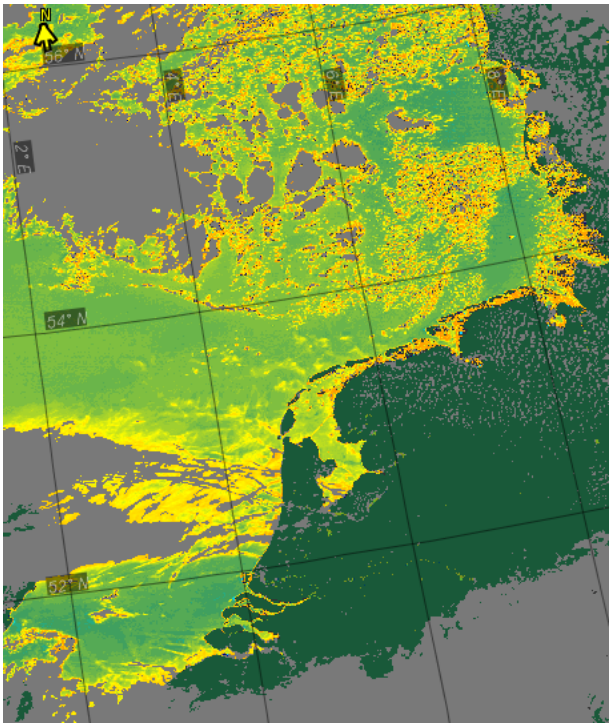

Colour	Value
	0.005
	0.011
	0.027
	0.062
	0.146
	0.341
	0.798
	1.867
	4.368

Figure 6.4: Map of the AOT product of OLCI for the Dutch North Sea on 17 July 2017. Colours in the legend represent AOT values. The land mask is given in green and the cloud mask in grey. From literature studies we know that AOT values ranging between 0 and 0.3 are expected in Dutch coastal areas. The values near clouds exceed these values. The cloudy area between 54° and 56° latitude shows unrealistic values of above 0.8. (Copyright 2017 EUMETSAT)

7

Conclusions & Recommendations

From the results shown in chapter 5 and the discussions in chapter 6 final conclusions were made. The conclusions are described in this chapter by answering the initial research questions, the elaborated research questions and the main research question. At the end of this chapter further research recommendations will be presented.

7.1. Answers to the initial research questions

The initial research question were formulated to gain knowledge on water quality monitoring using remote sensing. Answers to the initial questions were mainly found in chapter 1, 2 and 3. Their answers are presented in this paragraph.

Part 1: Evaluation of the chlorophyll and TSM product:

- *What is water quality?*
  The term water quality was explained as the suitability of water for a particular purpose. In this thesis I looked at the North Sea and therefore water quality can be seen as the status of North Sea ecosystem. Certain types of flora and fauna can become extinct when water quality changes. Two of the main components of water quality are chlorophyll (Chl) and Total Suspended Matter (TSM). Chl and TSM are mainly responsible for the amount of oxygen in water and the transport of nutrients and chemicals. Remote sensing has great potential in monitoring those two parameters and therefore Rijkswaterstaat is interested in the possibilities.

- *What are chlorophyll and TSM and why are those products important?*
  In this research chlorophyll and TSM are two parameters looked at. Chlorophyll is the pigment of phytoplankton which are micro algae. A change in chlorophyll means a change in algae which means a changes in water quality. Also TSM is an important parameter. TSM stands for Total Suspended Matter and is the amount of suspended particles in a litre of water. TSM causes a change in penetration depth of solar irradiance into the water. High TSM alternates light availability for photosynthesis in deeper layers.

- *How are the Sentinel-3 Level-2 chlorophyll, and TSM products created?*
  This study has shown that there are two chlorophyll products available in the OLCI Level-2 data product. One is based on the OC4Me algorithm the other one is based on a neural network. The TSM data product originates from the same neural network as the chlorophyll neural network product. After atmospheric correction the water-leaving radiance is determined and used as input for the OC4Me algorithm as well as for the neural network.

- *What is the precision and accuracy of the in-situ measurements taken by Rijkswaterstaat?*
  To conclude on the validity of remote sensing products it is important to know the precision and accuracy of the in-situ data which is the reference dataset used in this thesis. It was challenging to find an answer to this question. For the TSM in-situ measurements the uncertainty of the measurements was not stated in the datasets obtained from Rijkswaterstaat. Many factors influence the uncertainty

of TSM measurements for example the water depth at which the water sample is taken, the weighing of the wet and dry sediment load. Therefore no error bars where presented in the comparison plots of TSM. For chlorophyll an uncertainty of 23% was found in the datasets provided by Rijkswaterstaat. This uncertainty was provided by the laboratory where the water samples are analysed. We have to keep in mind that there are additional errors to the laboratory errors. Error bars for the chlorophyll comparisons used in the regression plots were based on the laboratory error only.

Phase 2: Verification of the normalised water-leaving reflectance and the aerosol optical thickness:

- *What is normalised water-leaving radiance and why it is important to verify this?*
  The normalised water-leaving radiance is the radiance leaving the water surface. The water-leaving radiance is influenced by the water constituents and can therefore be used to determine the content of those constituents. OLCI's Chl and TSM products are created from the normalised water-leaving reflectance products. It is therefore important to know the quality of the water-leaving radiance products as well. These products were verified by comparing it to the normalised water-leaving radiances of AERONET-OC station Thornton.
- *What is aerosol optical thickness and what is its importance?*
  The AOT is a measure of solar irradiance extinction. The atmospheric correction is important in obtaining correction water-leaving radiances. The AOT is a by-product of the atmospheric correction. The AOT product was compared to AERONET-OC and MODIS observations in order to evaluate the atmospheric correction.
- *How is the aerosol optical thickness Sentinel-3A Level-2 data product created?* The aerosol optical thickness is obtained through a method developed by Antoine and Morel in 1998. It originates from the Clear Water Atmospheric Correction (CWAC). Different aerosol models are fitted at bands 775 nm and 865 nm. The best fitting model is chosen in the atmospheric correction.

7.2. Answers to the elaborated research questions

Research questions which were further investigated in this thesis were called the elaborated research questions. Elaborated research was done to find answers to those questions. Answers to the elaborated research questions are presented in this paragraph.

Part 1: Evaluation of the chlorophyll and TSM product:

- *What is the precision and accuracy of the Sentinel-3A Level-2 reduced resolution data products?*
  The Sentinel-3 OLCI Level-2 data product contains per pixel error products for chlorophyll and TSM. These error products are used as error bars in the regression plots. We have to keep in mind that these error products are not calibrated and validated yet. The chlorophyll neural network product had an average value of 1.34 μg and an average error of 0.29 μg. The percentual error of OLCI's chlorophyll neural network product therefore becomes 21% and thus shows a large spread of data values. For chlorophyll OC4Me an average value of 5.78 μg was found with an average error of 0.73 μg. This results in a percentual error of approximately 12%. The regression plots of Chlorophyll OC4Me show an overestimation of a factor 2 and therefore the OC4Me product is precise but has a large offset. The average TSM value of OLCI is 2.05 mg/l. With an average error of 0.26 mg/l we can stated OLCI's TSM product has a percentual error of 13% and can thus be said to be precise. Comparison between TSM OLCI and in-situ measurements showed that OLCI had unrealistically low values and is therefore not very accurate.
- *What is the correlation between the chlorophyll and TSM Level-2 products and the in-situ measurements of chlorophyll and TSM?*
  From the comparison with MERIS and in-situ climatologies I conclude that the OLCI values of the chlorophyll neural network product seem to be lower than the MERIS and in-situ data. For the OC4Me data product this effect was less. The TSM product showed small underestimation when looking at the time series. Also a strong seasonal component was observed with higher values in the spring month and lower values in the winter months. The difference between the Case-1 and Case-2 waters was noticed here as well. Case-1 water showed lower values for Chl and TSM than the coastal waters. Regression plots were created to quantify those findings. The correlation coefficient between OLCI chlorophyll

originating from the neural network and in-situ measurements with a maximum time difference of 1 day was 0.77. The correlation coefficient between OLCI chlorophyll originating from the OC4Me algorithm and in-situ measurements with a maximum time difference of 1 day was 0.93. This was very high but when we took the slope into account an overestimation of a factor 2 was found of OLCI's OC4Me chlorophyll product. The correlation coefficient between OLCI TSM and in-situ measurements with a maximum time difference of 1 day was 0.18. There was almost no correlation found between OLCI and in-situ for TSM. An underestimation of a factor 4 was found for OLCI TSM as well.

- *What is the spatial variability of the chlorophyll and TSM Sentinel-3A Level-2 reduced resolution data product?*
  Unrealistically high values for chlorophyll and TSM occurred in the maps of the CHL_NN, CHL_OC4Me, and TSM_NN for pixels on cloud edges and near the coastline. From this we conclude that the algorithms to find the Chl and TSM content do not work well for those pixels. In order to get better products, these pixels should be masked. Another interesting feature noticed in the OC4Me maps was the number of invalid flagged pixels in the OC4Me product. Very often it occurred that there were many pixels marked as invalid for a large coastal area.

  Boxplots showed the spatial variability of the OLCI data products at each of the MWTL locations. The boxplots of the three data products showed largest spatial variability for stations close to the coast (<50km). The OC4Me dataset shows less outliers than the neural network data products but has a larger spatial variability and can thus be said to be more precise than the neural network datasets. Another interesting thing concluded from the boxplots was that fewer data samples could be found for the coastal stations than for the stations further from the coasts. This means that the flags filter out these pixels more often. Apparently it means that the algorithms often fail for determination of Chl or TSM in these areas.

Phase 2: Verification of the normalised water-leaving reflectance and the aerosol optical thickness:

- *What is the quality of the normalised water-leaving radiance product?*
  The normalised water-leaving radiance products were verified by comparison of normalised water-leaving radiances of AERONET-OC station Thornton. Regressions were created for the individual OLCI bands with the closest AERONET-OC bands. These regressions showed a large variability for the green and blue bands of OLCI. The red and NIR bands correlated well. Since the Chl and TSM products are partially created by the ratio of the green and blue bands, this can explain the variability in the Chl and TSM data products. For the NIR bands the atmospheric correction and the aerosol optical thickness product is derived therefore we expected a stable AOT. The error defined in the water-leaving radiance product of OLCI is very large, especially for the blue and green bands. This brings uncertainty to the verification of those bands.

- *What is the correlation between the aerosol optical thickness Sentinel-3A Level-2 OLCI data product and aerosol optical thickness measured at AERONET-OC?*
  From the time series and regression plot of OLCI and AERONET-OC it can be concluded that the OLCI AOT shows a large overestimation compared to AERONET-OC values. For clear-sky days without clouds, OLCI's values for the AOT were lower and more realistic but still higher than the AOT of AERONET-OC. Because this AERONET-OC station could not represent the AOT values of the whole research area, the AOT values of OLCI were compared with MODIS AOT values. Since the overestimation of AOT OLCI was unrealistically large, no correlation coefficient was calculated.

- *What is the correlation between the aerosol optical thickness Sentinel-3A Level-2 OLCI data products and the aerosol optical thickness product of MODIS?*
  The comparison with MODIS showed better results. The ranges of OLCI and MODIS were similar as shown in the time series and regression plots. A regression has been created for match-ups between OLCI and MODIS data at the MWTL locations for different time constraints. The regression with a time constraint of 2.5 hours between OLCI and MODIS showed good results. A linear least squares fit of this regression had a slope of 0.81 and an intercept of almost 0. The correlation coefficient between OLCI's AOT and MODIS AOT with a maximum time difference of 2 hours between the match-up data was 0.58. This correlation coefficient was determined using 22 match-ups. In Figure 5.20 the error bars of OLCI and MODIS were shown as well. Concluding from those error bars we can say that the OLCI AOT product is less precise than OLCI with spatial variations of more than 40% occurring sometimes.

- *What is the spatial variability of Sentinel-3A's Level-2 reduced resolution OLCI aerosol optical thickness data product?*
  The maps showed that OLCI's values for the AOT were unrealistically high around the edges of clouds and next to the coasts. This means that the cloud mask and land mask need to be adjusted in order to get this right. One of the major findings for the AOT of OLCI was the large variability and range of values. OLCI's AOT values were ranging from 0 to 0.6 while we would expect values of around 0.3 for Dutch coastal waters. The boxplots confirmed the large temporal and spatial variability for the OLCI data products. Differences of more than 40% were found for connecting pixels. This means that the AOT can differ by more than 40% per kilometre distance. The boxplots also showed that often the maximum AOT value of 0.6 was reached for AOT which is unrealistic for Dutch waters.

7.3. Conclusions

Formulating the conclusions of this master thesis was based on the answers of the initial and elaborated research questions. The main conclusions of this thesis are presented in this paragraph. The main question of this research was:

Main question: What are the possibilities and limitations of Sentinel-3 Level-2 reduced resolution data products for monitoring water quality of the Dutch North Sea?

I evaluated Sentinel-3 Level-2 reduced resolution data products to see if they can complement Rijkswaterstaat's water quality monitoring strategy. The amount of available data that can be used as match-up data is still limited. Strong conclusions on the quality and validity of Sentinel-3's data products require data over a longer period of time.

Comparison of OLCI's chlorophyll neural network product showed values in the same range as the in-situ measurements. A linear regression line fitted through match-up data with a maximum time difference of 1 day showed a correlation coefficient of 0.77 and a slope of almost 1. These results show that the chlorophyll neural network data is sufficient to complement Rijkswaterstaat's monitoring system. OLCI's OC4Me data product showed and overestimation of approximately factor 2. This means that the OC4Me data product still needs some improvements before it can be used for water quality monitoring of the Dutch North Sea. OLCI's TSM product showed values in the same range as the in-situ measurements when direct match-up data were compared. But unrealistically underestimations of OLCI TSM were found when the time difference between in-situ measurement and satellite overpass was increased. Further research with more match-up data should find out if the OLCI TSM product is suitable for the use of water quality monitoring. All of the three data products showed a large spatial variability in the coastal areas. Therefore, it will be useful to investigate if full resolution data products are more suitable in the coastal area for monitoring chlorophyll and TSM. The OLCI data products of offshore locations showed a minimal spatial variability thus reduced resolution data products are sufficient in these areas.

Verification of OLCI's water-leaving radiance and aerosol optical thickness (AOT) product showed the following patterns. The overall water-leaving radiance spectra of OLCI corresponded well with AERONET-OC observations. Small underestimations but large variabilities were found in the blue and green bands. The red and near-infra-red bands fall in the same range as AERONET-OC values at those bands. The atmospheric correction is based on the near-infra-red part of the spectrum so we do not expect problems here. The OLCI and MODIS AOT data products show both an overestimation comparing it to the range of AERONET-OC values and literature studies. Especially for OLCI this overestimation was unrealistically high. OLCI and MODIS AOT correlated well with a correlation coefficient of 0.58 when the time difference between the two satellite measurements was kept to a maximum of 2.5 hours. AOT values of OLCI were also observed to be high in coastal areas and around clouds. This indicates that the "AOT invalid flag" and cloud mask of OLCI are not yet strict enough and more pixels around clouds should be flagged as unreliable. In MODIS AOT product the same issues were found but the invalid flag was more often raised in coastal areas. This implies that both OLCI and MODIS AOT products are not sufficient to monitor the aerosol state of the atmosphere.

The use of Sentinel-3 data products can greatly improve geographical and temporal coverage of monitoring North Sea water quality. But the results of this research imply that further research into the software implementation of the atmospheric correction, neural networks and validation methods is needed to get a better representation of the validity of the new Sentinel-3 products for monitoring North Sea water quality.

7.4. Recommendation

In the conclusion was stated that more research is needed to improve OLCI's data products. Furthermore, validation studies need to continue to investigate the validity of Level-2 datasets for monitoring of water quality and atmosphere. Recommendations for further research are presented in this paragraph.

7.4.1. Additional validation data

In order to obtain more match-up data in-situ measurements from other sources should have been included as well. For example the meetvis could be implemented (paragraph 4.1.4). This would also improve the research on spatial variability since the meetvis measures the water quality continuously. Also the use of ferrybox data could greatly improve the number of match-up data. Other European countries like Norway use this technique already [41]. The ferrybox is an instrument similar to that of the meetvis. It pumps water from the sea into the measuring device where the water quality parameters are then obtained. A picture of a ferrybox is given in Figure 7.1. On board of the Rijkswaterstaat measurement ship is a ferrybox installed which could be used immediately.

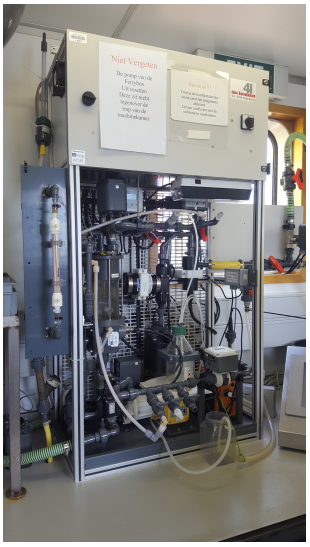

Figure 7.1: Picture of the ferrybox. Water from the sea is pumped through the ferrybox which measures water quality parameters.

Another possibility in obtaining more water-leaving radiance data is the use of hand-held spectrometers. The WISP of Water Insight B.V. is an option for this. The WISP is an hand-held spectrometer measuring solar irradiance, sky radiance and water-leaving radiance using three spectrometers. In this research comparisons between WISP measurements and OLCI data products were left out due to overcast during the measurement campaign. The WISP is a very user friendly device which can easily increase the number of in-situ measurements available for the North Sea. A picture of a WISP device is shown in Figure 7.2. From the spectrometer measurements chlorophyll and TSM contents can be derived.

Figure 7.2: Picture of the WISP. The WISP uses 3 spectrometers to observe the solar irradiance, the water-leaving radiance and the sky radiance. From these measurements chlorophyll and TSM products can be determined.

7.4.2. Algorithm development

The Dutch North Sea is a complicated area for monitoring water quality using remote sensing data, because it predominantly consists of complex coastal waters. Water-leaving radiances, chlorophyll and TSM concentrations are measured at ground-level during cruises are available these days. Also databases of inherent optical properties are available. Water-leaving radiances can be determined from inherent optical properties and concentration measurements. These determined water-leaving radiances can be compared to the water-leaving radiance product of OLCI to validate this product. Prerequisite that te OLCI water-leaving radiance products are valid, they can then be used in algorithms to derive chlorophyll and TSM parameters. The derived chlorophyll and TSM concentrations can be used to validate the algorithm or neural network of OLCI. For this research it is important to have broad measurements of all water types. International collaboration between different countries can achieve this.

7.4.3. Atmospheric correction

The atmosphere has a very large influence on the water-leaving radiance measure by the Sentinel-3 OLCI instrument. Approximately 90% of the measured radiance originates from reflectance in the atmosphere. It the therefore important that the atmospheric correction is accurate and correctly applied in obtaining water-leaving radiances. In this research we chose to verify the aerosol optical thickness product as a measure for the atmospheric correction. The AOT product of OLCI is only a by-product of the atmospheric correction and therefore more research into the atmospheric correction should be done. A proposed method would be to apply different atmospheric corrections to the Level-1 data after which the obtained water-leaving reflectance can be compared with water-leaving reflectance measured at ground level. Water-leaving reflectance at ground-level can be measured using AERONET-OC measurements or hand-held spectrometers.

7.4.4. Full resolution data

In this research we have chosen to use reduced resolution Level-2 data products of OLCI. The spatial resolution of those data products was approximately 1 km x 1 km. Since the spatial variability was very high in some of the data products more research into the full resolution data product is needed. Especially in coastal areas and in the aerosol optical thickness products a large variability was found between adjacent pixels. A research using the full resolution data product could find out more about these patterns.The full resolution data product has a spatial resolution of 300 m x 300 m. More detailed patterns can be observed. The question remains if a full resolution data product is necessary/better to monitor North Sea water quality.

A

Mean maps of chlorophyll per month obtained from MERIS satellite data

In this appendix chlorophyll monthly mean maps are presented for the years 2002 until 2011. The data for these maps comes from the Copernicus Marine Environment Monitoring Service [11]. The title of the figures shows which year and month is presented. The colour bars give chlorophyll values in μg/l. The same spatial and seasonal variations were observed as presented in paragraph 2.3. Higher chlorophyll values occur in the spring and autumn months. During the summer months the chlorophyll concentrations decrease due to a decrease in water turbulence which causes the phytoplankton to sink. White gaps in the data occur in the presence of clouds.

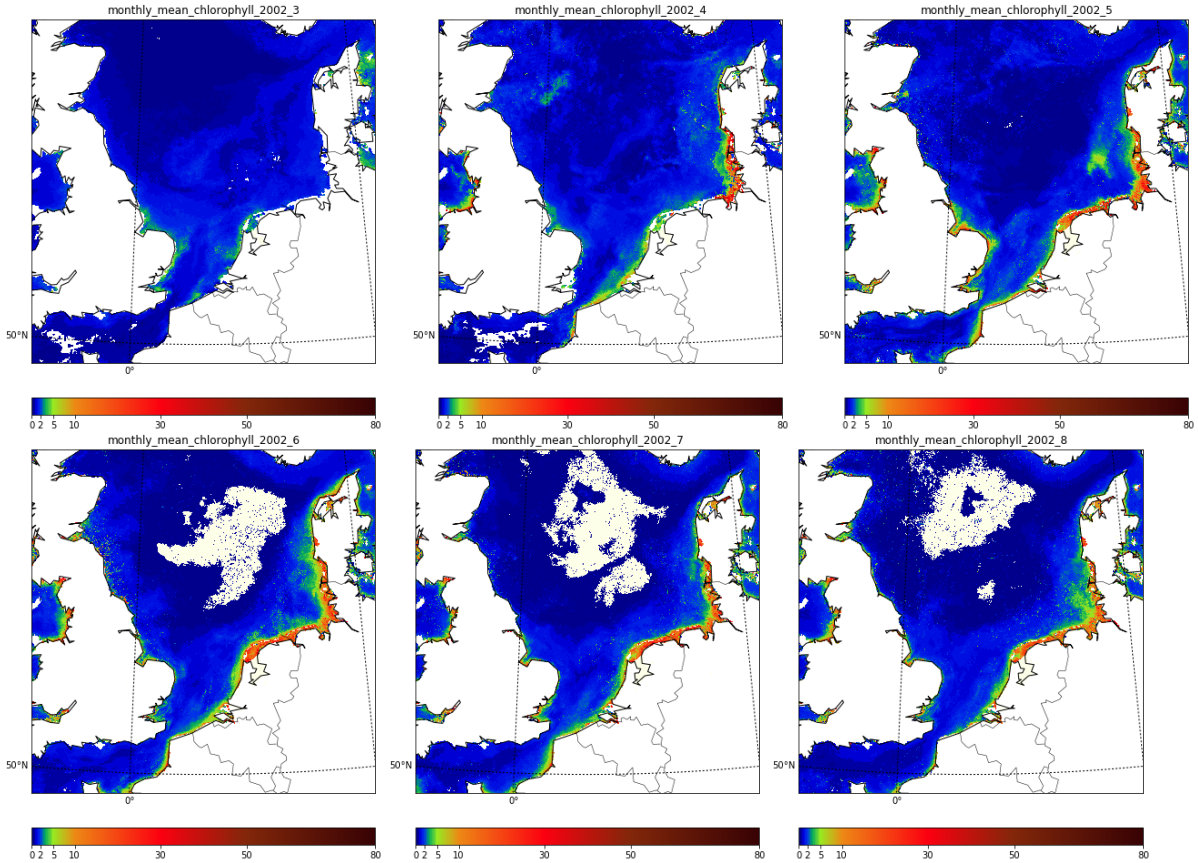

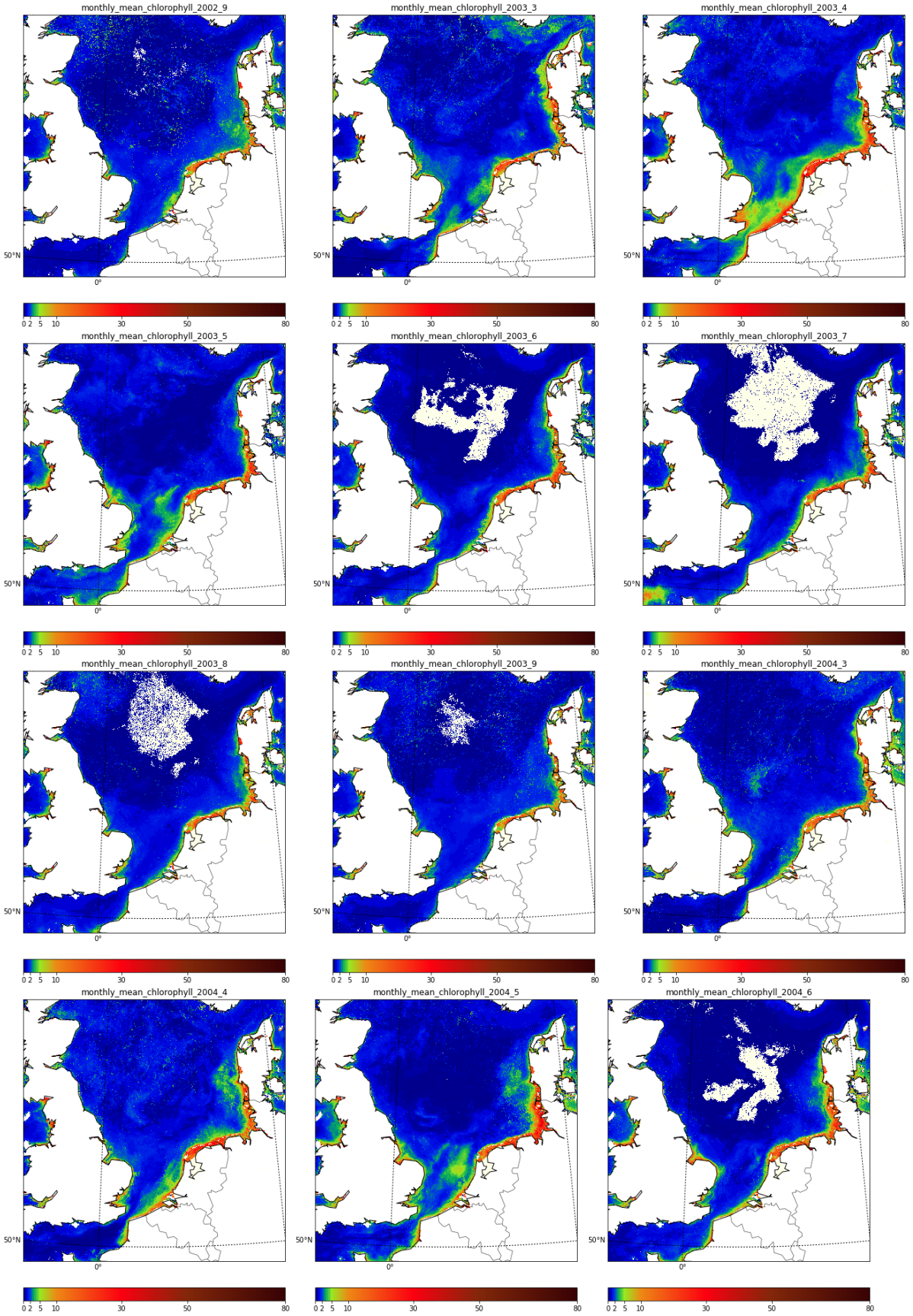
monthly_mean_chlorophyll_2002_9
monthly_mean_chlorophyll_2003_3
monthly_mean_chlorophyll_2003_4
monthly_mean_chlorophyll_2003_5
monthly_mean_chlorophyll_2003_6
monthly_mean_chlorophyll_2003_7
monthly_mean_chlorophyll_2003_8
monthly_mean_chlorophyll_2003_9
monthly_mean_chlorophyll_2004_3
monthly_mean_chlorophyll_2004_4
monthly_mean_chlorophyll_2004_5
monthly_mean_chlorophyll_2004_6
50°N
0°
0 2 5 10 30 50 80

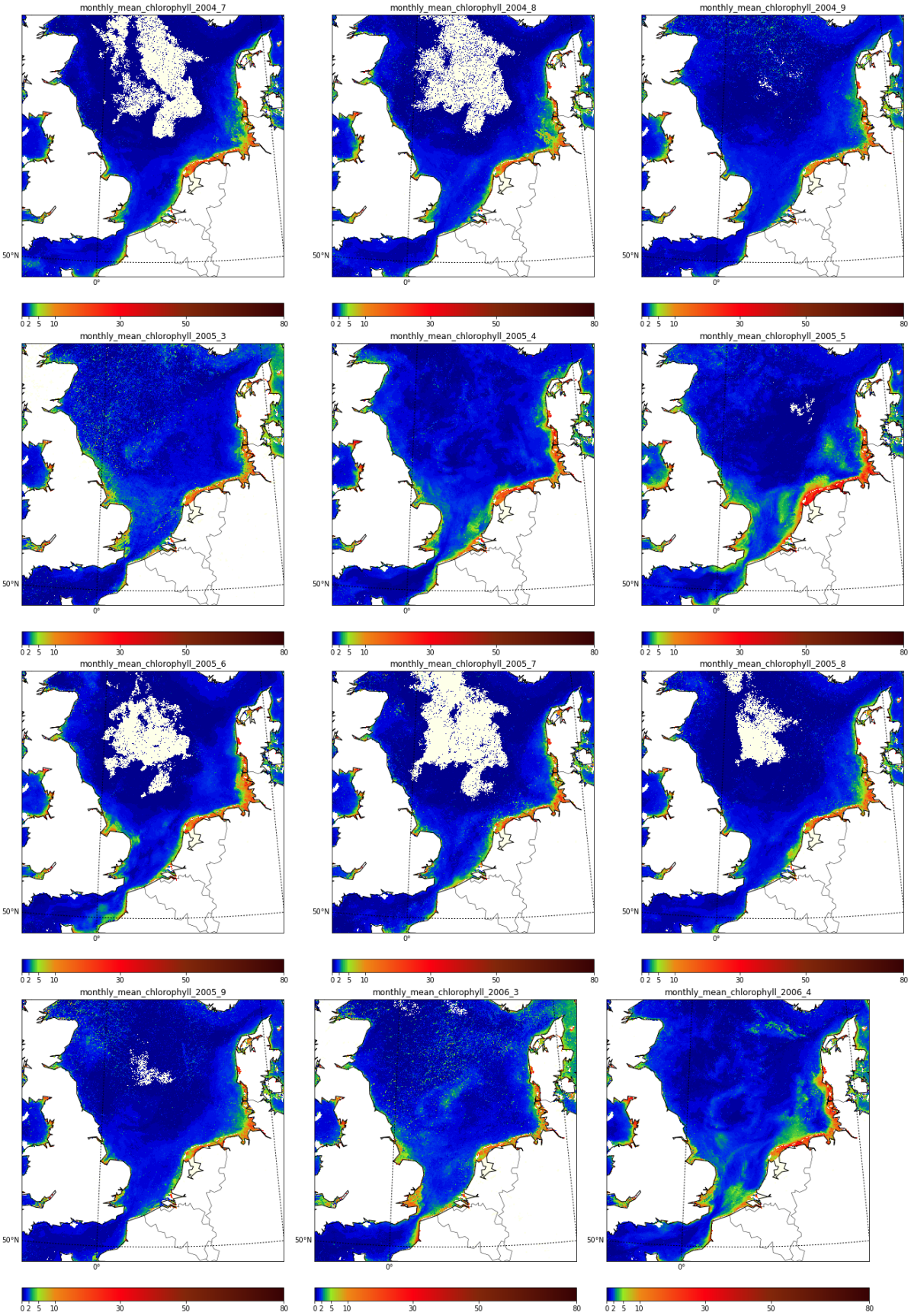
monthly_mean_chlorophyll_2004_7
monthly_mean_chlorophyll_2004_8
monthly_mean_chlorophyll_2004_9
monthly_mean_chlorophyll_2005_3
monthly_mean_chlorophyll_2005_4
monthly_mean_chlorophyll_2005_5
monthly_mean_chlorophyll_2005_6
monthly_mean_chlorophyll_2005_7
monthly_mean_chlorophyll_2005_8
monthly_mean_chlorophyll_2005_9
monthly_mean_chlorophyll_2006_3
monthly_mean_chlorophyll_2006_4
50°N
0°
0 2 5 10 30 50 80

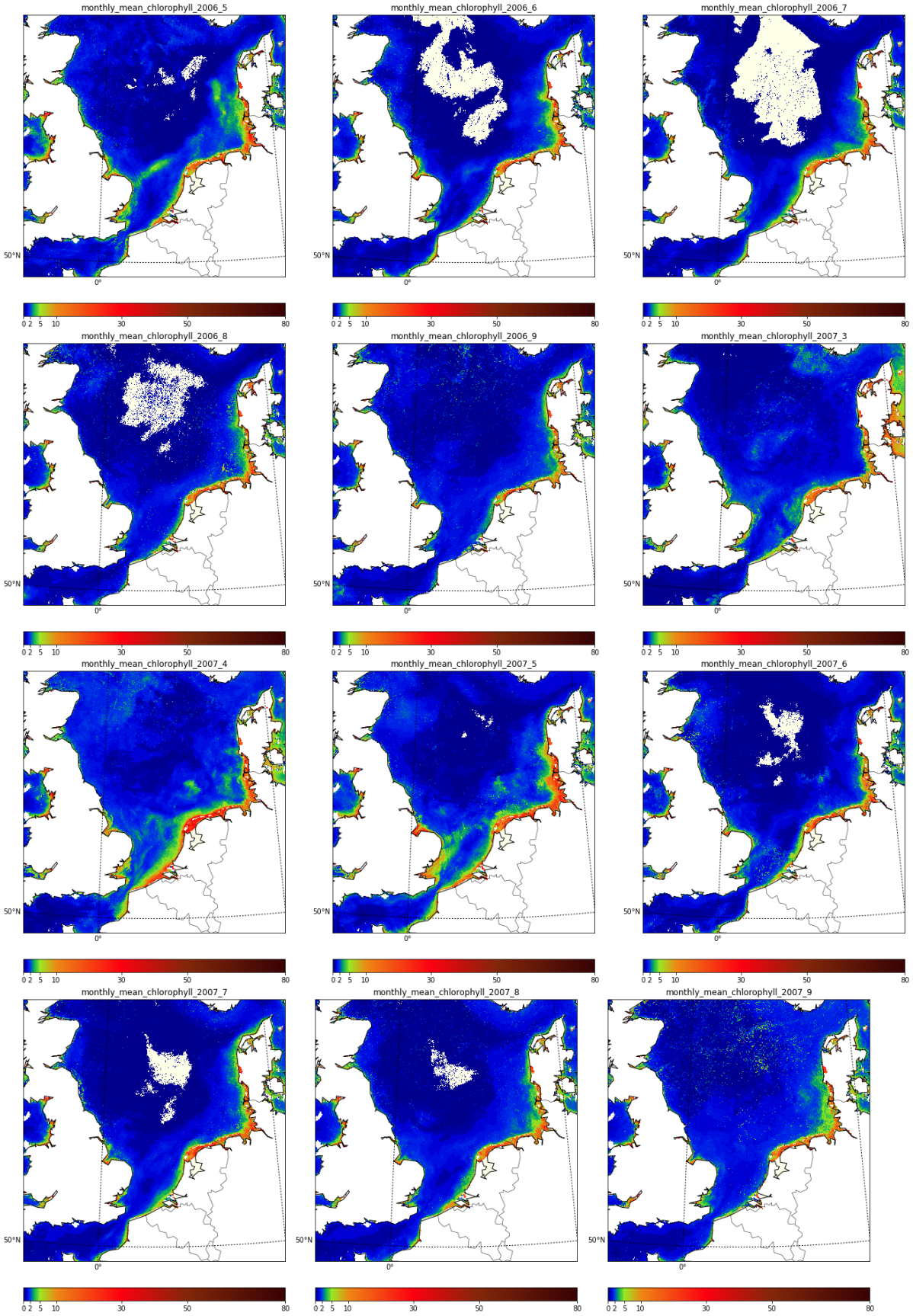
monthly_mean_chlorophyll_2006_5
monthly_mean_chlorophyll_2006_6
monthly_mean_chlorophyll_2006_7
monthly_mean_chlorophyll_2006_8
monthly_mean_chlorophyll_2006_9
monthly_mean_chlorophyll_2007_3
monthly_mean_chlorophyll_2007_4
monthly_mean_chlorophyll_2007_5
monthly_mean_chlorophyll_2007_6
monthly_mean_chlorophyll_2007_7
monthly_mean_chlorophyll_2007_8
monthly_mean_chlorophyll_2007_9
50°N
0°
0 2 5 10 30 50 80

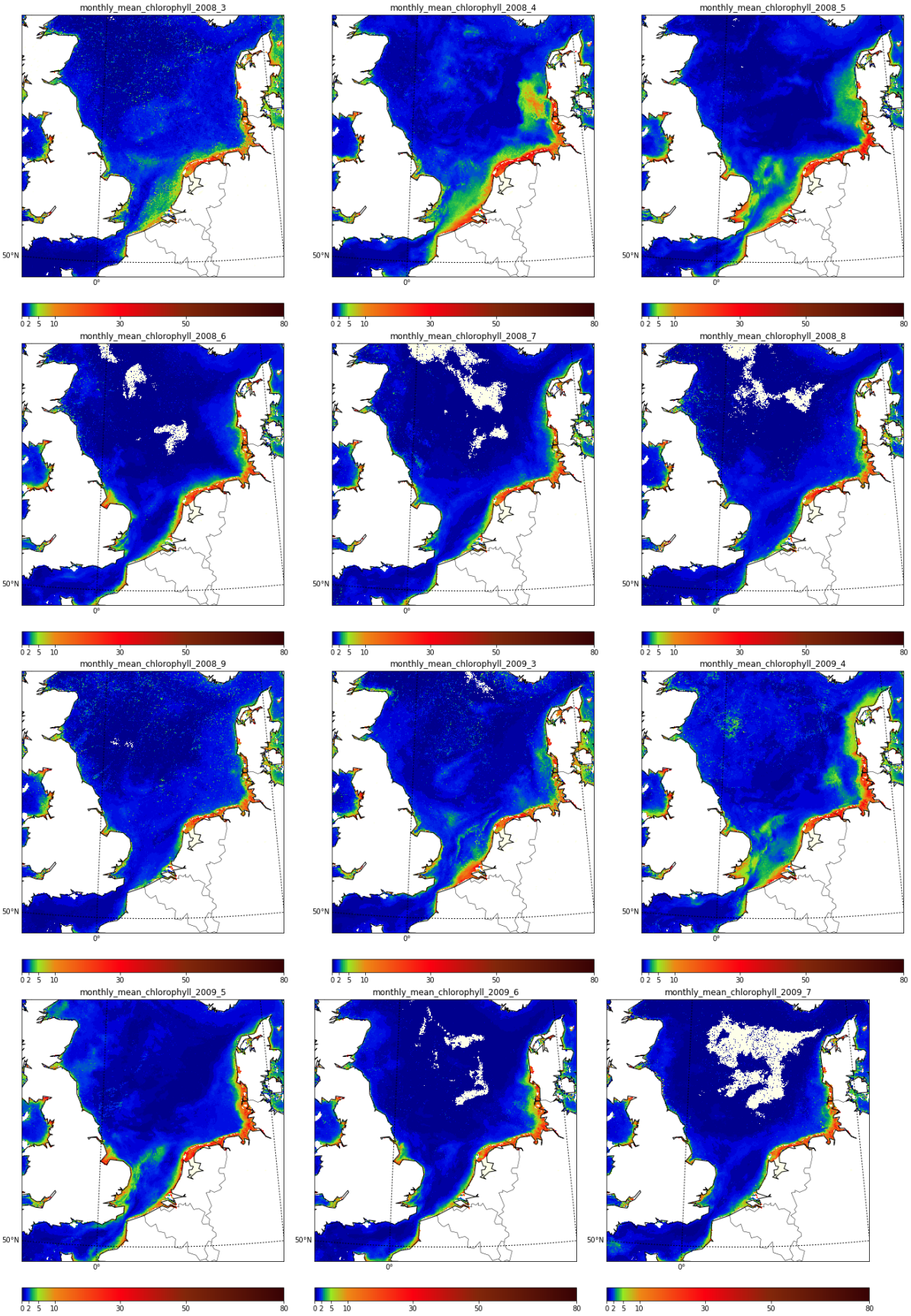
monthly_mean_chlorophyll_2008_3
monthly_mean_chlorophyll_2008_4
monthly_mean_chlorophyll_2008_5
monthly_mean_chlorophyll_2008_6
monthly_mean_chlorophyll_2008_7
monthly_mean_chlorophyll_2008_8
monthly_mean_chlorophyll_2008_9
monthly_mean_chlorophyll_2009_3
monthly_mean_chlorophyll_2009_4
monthly_mean_chlorophyll_2009_5
monthly_mean_chlorophyll_2009_6
monthly_mean_chlorophyll_2009_7
50°N
0°
0 2 5 10 30 50 80

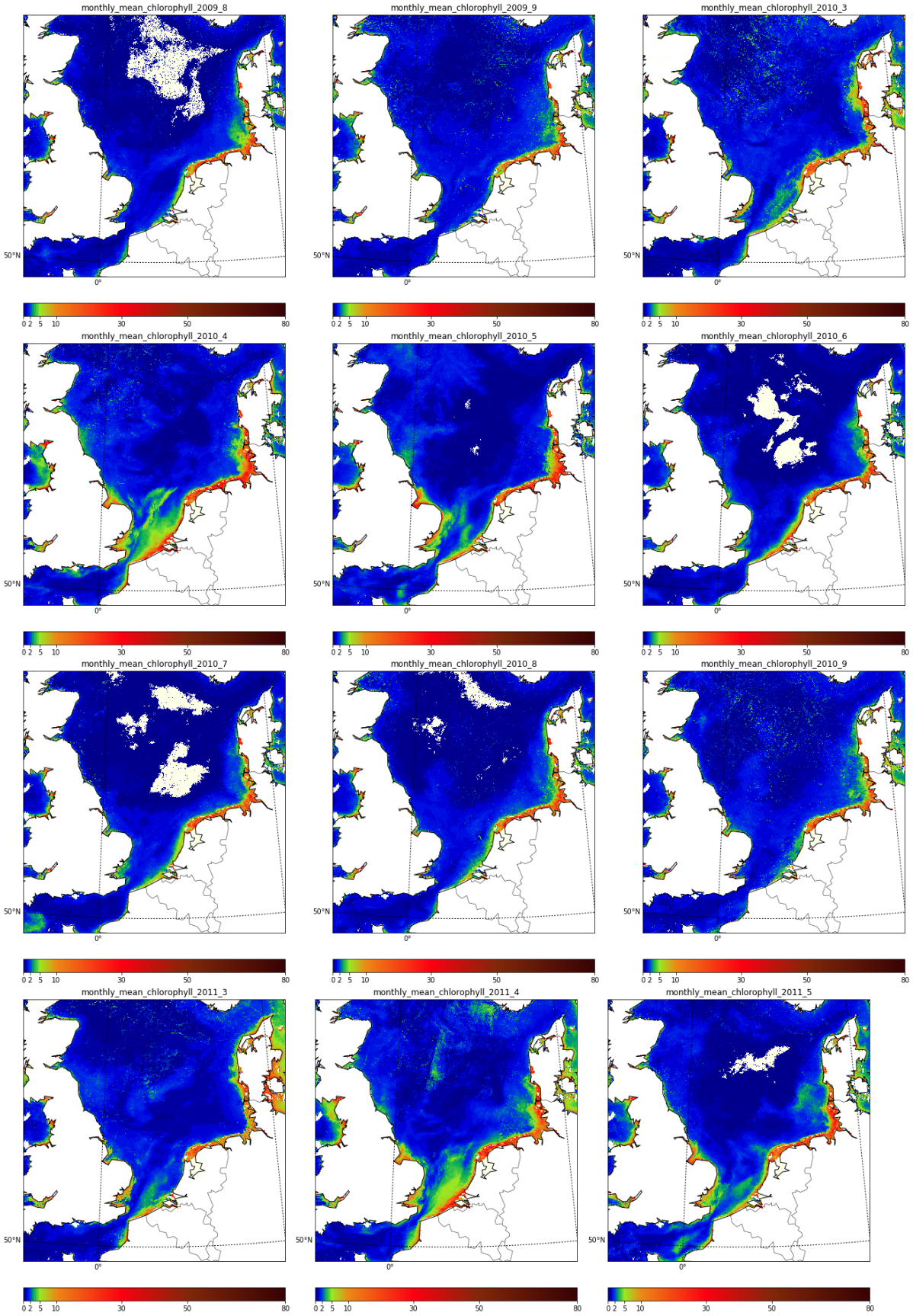
monthly_mean_chlorophyll_2009_8
monthly_mean_chlorophyll_2009_9
monthly_mean_chlorophyll_2010_3
monthly_mean_chlorophyll_2010_4
monthly_mean_chlorophyll_2010_5
monthly_mean_chlorophyll_2010_6
monthly_mean_chlorophyll_2010_7
monthly_mean_chlorophyll_2010_8
monthly_mean_chlorophyll_2010_9
monthly_mean_chlorophyll_2011_3
monthly_mean_chlorophyll_2011_4
monthly_mean_chlorophyll_2011_5
50°N
0°
0 2 5 10 30 50 80

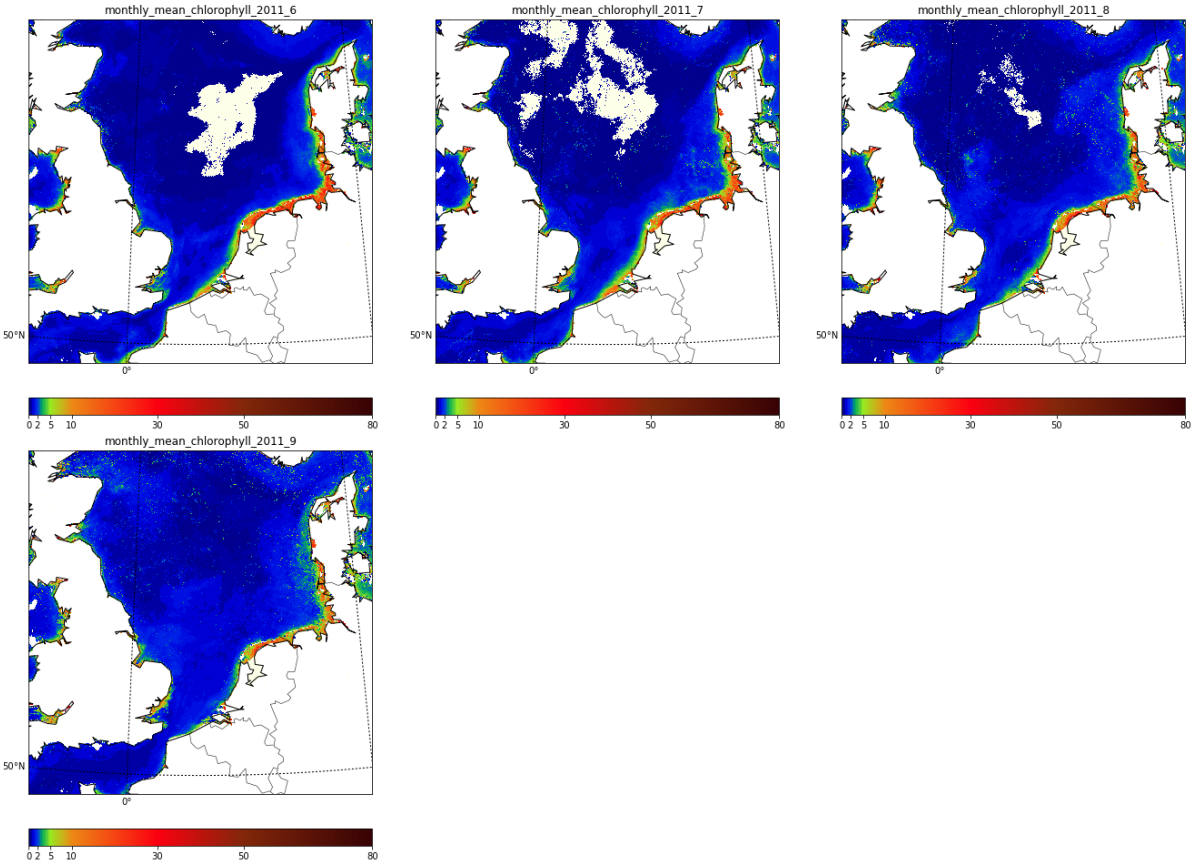
monthly_mean_chlorophyll_2011_6
monthly_mean_chlorophyll_2011_7
monthly_mean_chlorophyll_2011_8
monthly_mean_chlorophyll_2011_9
50°N
0°
0 2 5 10 30 50 80

B

Time series of chlorophyll (Chl) and total suspended matter (TSM)

In this appendix time series of chlorophyll and TSM are presented. All the plots combine MERIS, in-situ and OLCI data. The titles above the plots show at which of the Rijkswaterstaat measurement location the time series is valid for. An interesting pattern that is observed is the seasonal variation. The chlorophyll values are higher during the spring months especially at the coastal stations. This is caused by a spring bloom. For TSM counts that the TSM values are higher during autumn and winter months. This is most probably to do with the frequency of storms occurring in those months. Strong wind causes high turbulence of the water and an increase in sediments in the surface waters. The difference between coastal and off-shore stations (>50 km) is clearly seen as well. The coastal stations show higher values for TSM and chlorophyll throughout the whole year.

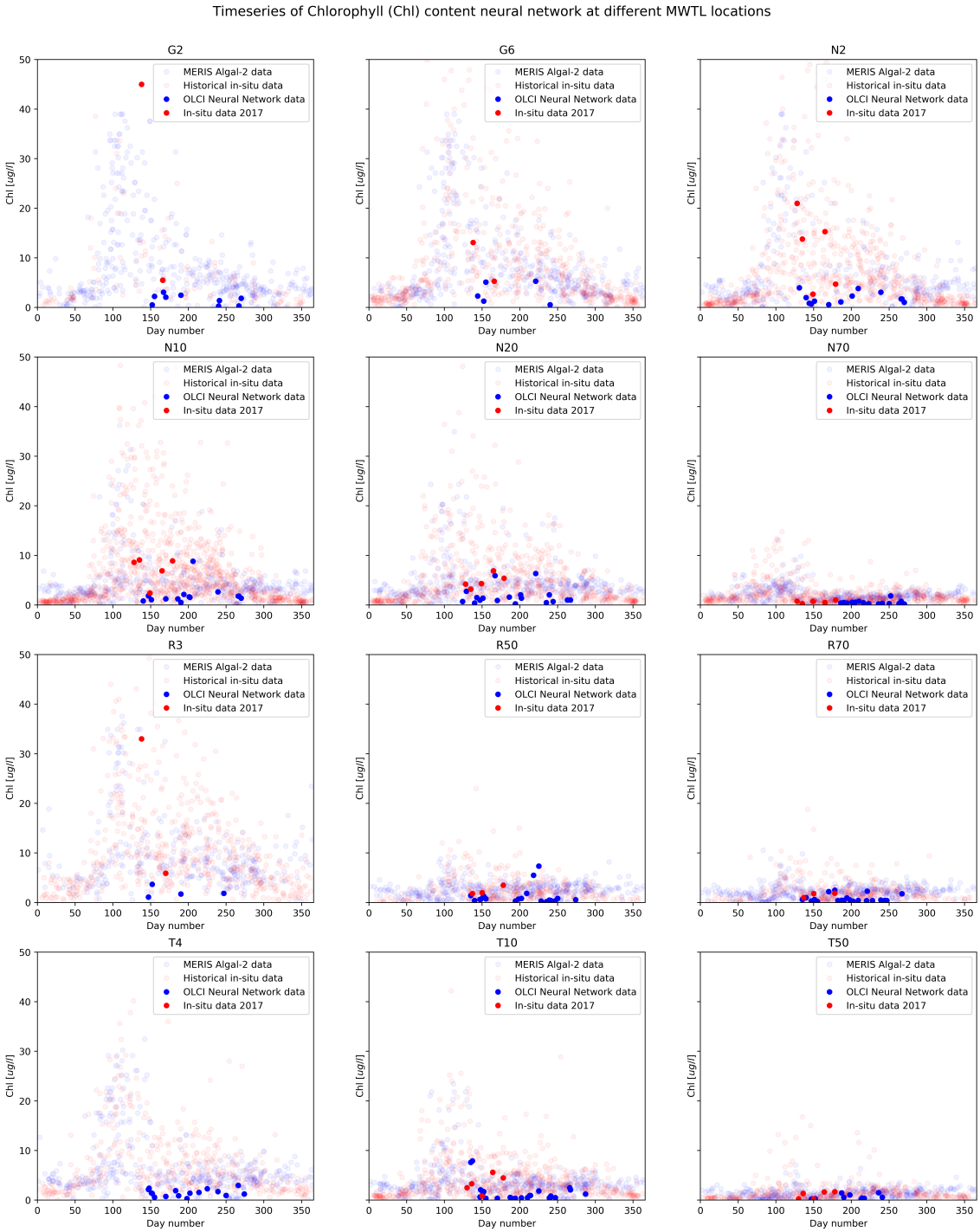
Timeseries of Chlorophyll (Chl) content neural network at different MWTL locations
G2
G6
N2
N10
N20
N70
R3
R50
R70
T4
T10
T50
MERIS Algal-2 data
Historical in-situ data
OLCI Neural Network data
In-situ data 2017
Chl [ug/l]
Day number

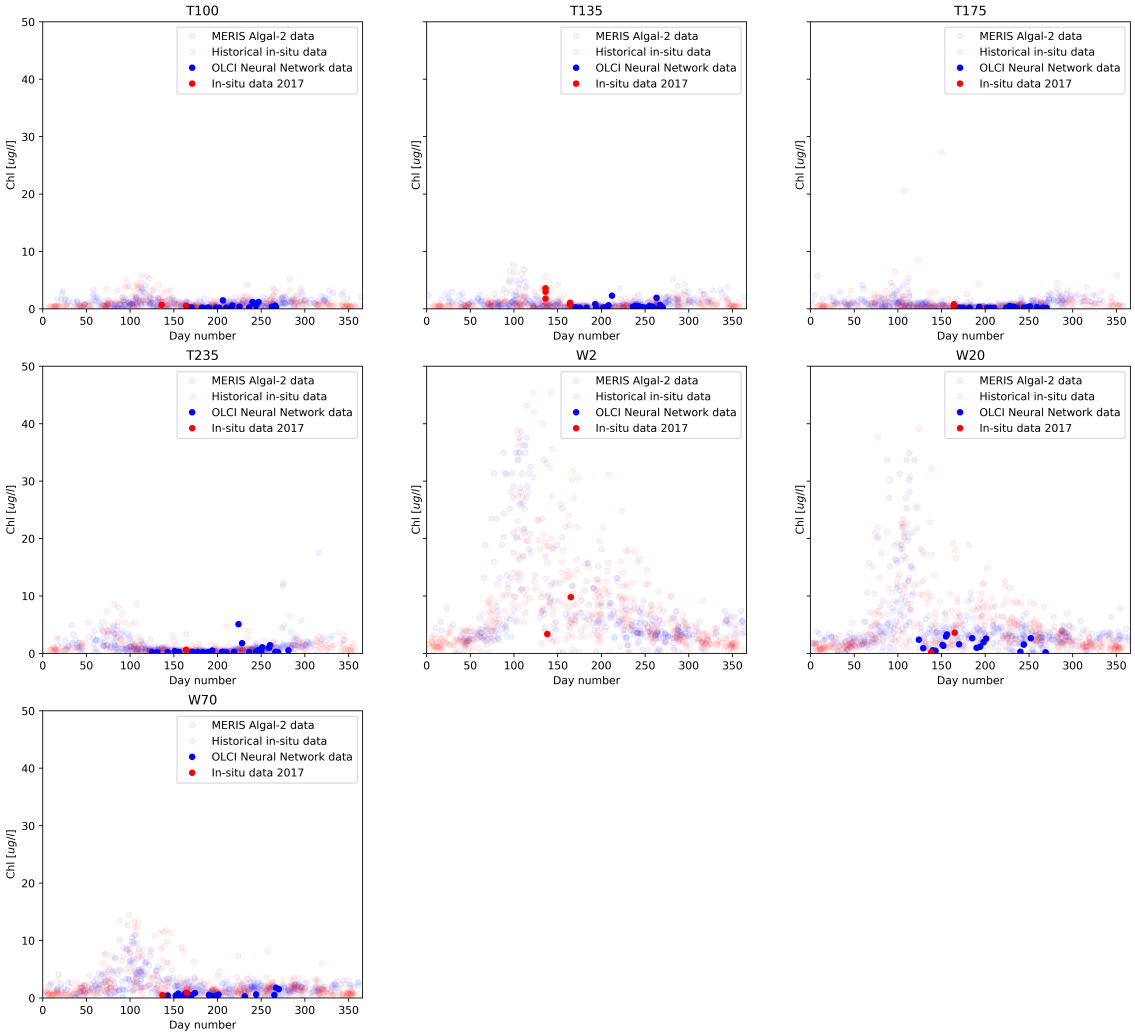

Figure B.1: Time series for all the used MWTL locations. The red dots represent in-situ data of which the bright dots are in-situ data of 2017, the transparent dots are historical data points. The blue dots represent satellite remote sensing data of which the bright blue dots represent OLCI data, the transparent dots represent historical MERIS data. Here the OLCI data is based on Neural Network measurements and MERIS on Algal2 measurements.

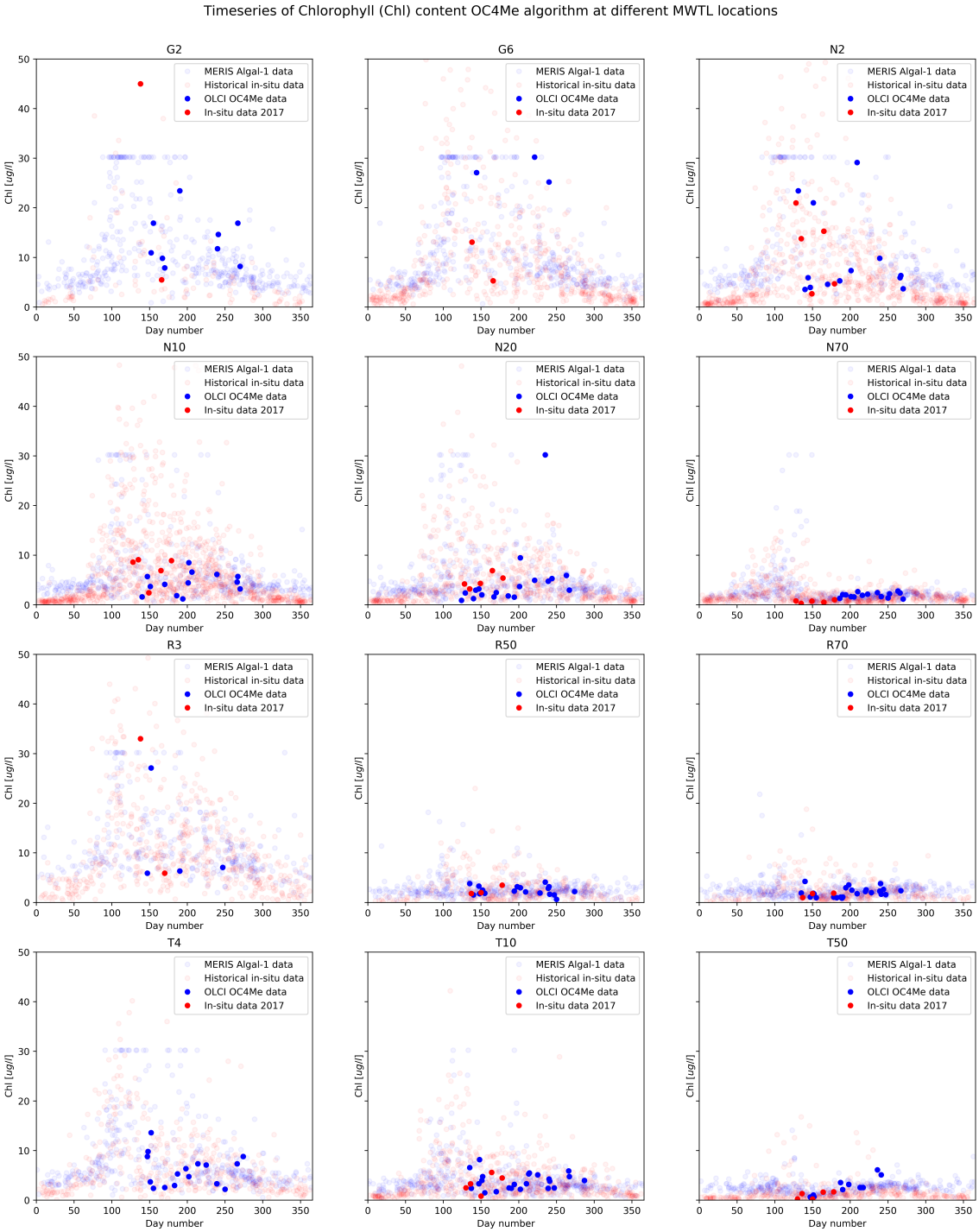
Timeseries of Chlorophyll (Chl) content OC4Me algorithm at different MWTL locations
G2
G6
N2
N10
N20
N70
R3
R50
R70
T4
T10
T50
MERIS Algal-1 data
Historical in-situ data
OLCI OC4Me data
In-situ data 2017
Chl [ug/l]
Day number

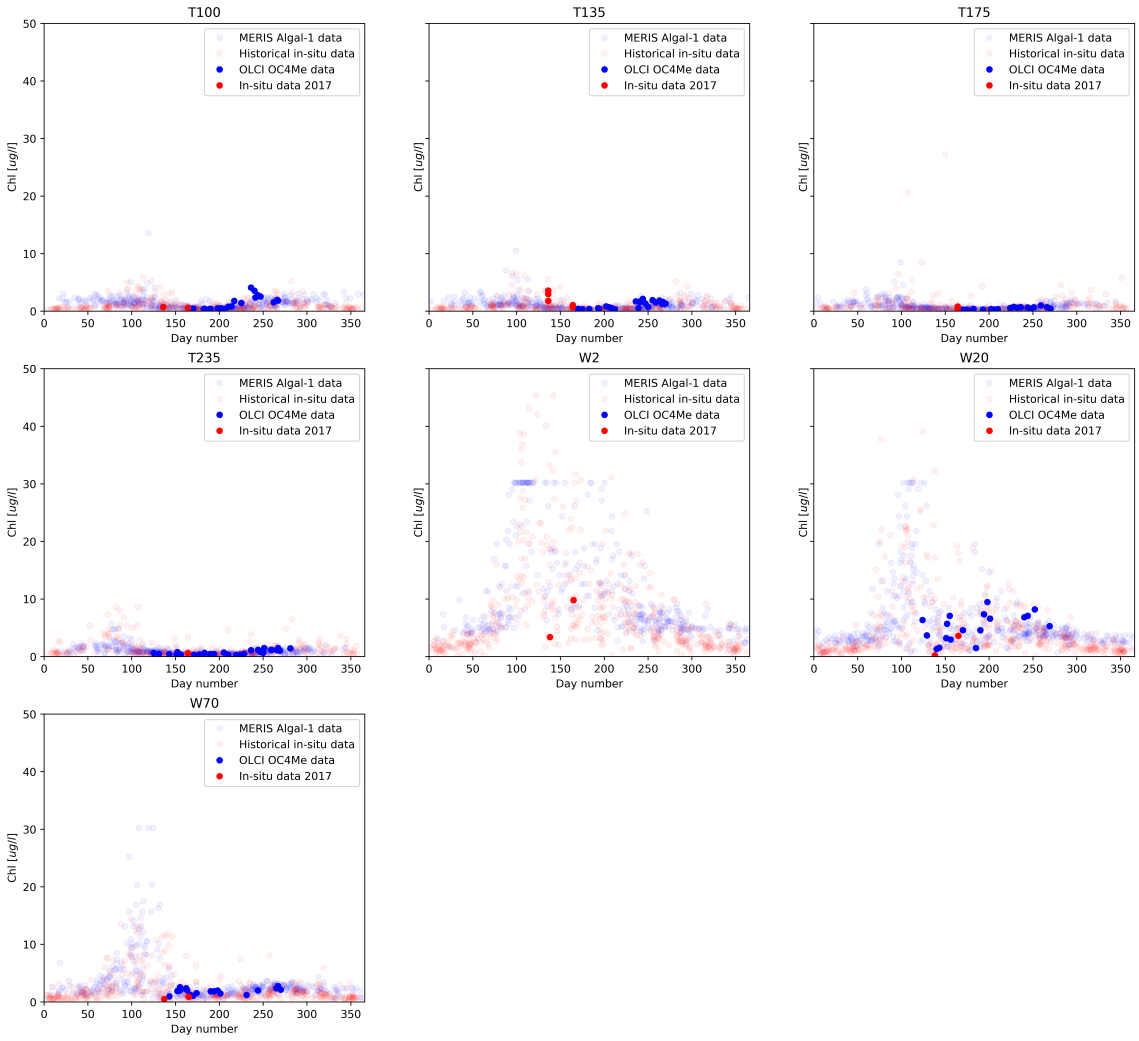

Figure B.2: Time series for all the used MWTL locations. The red dots represent in-situ data of which the bright dots are in-situ data of 2017, the transparent dots are historical in-situ data points. The blue dots represent satellite remote sensing data of which the bright blue dots represent OLCI data, the transparent dots represent historical MERIS data. The OLCI data is based on the OC4Me-algorithm and MERIS on the Algal1 algorithm.

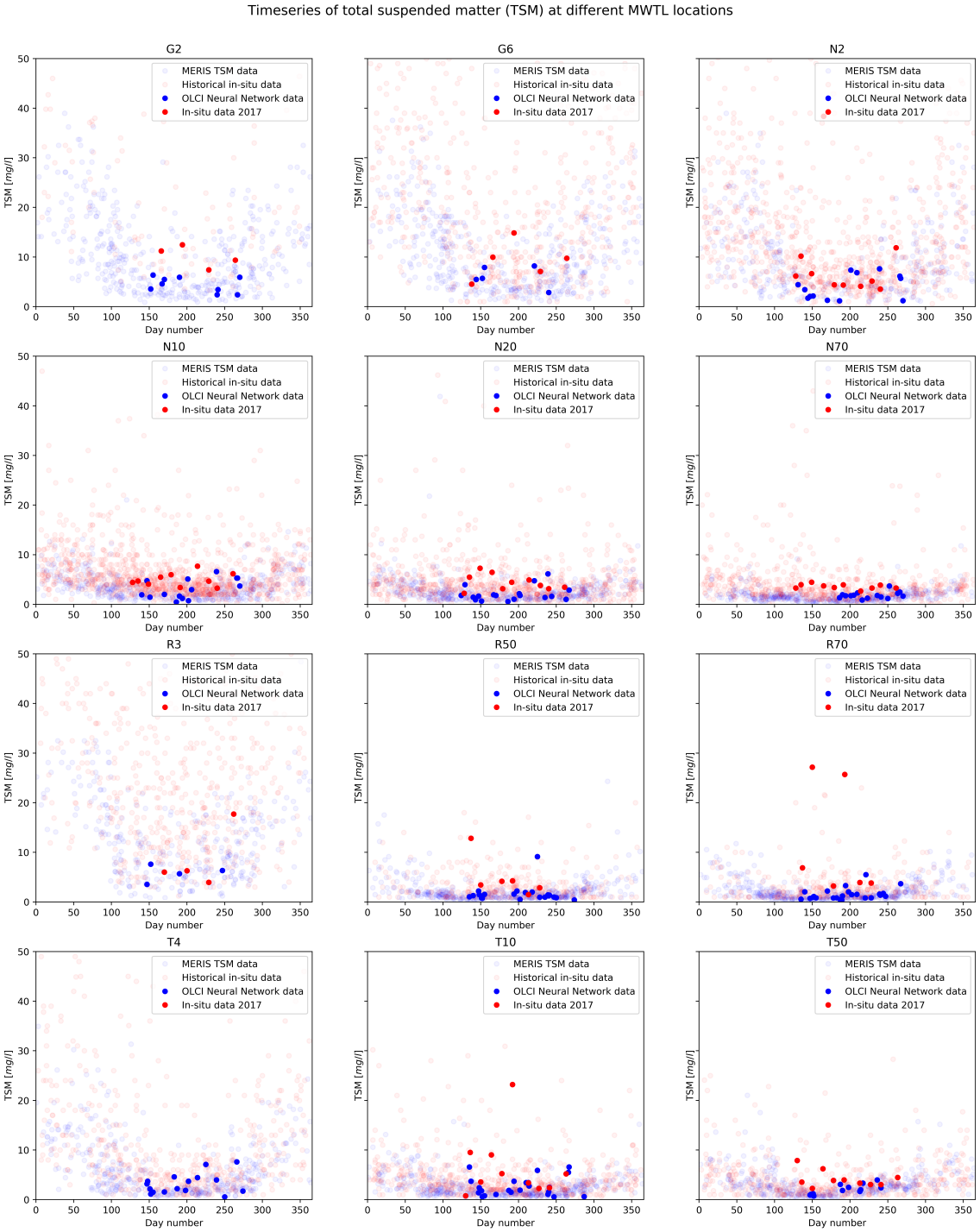
Timeseries of total suspended matter (TSM) at different MWTL locations
G2
G6
N2
N10
N20
N70
R3
R50
R70
T4
T10
T50
MERIS TSM data
Historical in-situ data
OLCI Neural Network data
In-situ data 2017
TSM [mg/l]
Day number

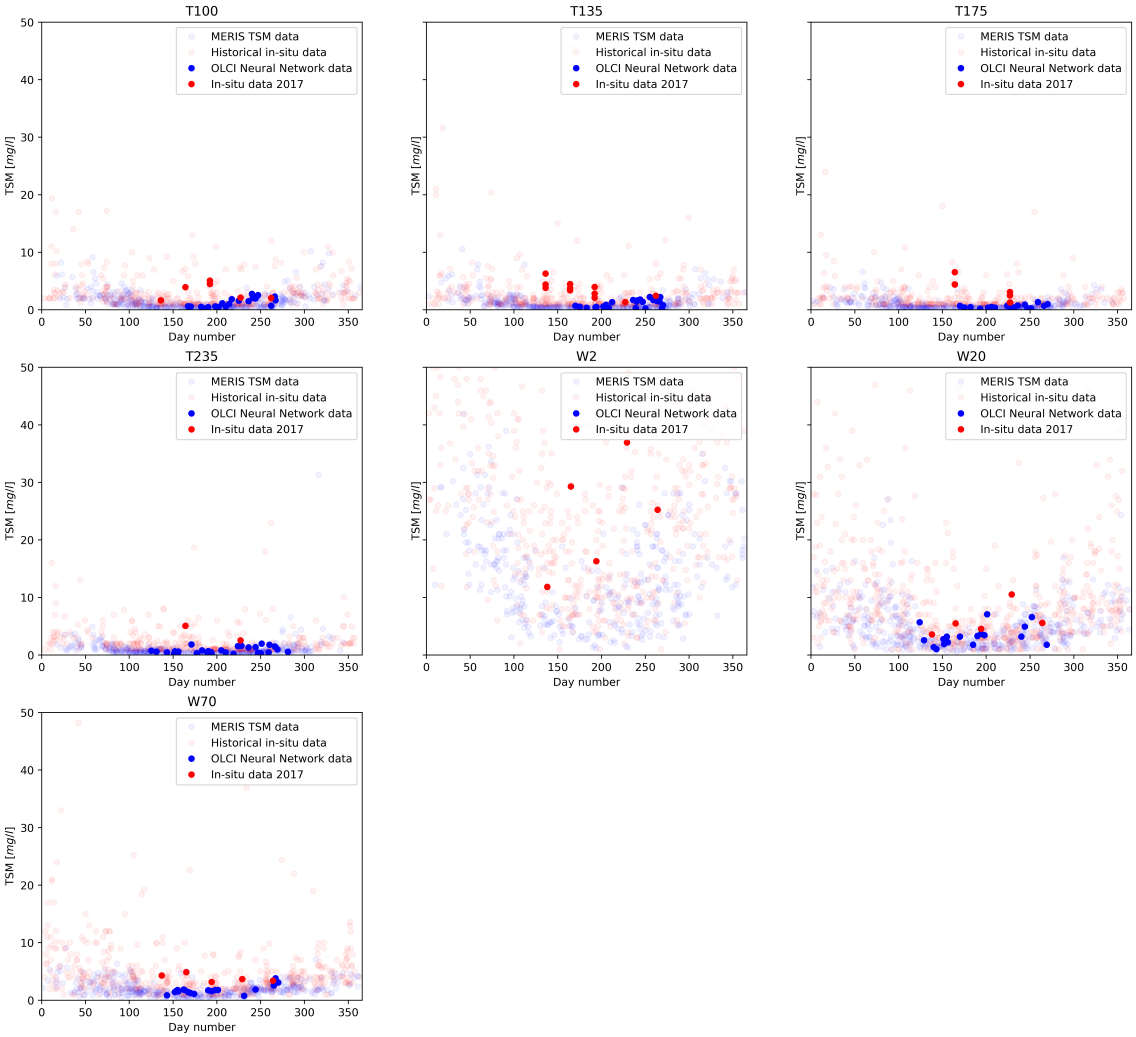

Figure B.3: Time series for all the used MWTL locations. The red dots represent in-situ data of which the bright dots are in-situ data of 2017, the transparent dots are historical data points. The blue dots represent satellite remote sensing data of which the bright blue dots represent OLCI data, the transparent dots represent historical MERIS data. All remote sensing data is based on results from a neural network.

C

Regression results of the old processing line

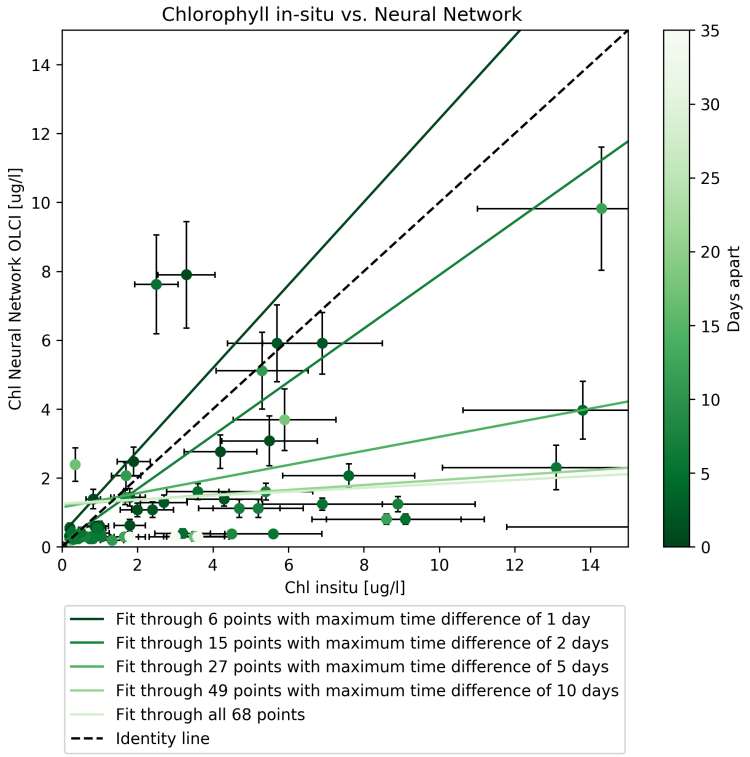

Figure C.1: This plot covers data of the old processing line and data before 6 July 2017. Regressions between chlorophyll in-situ measurements on the x-axis and chlorophyll neural network values of OLCI on the y-axis are shown. The different dots represent match-ups data at Rijkswaterstaat's measurement locations. The greenness of the points indicates what the time difference was between the in-situ measurement and the satellite overpass time.

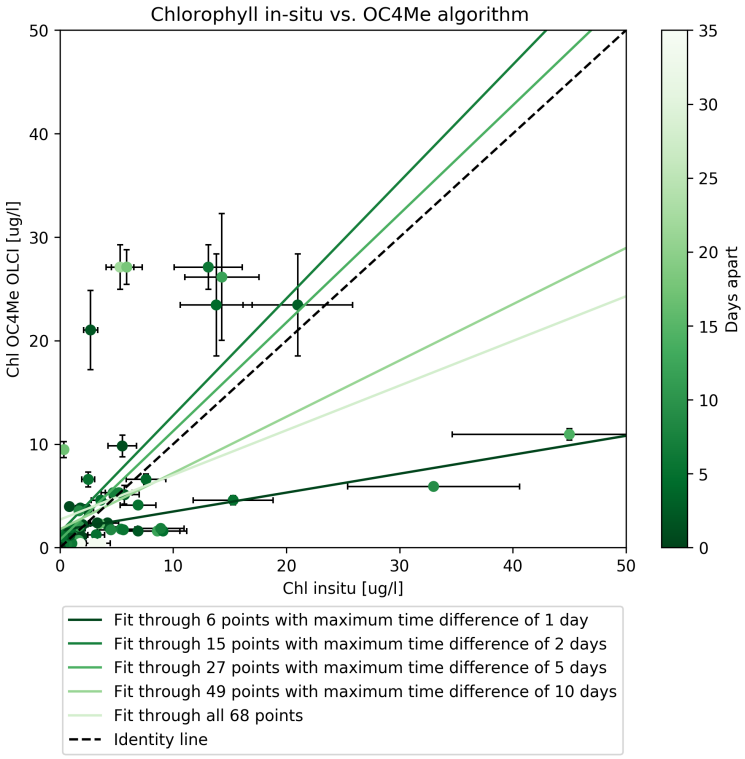

Figure C.2: This plot covers data of the old processing line and data before 6 July 2017. Regressions between chlorophyll in-situ measurements on the x-axis and chlorophyll OC4Me algorithm values of OLCI on the y-axis are shown. The different dots represent match-ups data at Rijkswaterstaat's measurement locations. The greenness of the points indicates what the time difference was between the in-situ measurement and the satellite overpass time.

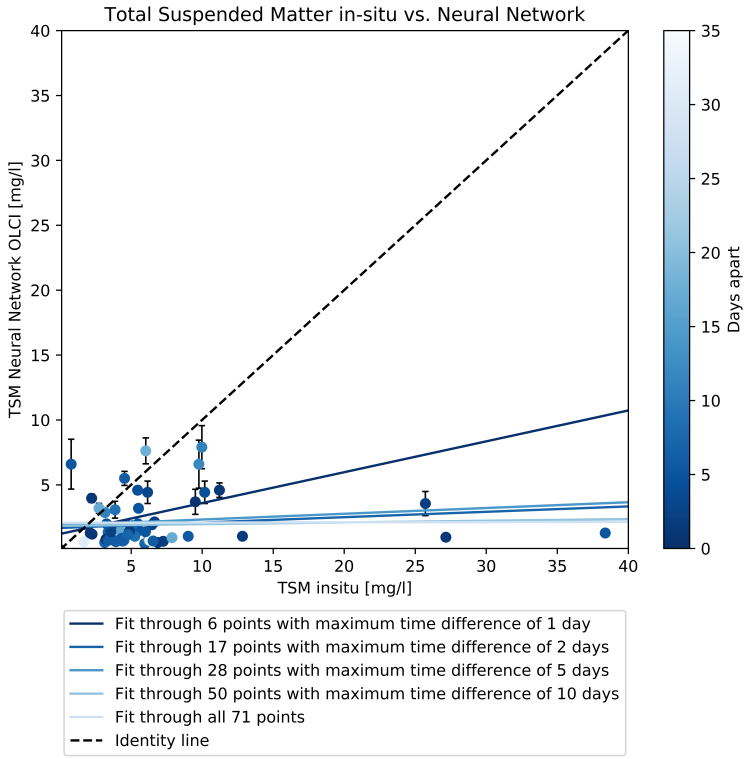

Figure C.3: This plot covers data of the old processing line and data before 6 July 2017. Regressions between TSM in-situ measurements on the x-axis and TSM neural network values of OLCI on the y-axis are shown. The different dots represent match-ups data at Rijkswaterstaat's measurement locations. The blueness of the points indicates what the time difference was between the in-situ measurement and the satellite overpass time.

D

Time series of aerosol optical thickness (AOT)

In this appendix time series of chlorophyll and TSM are presented. All the plots combine MERIS, in-situ and OLCI data. The titles above the plots show at which of the Rijkswaterstaat measurement location the time series is valid for. An interesting pattern that is observed is the seasonal variation. The chlorophyll values are higher during the spring months especially at the coastal stations. This is caused by a spring bloom. For TSM counts that the TSM values are higher during autumn and winter months. This is most probably to do with the frequency of storms occurring in those months. Strong wind causes high turbulence of the water and an increase in sediments in the surface waters. The difference between coastal and off-shore stations (>50 km) is clearly seen as well. The coastal stations show higher values for TSM and chlorophyll throughout the whole year.

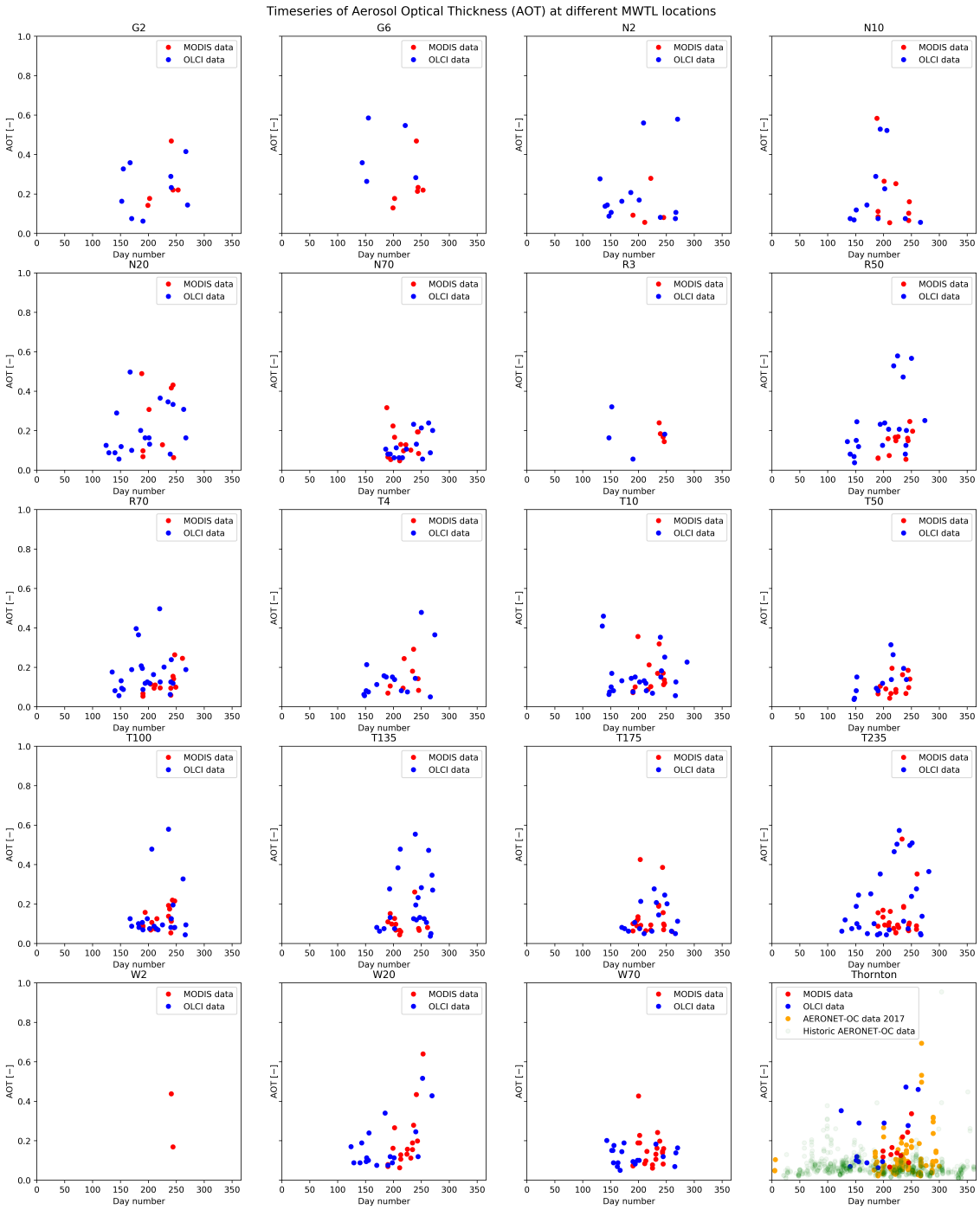

Figure D.1: Time series for all the used MWTL locations. The red dots represent in-situ data of which the bright dots are in-situ data of 2017, the transparent dots are historical data points. The blue dots represent satellite remote sensing data of which the bright blue dots represent OLCI data, the transparent dots represent historical MERIS data. All remote sensing data is based on results from a neural network.

E

Boxplots of chlorophyll (Chl) and total suspended matter (TSM)

Boxplots are created for each of the MWTL locations when a pixel extraction area of 3x3 pixels is extracted. The orange line indicates the mean value within a box, the box is defined by the first and third quartile. The whiskers indicate value of 3x standard deviation. The points that are outside the whiskers can be considered as outliers.

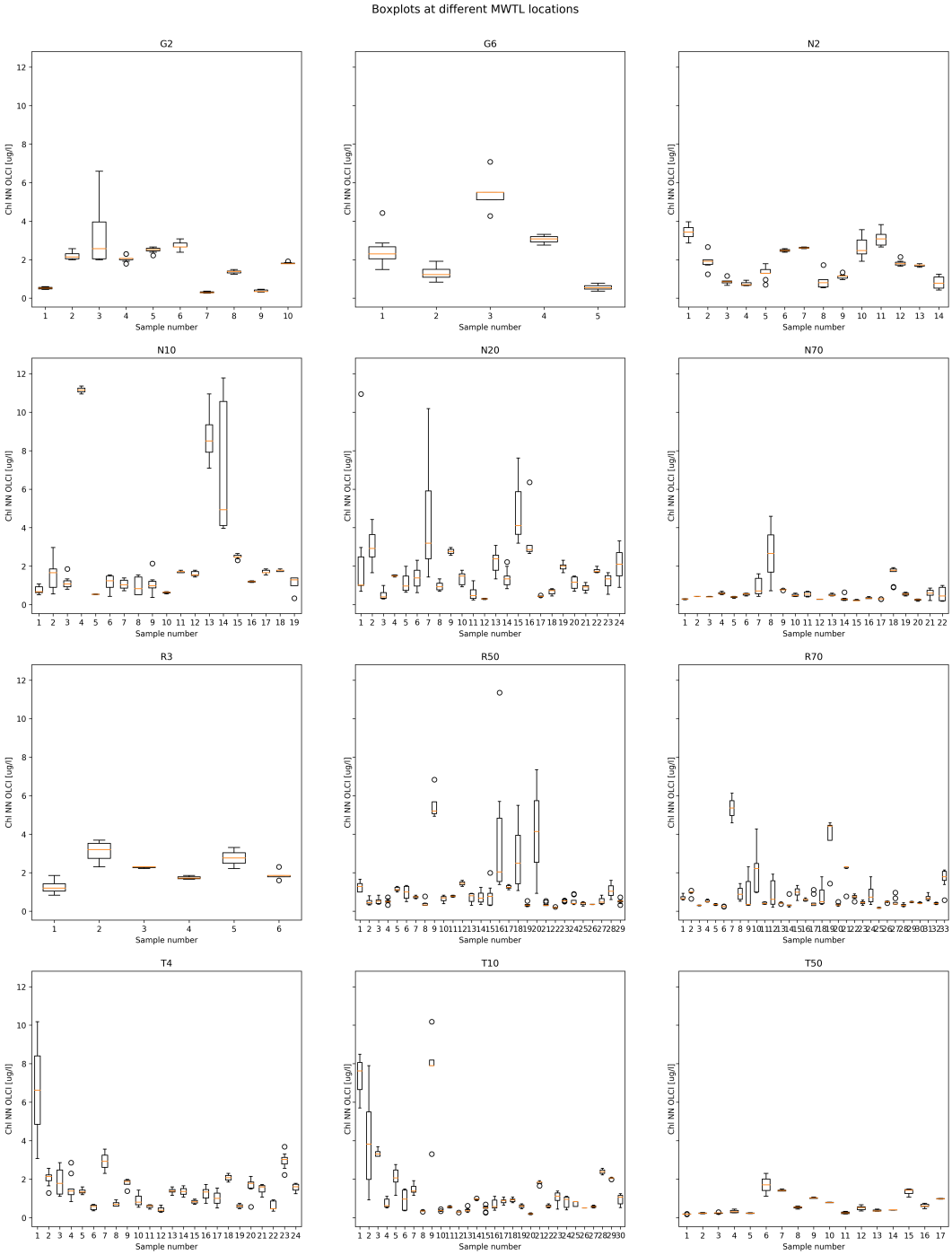
Boxplots at different MWTL locations
G2
G6
N2
N10
N20
N70
R3
R50
R70
T4
T10
T50
Chl NN OLCI [ug/l]
Sample number

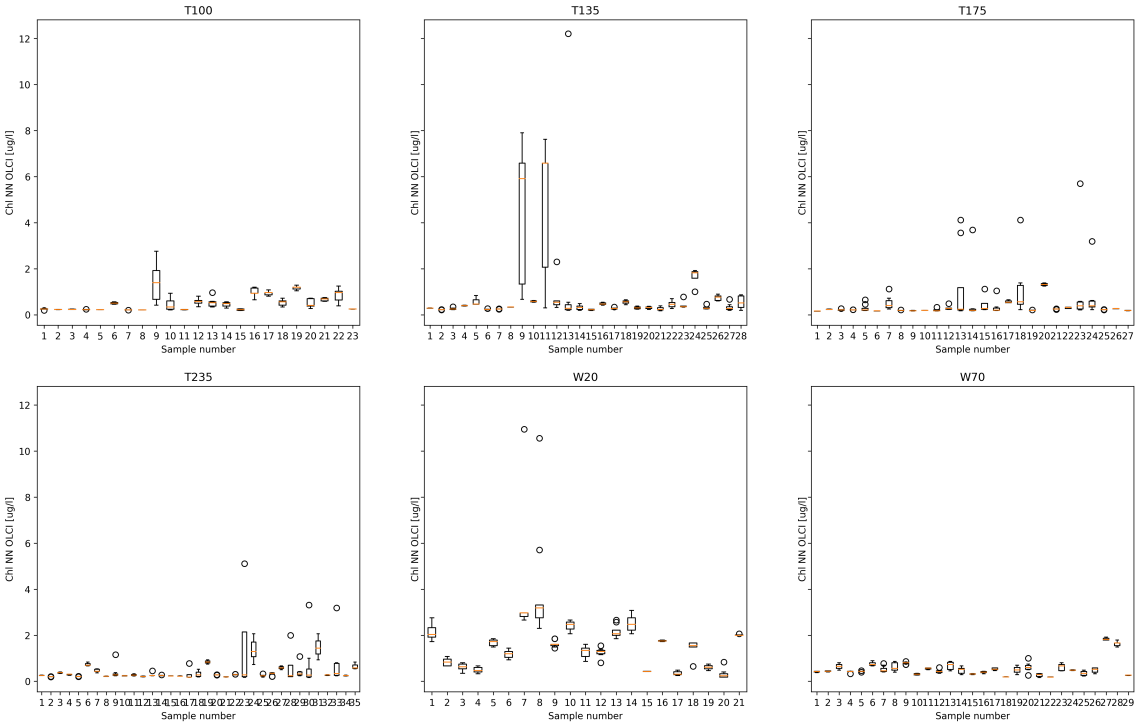

Figure E.1: Boxplots of the Chl neural network at all MWTL locations.

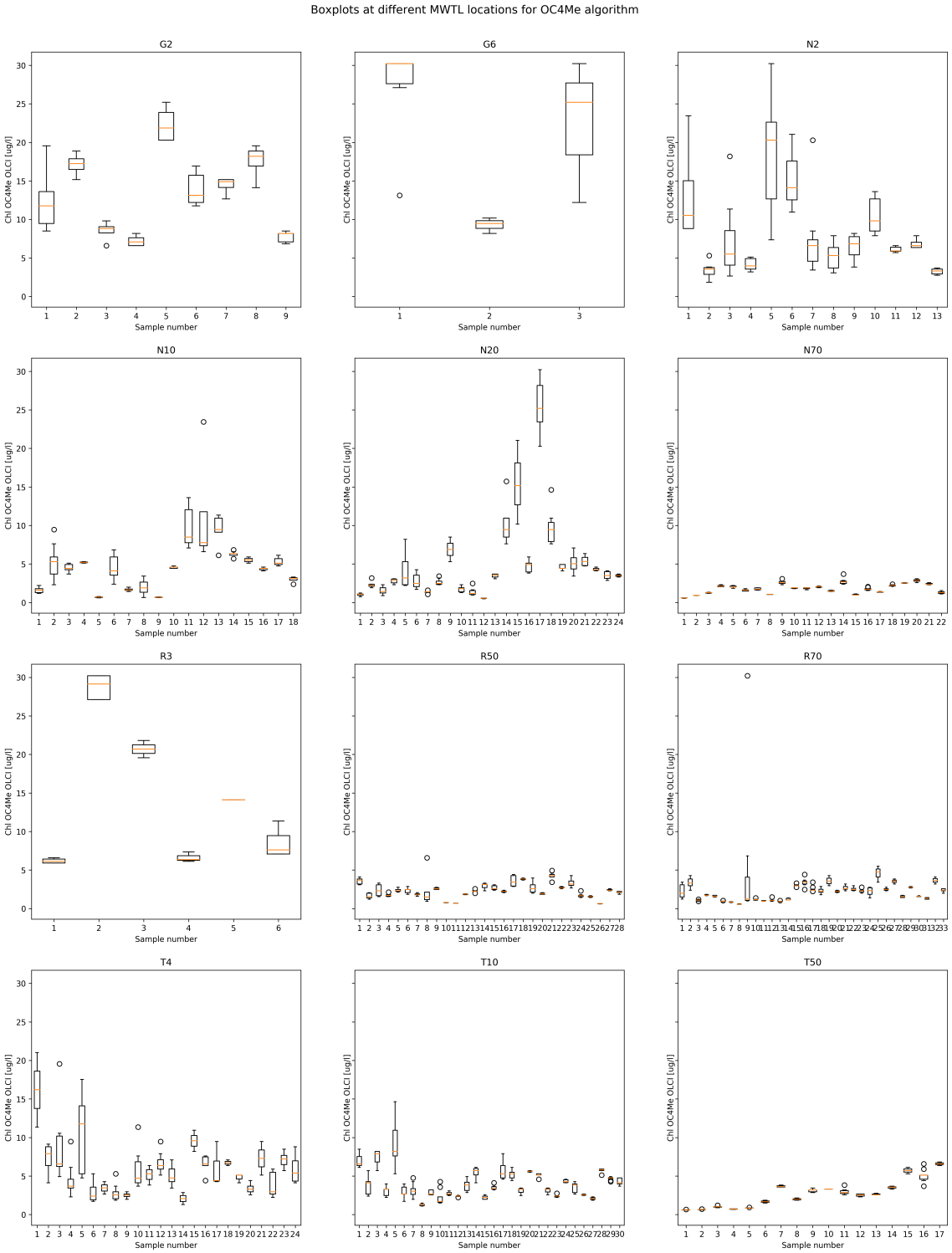
Boxplots at different MWTL locations for OC4Me algorithm
G2
G6
N2
N10
N20
N70
R3
R50
R70
T4
T10
T50
Chl OC4Me OLCI [ug/l]
Sample number

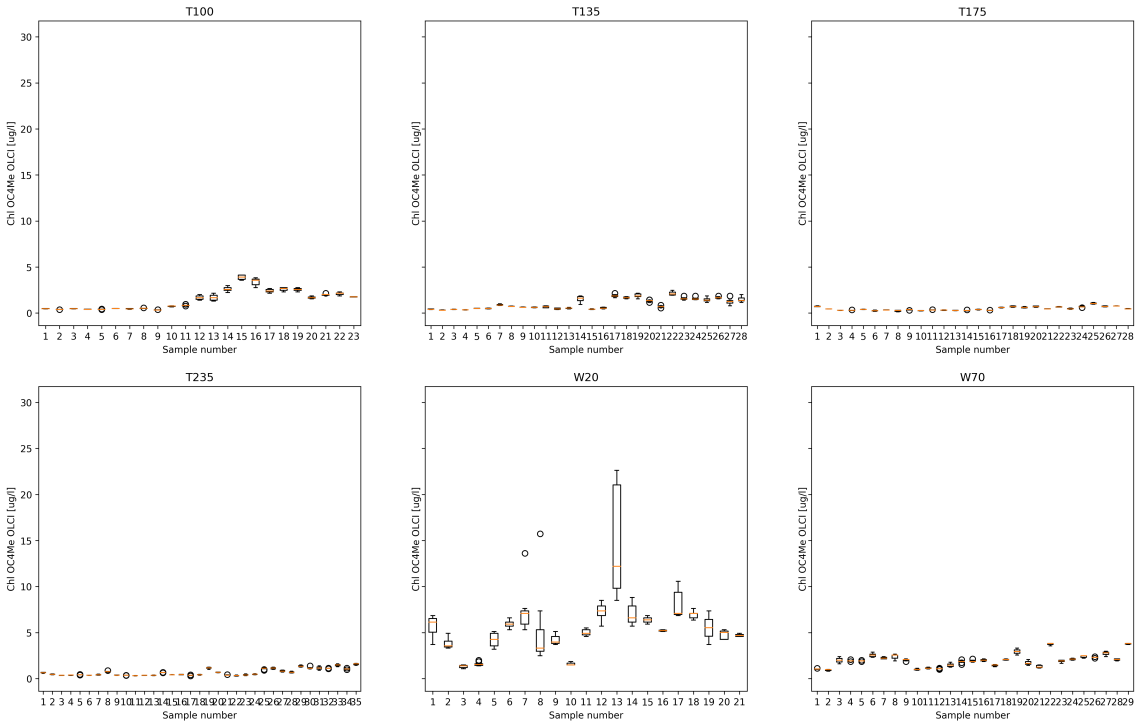

Figure E.2: Boxplots for the Chl OC4Me data product for each of the MWTL locations.

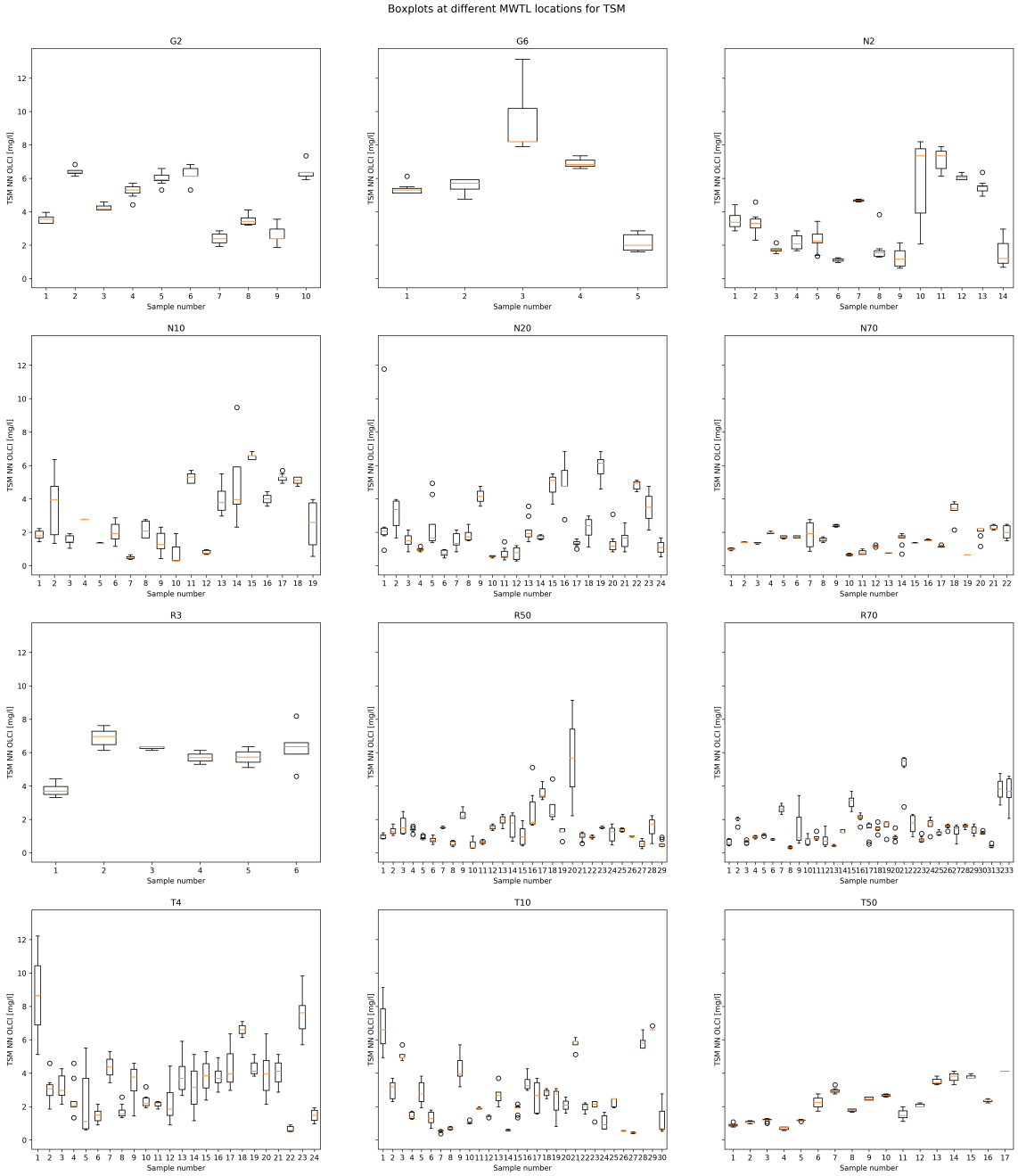
Boxplots at different MWTL locations for TSM
G2
G6
N2
N10
N20
N70
R3
R50
R70
T4
T10
T50
TSM NN OLCI [mg/l]
Sample number

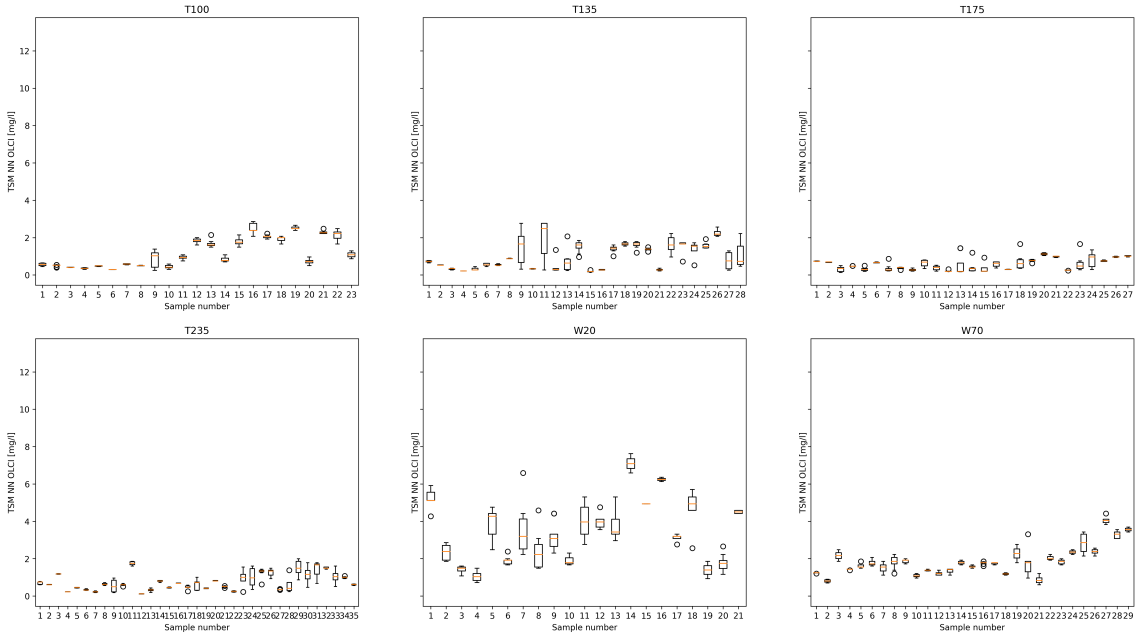

Figure E.3: Boxplots for the TSM values found at each of the MWTL locations.

F

Boxplots of aerosol optical thickness (AOT)

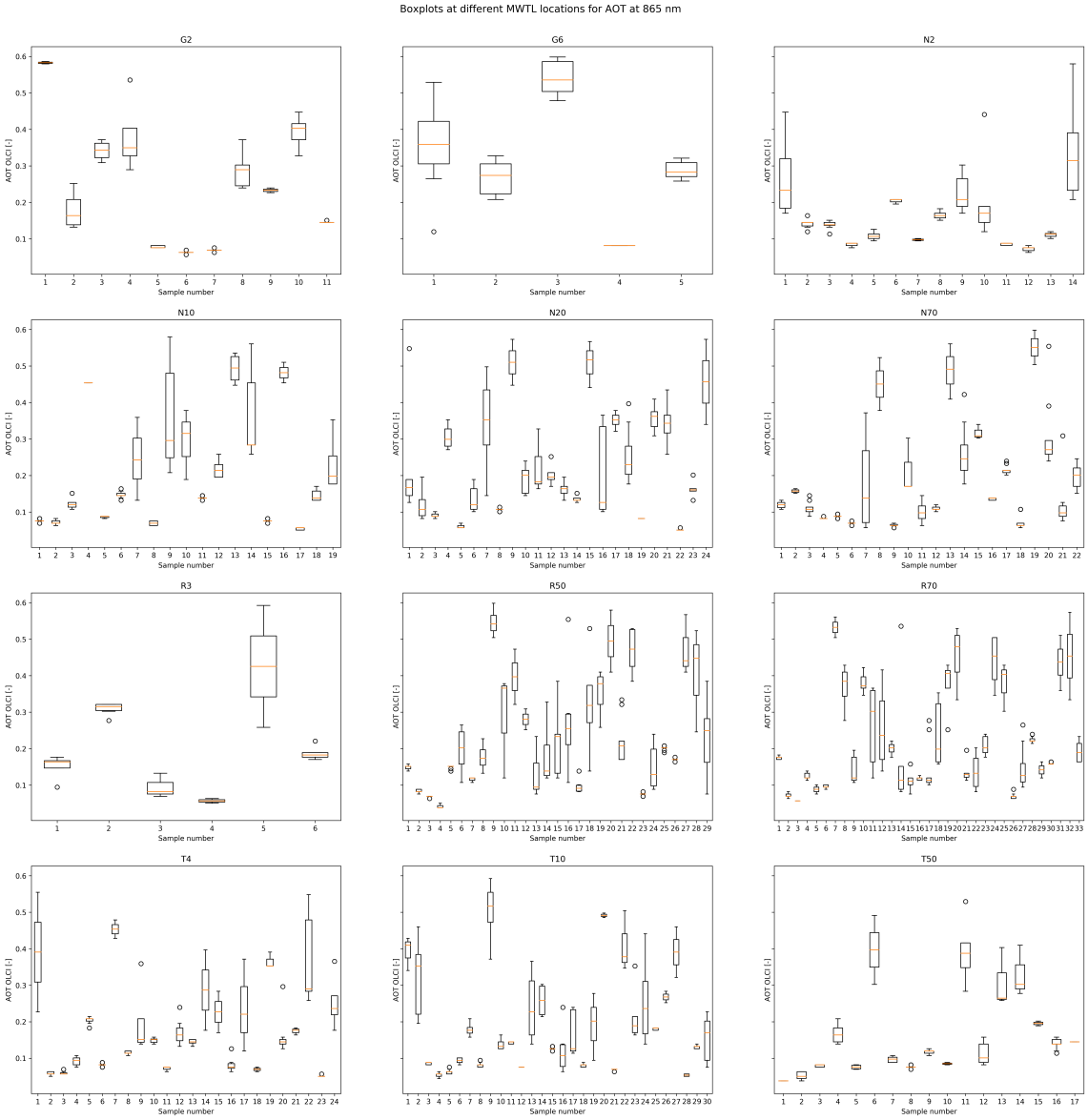

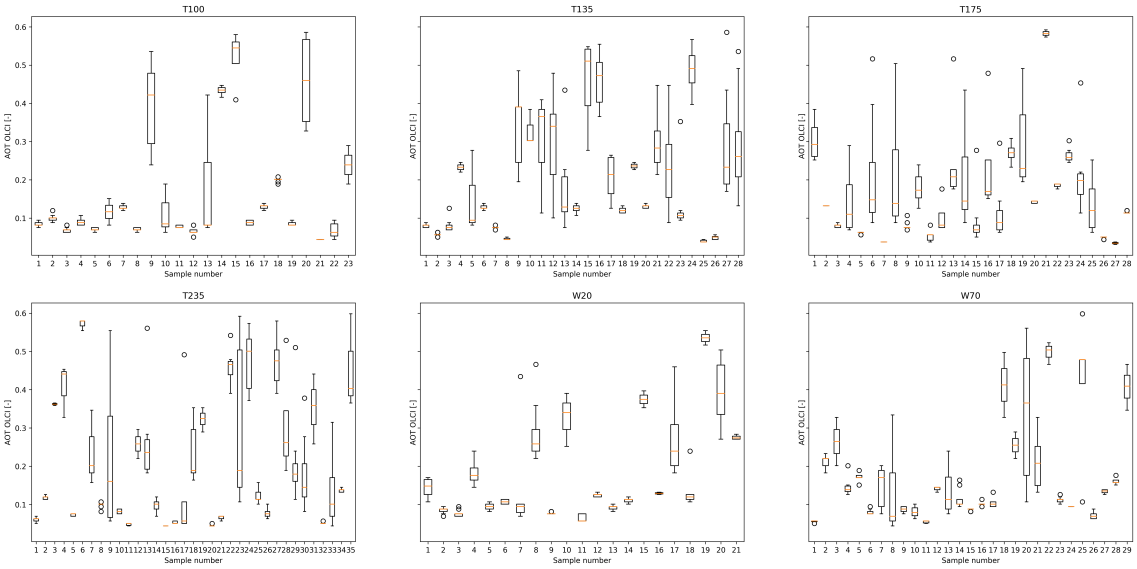

Figure F.1: Boxplots of the AOT at all MWTL locations.

Bibliography

[1] D. Antoine. OLCI Level 2 ATBD: Ocean Colour Products in case 1 waters. pages 1–31, 2010.

[2] D. Antoine. OLCI Level 2 ATBD - Atmospheric corrections over Case 1 waters. pages 1–37, 2010.

[3] D. Antoine and A. Morel. Relative importance of multiple scattering by air molecules and aerosols in forming the atmospheric path radiance in the visible and near-infrared parts of the spectrum. *Applied optics*, 37:2245–2259, 1998.

[4] D. Antoine and A. Morel. MERIS ATBD 2.7 — Atmospheric Correction of the MERIS observations Over Ocean Case 1 waters. 2011.

[5] M. Babin, A. Morel, V. Fournier-Sicre, F. Fell, and D. Stramski. Light scattering properties of marine particles in coastal and open ocean waters as related to the particle mass concentration. *Limnology and Oceanography*, page 843–859, 2003.

[6] Biodivcanada. Primary Productivity, 2014. http://www.biodivcanada.ca/default.asp?lang=En&n=71EC8678-1, Accessed on 2017-12-13.

[7] D. Blondeau-Patissier, J. F. R. Gower, A. G. Dekker, S. R. Phinn, and V. E. Brando. A review of ocean color remote sensing methods and statistical techniques for the detection, mapping and analysis of phytoplankton blooms in coastal and open oceans. *Progress in Oceanography*, 123:123–144, 2014. ISSN 00796611. doi: 10.1016/j.pocean.2013.12.008.

[8] D. G. Boyce, M. R. Lewis, and B. Worm. Global phytoplankton decline over the past century. *Nature*, 466: 591–596, 2010.

[9] R. J. W. Brewin, S. J. Lavender, N. J. Hardman-Mountford, and T. Hirata. A spectral response approach for detecting dominant phytoplankton size class from satellite remote sensing. *Acta Oceanologica Sinica*, 29:14–32, 2010.

[10] Brockmann Consult and ESA. Sentinel Application Platform (SNAP). http://step.esa.int/main/toolboxes/snap/, Accessed on 2017-12-13.

[11] CMEMS. Copernicus marine environment monitoring service - north atlantic surface chlorophyll concentration from satellite observations: monthly and 8-days. http://marine.copernicus.eu/, Accessed on 2017-12-13.

[12] Copernicus. Overview | Copernicus, 2016. URL `http://www.copernicus.eu/main/overview`.

[13] G. E. Cordy (USGS). A primer on water quality. https://pubs.usgs.gov/fs/fs-027-01/, Accessed on 2017-12-13.

[14] R. Doerffer. Olci level 2 atbd - ocean colour turbid water. *GKSS Research Centre*, 2010.

[15] R. Doerffer. OLCI Level 2 ATBD Alternative Atmospheric Correction. page 10, 2010.

[16] R. Doerffer and H. Schiller. Atbd 2.12 — pigment index, sediment and gelbstoff retrieval from directional water leaving radiance reflectances using inverse modelling technique. *GKSS Research Centre*, 1997.

[17] R. Doerffer and H. Schiller. The meris case 2 water algorithm. *International Journal of Remote Sensing*, 28(3-4):517–535, 2007. doi: 10.1080/01431160600821127.

[18] C. Donlon, B. Berruti, A. Buongiorno, M. H. Ferreira, P. Femenias, J. Frerick, P. Goryl, U. Klein, H. Laur, C. Mavrocordatos, J. Nieke, H. Rebhan, B. Seitz, J. Stroede, and R. Sciarra. The Global Monitoring for Environment and Security (GMES) Sentinel-3 mission. *Remote Sensing of Environment*, 120:37–57, 2012.

[19] M. A. Eleveld, R. Pasterkamp, H. J. Van der Woerd, and J. D. Pietrzak. Remotely sensed seasonality in the spatial distribution of sea-surface suspended particulate matter in the southern North Sea. *Estuarine, Coastal and Shelf Science*, page 103–113, 2008.

[20] ESA. Sentinel-3 olci technical guide - level-2 olci processing algorithms, . https://sentinel.esa.int/web/sentinel/technical-guides/sentinel-3-olci/level-2/processing, Accessed on 2017-12-13.

[21] ESA. User Guides - Sentinel-3 OLCI - Coverage, . https://sentinel.esa.int/web/sentinel/user-guides/sentinel-1-sar/acquisition-modes/interferometric-wide-swath, Accessed on 2017-12-13.

[22] ESA. Algal Pigment Index i, . http://envisat.esa.int/handbooks/meris/CNTR2-7-2-2-2-2.html, Accessed on 2017-12-13.

[23] ESA. Algal pigment index ii, . https://earth.esa.int/handbooks/meris/CNTR2-7-2-2-2-3.html, Accessed on 2017-12-13.

[24] ESA. Technical guides - ocean quality and science flags, . https://sentinels.copernicus.eu/web/sentinel/technical-guides/sentinel-3-olci/level-2/quality-and-science-flags-op, Accessed on 2017-12-13.

[25] EUMETSAT. Sentinel-3a product notice 05 july 2017 - olci level-2 ocean colour. 2017.

[26] European Community. Directive 2000/60/EC of the European Parliament and of the Council of 23 October 2000 establishing a framework for Community action in the field of water policy. *Official Journal of the European Parliament*, L327, 2000.

[27] G. C. Feldman (NASA). An overview of seawifs and the seastar spacecraft. https://oceancolor.gsfc.nasa.gov/SeaWiFS/, Accessed on 2017-12-13.

[28] J. Fischer, R. Preusker, and R. Lindstrot. Olci level 2 algorithm theoretical basis document - correction of the impact of the absorption of atmospheric gases. *Free University Berlin*, 2010.

[29] M. Gergely and G. Zibordi. Assessment of aeronet-oc l wn uncertainties. *Metrologia*, 51(1):40, 2014.

[30] Heliospectra. Spectrum 101: The Action Spectra | Heliospectra, provider of energy-efficient, fully controllable LED grow lights for greenhouses, indoor growers and researchers, 2015. https://www.heliospectra.com/blog/spectrum-101-action-spectra, Accessed on 2017-12-13.

[31] W. C. Hinds. Properties, behavior, and measurement of airborne particles. *John Wiley and Sons*, page 3, 1999.

[32] J. Kusmierczyk-Michulec, .G De Leeuw, and M. M. Moerman. Physical and optical aerosol properties at the Dutch North Sea coast based on AERONET observations. *Atmospheric Chemistry and Physics*, 7: 3481–3495, 2007.

[33] J. Li, B. E. Carlson, and A. A. Lacis. How well do satellite aod observations represent the spatial and temporal variability of pm2.5 concentration for the united states? *Atmospheric Environment*, 102:260–273, 2015.

[34] B. Maccherone and S. (NASA) Frazier. Modis - moderate resolution imaging spectroradiometer - data. https://modis.gsfc.nasa.gov/about/, Accessed on 2017-12-13.

[35] C. D. Mobley. Overview of optical oceanography - inherent optical properties. http://www.oceanopticsbook.info/view/overview-of-optical-oceanography/inherent-optical-properties, Accessed on 2017-12-13.

[36] C. D. Mobley. Ocean Optics Web Book - Atmospheric Correction, 2016. http://www.oceanopticsbook.info/view/atmospheric_correction, Accessed on 2017-12-13.

[37] G. Moore and S. Lavender. ATBD - OLCI Bright Waters AC (mesotrophic to high turbidity). Algorithm Theoretical Basis Document. 2010.

[38] A. Morel and D. Antoine. Atbd 2.9 — pigment index retrieval in case 1 waters. *Laboratoire d'Océanographie de Villefranche*, 2011.

[39] A. Morel and L. Prieur. Analysis of variations in ocean color. *Limnology and Oceanography*, 22(4):709–722, 1977. ISSN 00243590. doi: 10.4319/lo.1977.22.4.0709.

[40] A. Morel, B. Gentili, H. Claustre, M. Babin, A. Bricaud, J. Ras, and F. Tieche. Optical properties of the "clearest" natural waters. *Limnology and Oceanography*, 52:217–229, 2007.

[41] NIVA. Ferrybox - ships of opportunity. http://www.niva.no/en/miljoedata-paa-nett/ferrybox-og-satellittdata, Accessed on 2017-12-13.

[42] U.S. Department of the Interior and U.S. Geological Survey. Land processes distributed active archive center - modis overview. https://lpdaac.usgs.gov/dataset-discovery/modis, Accessed on 2017-12-13.

[43] Y.J. Park, K. Ruddick, and G. Lacroix. Detection of algal blooms in european waters based on satellite chlorophyll data from meris and modis. *International Journal of Remote Sensing, Volume 31*, pages 6567–6583, 2010.

[44] R. Pasterkamp, M. Van Drunen, and E. Hoogenboom. Noordzee-atlas voor zwevend stof op basis van satellietbeelden in 2000. 2002.

[45] S.W.M. Peters, M. A. Eleveld, R. Pasterkamp, H. Van der Woerd, M. Devolder, S. Jans, Y. Park, K. Ruddick, T. Block, C. Brockmann, R. Doerffer, H. Krasemann, R. Röttgers, W. Schönfeld, P. V. Jørgensen, G. Tilstone, V. Martinez-Vicente, G. Moore, K. Sørensen, J. Høkedal, T. M. Johnsen, E.R. Lømsland, and E. Aas. Atlas of chlorophyll-a concentration for the north sea based on meris imagery of 2003. 2005. doi: 90-5192-026-1.

[46] L. Prieur and S. Sathyendranath. An optical classification of coastal and oceanic waters based on the specific spectral absorption curves of phytoplankton pigments, dissolved organic matter, and other particulate materials1. *Limnology and Oceanography*, 26:671–689, 1981.

[47] D. E. Raitsos, Y. Pradhan, R. J. W. Brewin, and G. Stenchikov. Remote Sensing the Phytoplankton Seasonal Succession of the Red Sea. *PLoS ONE*, 8, 2013.

[48] Rijksoverheid. Noordzeeloket Waterkwaliteit. https://www.noordzeeloket.nl/functies-en-gebruik/waterkwaliteit/index.aspx, Accessed on 2017-12-13.

[49] K. Ruddick, Y. Park, R. Astoreca, Borges A., G. Lacroix, C. Lancelot, and V. Rousseau. Application of the meris algal pigment products in belgian waters. *Proceedings of the 2nd MERIS/(A)ATSR workshop ESA SP 666*, 2008.

[50] R. P. Stumpf, T. W. Davis, T. T. Wynne, J. L. Graham, K. A. Loftin, T. H. Johengen, D. Gossiaux, D. Palladino, and A. Burtner. Challenges for mapping cyanotoxin patterns from remote sensing of cyanobacteria. *Harmfull Algae*, (1):160–173, 2016.

[51] G. H. Tilstone, S. W. M. Peters, H. J. van der Woerd, M. A. Eleveld, K. Ruddick, W. Schonfeld, H. Krasemann, V. Martinez-Vicente, D. Blondeau-Patissier, R. Rottgers, K. Sorensen, P. V. Jorgensen, and J. D. Shutler. Variability in specific-absorption properties and their use in a semi-analytical ocean colour algorithm for MERIS in North Sea and Western English Channel Coastal Waters. *Remote Sensing of Environment*, 118:320–338, 2012. doi: 10.1016/j.rse.2011.11.019.